Functional Evaluation of Noncovalent Interactions in Neuroreceptors and Progress Toward the Expansion of Unnatural Amino Acid Methodology

Thesis by

Kristina Nicole-McCleary Daeffler

In Partial Fulfillment of the Requirements for the degree

of

Doctor of Philosophy

CALIFORNIA INSTITUTE OF TECHNOLOGY

Pasadena, California

2014

(Defended May 2, 2014)

Acknowledgements

This degree would not have been as fulfilling as it was without the support and friendship of so many people. First of all (and most importantly), I would like to thank my advisor, Dennis Dougherty, for providing us with the means and freedom to embark on our scientific quests, and for being a constant source of optimism when I most certainly needed it. We have also been lucky in our collaboration with the Lester lab, which has afforded us a wealth of knowledge and experience (and constructs). Henry himself has been a wonderful collaborator, and has provided invaluable insight into my projects for which I am grateful. I would also like to thank my committee, Professors Jackie Barton, Jim Heath, and Doug Rees, for wonderful discussions and encouragement in all of our meetings.

I have had the pleasure of overlapping with many group members who have all left me a better and more capable scientist (and person). Kiowa Bower helped convince me to join the lab, and taught me most of what I know about group lore as my mentor. Angela Blum, Walrati (Kay) Limapichat, and Nyssa Puskar were the first group members that I formed a strong friendship with. They are incredible scientists, coworkers, and people, and have provided me with wisdom beyond my years.

To the North Bay Nation (and those of you who wish you were a part): you are the best. You are all the best. I cannot imagine what my degree would have been like if you had been any different. No workplace has any business being as fun as ours is on any given day. From good times on the veranda to deep scientific discussions, we have evolved to be an extremely cohesive group, which makes the inherent frustrations of graduate school seem insignificant. It would be a tall order to fill to find another group of scientists

as motivated, intelligent, and down-to-earth, as you all are, and there are so many little things I will miss about our interactions.

I have so much to say about everyone in the group, but I will keep it short. Noah Duffy is my graduation buddy and a great friend. He has been both motivating and supportive through our final months here and our departure will considerably decrease the average age of the north bay. Ethan Van Arnam and Ximena da Silva Tavares joined the lab the same year as me. I was fortunate to work with Ethan at the beginning of our degrees on the GPCR projects, and we have all been fortunate to be acquainted with his finger toes. I've enjoyed many meaningful conversations with Ximena and wish her good luck with her future adventures. Chris Marotta is a fellow Connecticutian and football lover, and I've enjoyed our collaboration and friendship over the years. Maybe some day the Bills will actually be good. Tim Miles is one of the most well-read scientists I know. I will miss hearing "hmm, that's interesting" as an invitation to turn around and learn about whatever interesting research article he found, or if I was really lucky, some wonderful distraction on the internet that would make many potential hours of productivity disappear. Matt Rienzo and Mike Post have been two of my best friends in the group. I will miss you both so much, and can't wait to hear about the awesome science you will have done by the time you graduate. I'd like to thank Kayla Busby and Betty Wong for joining the group so that the female presence was stronger. Also, Kayla for organizing daily trips to red door. I'll certainly miss (David) Paul Walton's antics, Matt Davis's constant enthusiasm, and conversations about Texas with Clint Regan. And finally to the first years and future group members, good luck. And if you get the mammalian project, I wish you even more luck.

I would also like to thank my family, for whom I would not have gotten to where I am without. I'd like to thank my parents for being generally awesome and supportive, and for not making me fly home to visit, especially on holidays. Also, my wonderful husband Chris: you make life so much more fun and easy, and give me a constant supply of things to look forward to in life. And finally, thank you to my non-Dougherty group friends. Matthew and Catrina were our partners in crime throughout our degrees. I already miss our late night board games, and will be forever impressed that friendship always won over our competitiveness.

Abstract

This dissertation primarily describes chemical-scale studies of G protein-coupled receptors and Cys-loop ligand-gated ion channels to better understand ligand binding interactions and the mechanism of channel activation using recently published crystal structures as a guide. These studies employ the use of unnatural amino acid mutagenesis and electrophysiology to measure subtle changes in receptor function.

In Chapter 2, the role of a conserved aromatic microdomain predicted in the D3 dopamine receptor is probed in the closely related D2 and D4 dopamine receptors. This domain was found to act as a structural unit near the ligand binding site that is important for receptor function. The domain consists of several functionally important noncovalent interactions including hydrogen bond, aromatic-aromatic, and sulfur-π interactions that show strong couplings by mutant cycle analysis. We also assign an alternate interpretation for the linear fluorination plot observed at W6.48, a residue previously thought to participate in a cation-π interaction with dopamine.

Chapter 3 outlines attempts to incorporate chemically synthesized and *in vitro* acylated unnatural amino acids into mammalian cells. While our attempts were not successful, method optimizations and data for nonsense suppression with an *in vivo* acylated tRNA are included. This chapter is aimed to aid future researchers attempting unnatural amino acid mutagenesis in mammalian cells.

Chapter 4 identifies a cation-π interaction between glutamate and a tyrosine residue on loop C in the GluClβ receptor. Using the recently published crystal structure of the homologous GluClα receptor, other ligand-binding and protein-protein interactions are probed to determine the similarity between this invertebrate receptor and other more distantly related vertebrate Cys-loop receptors. We find that many of the interactions previously observed are conserved in the GluCl receptors, however care must be taken when extrapolating structural data.

Chapter 5 examines inherent properties of the GluClα receptor that are responsible for the observed glutamate insensitivity of the receptor. Chimera synthesis and mutagenesis reveal the C-terminal portion of the M4 helix and the C-terminus as contributing to formation of the decoupled state, where ligand binding is incapable of triggering channel gating. Receptor mutagenesis was unable to identify single residue mismatches or impaired protein-protein interactions within this domain. We conclude that M4 helix structure and/or membrane dynamics are likely the cause of ligand insensitivity in this receptor and that the M4 helix has an role important in the activation process.

Table of Contents

Chapter 1

Introduction

Chemistry at the synapse

The brain is the most complex object in nature. Within a human brain are approximately 10^{11} neurons that make between one and ten thousand connections to each other through synapses. It is at these synapses that most of the information processing in the brain occurs. Connected neurons communicate with each other through a process called synaptic transmission. In this process, an electrical signal, known as an action potential, propagates down the axon of a neuron. Once the electrical signal reaches the axon terminal, it stimulates the mobilization of vesicles containing neurotransmitters. These vesicles fuse with the cell membrane and release their contents into the synaptic cleft, which is the space between the two cells. Neurotransmitters then diffuse across the synapse and bind to neuroreceptors on the second neuron. Upon binding, these neuroreceptors either directly or indirectly produce an electrical signal, which can promote or inhibit the firing of an action potential in this second neuron (Figure 1.1).

Two major classes of neuroreceptors exist at the synapse: G protein-coupled receptors (GPCRs) and ligand-gated ion channels (LGICs). These neuroreceptors are found in both the central nervous system and the peripheral nervous system and are located on both presynaptic and postsynaptic neurons. GPCRs are often involved in slow synaptic transmission by acting through second messenger pathways, including G proteins and β-arrestins, and ligand-gated ion channels are involved in fast synaptic transmission through the direct passage of ions across the membrane upon activation.

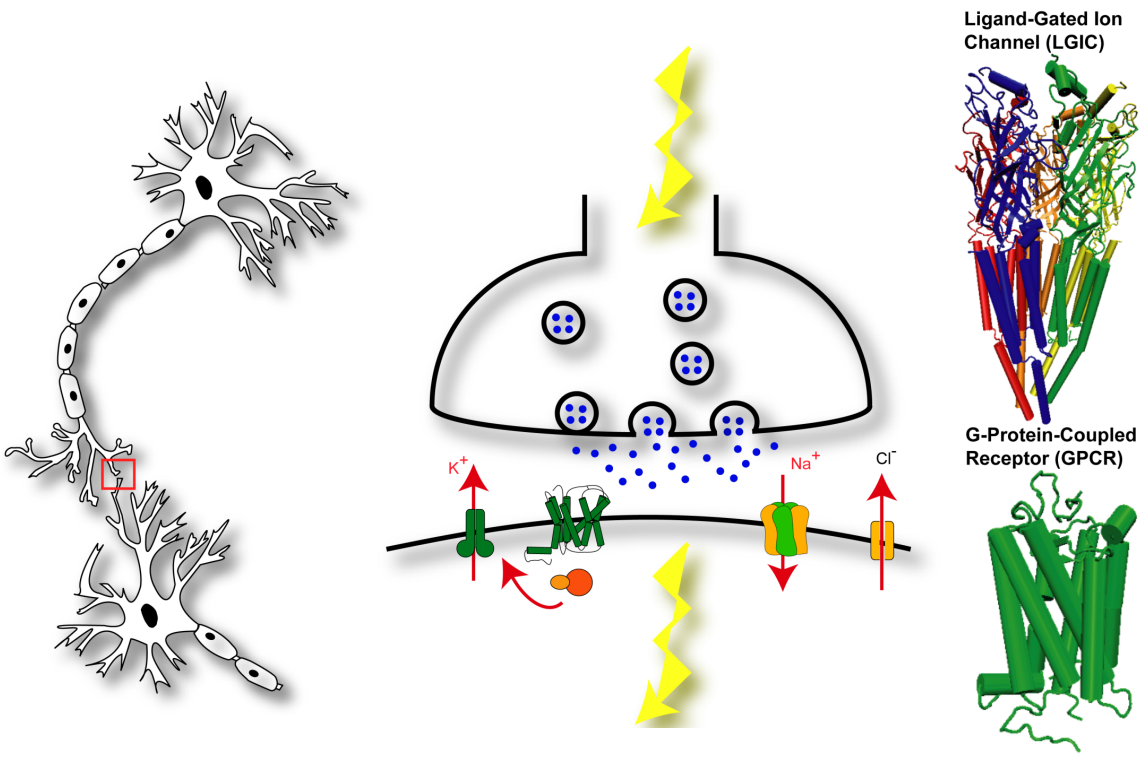

Figure 1.1 Synaptic transmission by neuroreceptors.

These receptors bind a variety of ligands including small aminergics, peptides, and fatty acids. And to add to this complexity, multiple inputs from a diverse array of neurotransmitters are received simultaneously at the post-synaptic neuron leading to an interplay of signals that gives rise to our higher-order brain processing. Because of the complexity of these neuroreceptors, we are interested in elucidating the binding interactions between neurotransmitter ligands and their cognate neuroreceptors, and how these binding events lead to cellular signaling.

G protein-coupled receptors

G protein-coupled receptors are an important class of signaling proteins found throughout the eukaryotic kingdom. These receptors comprise the largest family of

membrane proteins and represent an important class of drug targets because of their integral role in cellular signaling. GPCRs are located in all cell types in the human body and are involved in a number of intracellular signaling pathways required for proper cellular function.

GPCRs are an evolutionarily and structurally homologous family of integral membrane proteins that consist of seven transmembrane helices and a G protein-binding

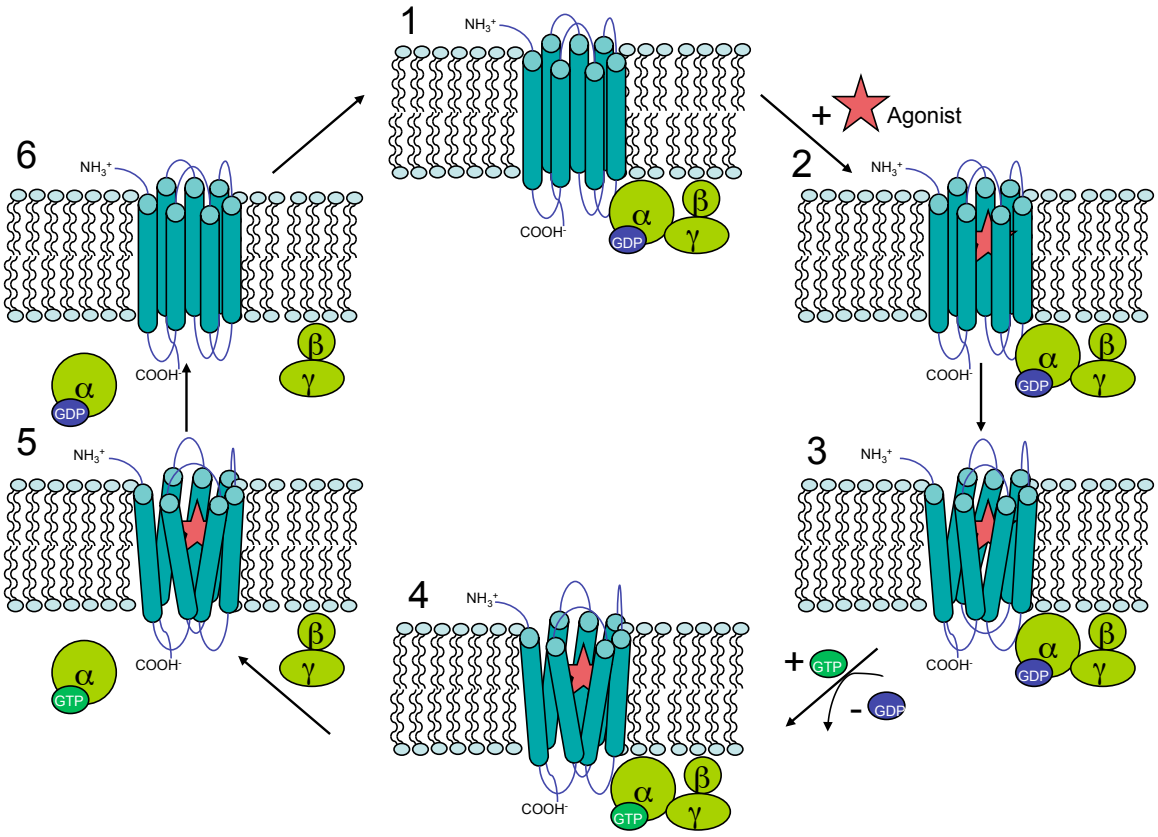

Figure 1.2: *GPCR activation and G protein signaling*. Binding of an agonist to the receptor (2) induces a conformational change of the receptor's helices (3). This conformational change causes activation of the heterotrimeric G protein. As a result, GDP is exchanged for GTP on the G_α subunit (4), which causes dissociation of the G_α and $G_{\beta\gamma}$ subunits from the GPCR (5). These subunits are then free to interact with downstream effector proteins. The cycle is complete (1) when the agonist dissociates from the GPCR, the receptor returns to its resting state conformation, and GTP is exchanged for GDP (6) on the G_α subunit.

domain created by the three intracellular loops of the receptor. GPCRs function by recognizing an extracellular stimulus (in the form of neurotransmitters, chemokines, light, odors, and other signaling molecules) and transducing this signal across the membrane to initiate downstream intracellular signaling pathways (Figure 1.2). Based on sequence homology, GPCRs are placed into one of six classes termed A-F. Class A (or the rhodopsin-like GPCRs) is the largest class of GPCRs and has the most solved crystal structures. These receptors are mostly activated by light, neurotransmitters, and hormones through binding of the ligand to the transmembrane domain of the receptor. It is this class of GPCRs that contains the well-studied rhodopsin, adrenergic (including β2-adrenergic receptor), and dopamine receptors.

Receptor activation occurs via ligand binding (or light activation) and results in a series of conformational changes in protein structure, which leads to activation of the bound heterotrimeric G protein (Figure 1.3). Activation of the G protein results in the exchange of GDP for GTP and dissociation of the G_{α} and $G_{\beta\gamma}$ subunits. These subunits are then free to interact with downstream signaling effector proteins, depending on the identity of the subunits, resulting in signal transduction. These pathways include activating or inhibiting production of cyclic AMP ($G_{\alpha s}$ or $G_{\alpha i/o}$, respectively), phospholipase C-dependent activation of the IP_3 pathway ($G_{\alpha q/11}$), Rho family GTPase signaling ($G_{\alpha 12/13}$), or hyperpolarization of the membrane for vision ($G_{\alpha t}$). The $G_{\beta\gamma}$ subunits are also free to interact with other molecules, and, in the case of $G_{\alpha i/o}$-associated GPCRs, can result in the opening of GIRK channels[2-6].

Due to the difficulties in obtaining crystal structures for integral membrane proteins, GPCRs are under-represented in the Protein Data Bank. However, recent

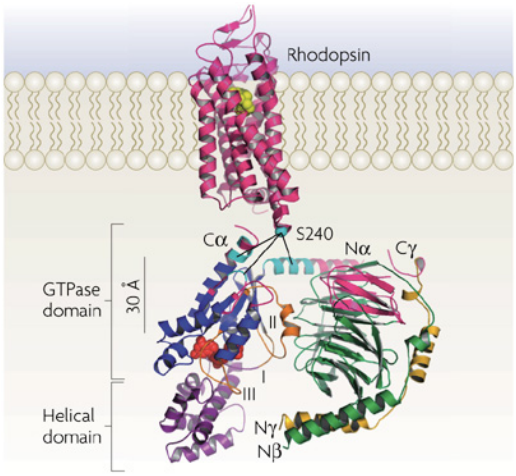

Figure 1.3. Crystal structure of rhodopsin with juxtaposed heterotrimeric G protein (PDB IDs: 1GZM and 1GOT) (taken from [1])

advances in crystallography have led to the elucidation of many new high-resolution crystal structures in the last few years[7-12]. Despite these advances, very few of the hundreds of known GPCRs have solved crystal structures, and we are therefore forced to extrapolate from structural data of related receptors. Likewise, while these crystal structures provide important structural information that was not previously available, the structures are a static image of the receptor, which provides minimal information about the activation process. Attempts have been made to capture the receptor in a permanently active conformation through either mutagenesis[13], the binding of a high affinity agonist[12,14], the binding of a G protein mimicking "nanobody" to the intracellular surface of the receptor[10], or by complexation of the receptor with its cognate G_α subunit[11]. Despite the promise of these new active-like structures, they are few and still provide only a static image. It is also unknown whether these structures represent a physiologically relevant active structure or are altered through the crystallization process. The lack of structural characterization of this large class of proteins, particularly in the activated state, has required a large effort in the form of structure-function studies to elucidate the mechanism of receptor activation as well as to probe the ability to target these molecules for therapeutic applications.

Cys-loop receptor ligand-gated ion channels

The Cys-loop receptors are a subfamily of ligand-gated ion channels and are named for a characteristic loop in the extracellular ligand-binding domain formed by a conserved disulfide bond. Receptors in this family include the excitatory, cation-permeable, nicotinic acetylcholine receptors (nAChRs) and 5-HT_{3A} receptor, and the inhibitory, anion-permeable, $GABA_A$, $GABA_C$, glycine, and GluCl receptors. These receptors are pentameric, and are either homomeric with five identical subunits or are heteromeric and have between two to four different subunits. All subunits are composed of an N-terminal extracellular ligand binding domain and four transmembrane helices (M1-M4), with the second transmembrane helix, known as M2, forming the ion-conducting pore (Figure 1.4).

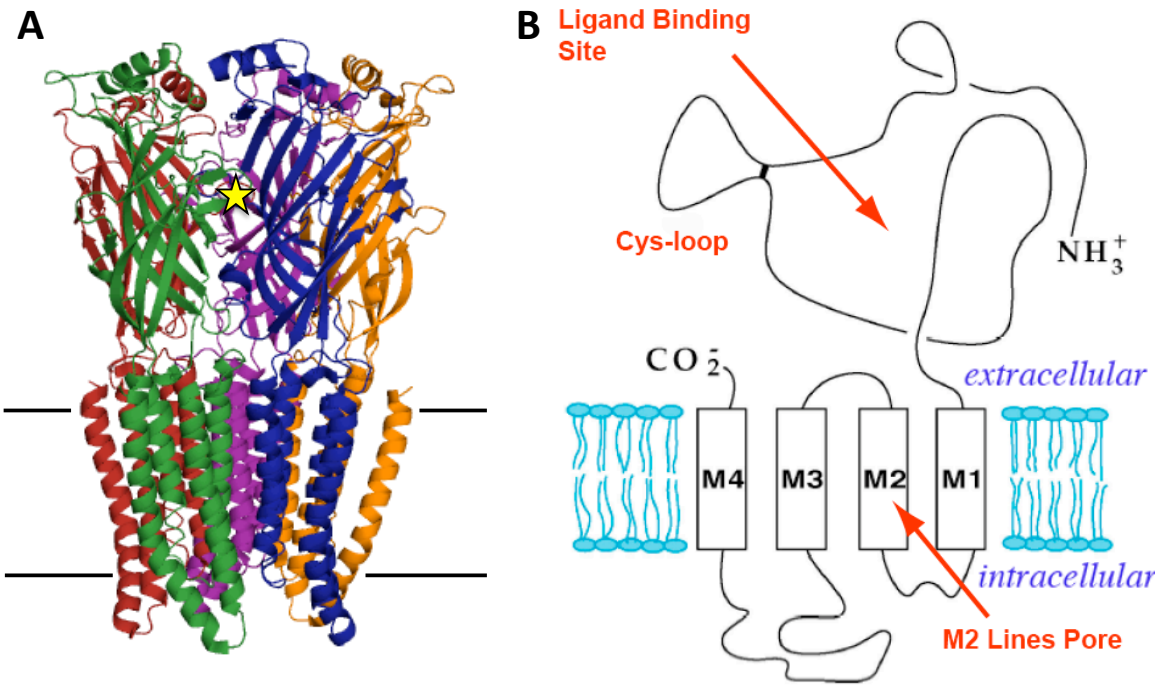

Figure 1.4. Structure of a Cys-loop receptor. **(A)** Crystal structure of the homomeric GluClα receptor (PDB ID: 3RIF). The ligand binding site is indicated by a yellow star. **(B)** Schematic of a typical Cys-loop receptor subunit.

Ligand binding occurs at the interface between two subunits in the extracellular domain, and the number of ligand binding sites is determined by the identity of the subunits in the receptor. In the absence of an agonist, the receptor exists in a non-conducting closed state. Upon ligand binding, a series of conformational changes occur near the binding site, which is translated approximately 60Å to the channel gate in the M2 helix. The net result of these movements is opening of the channel pore and ion conduction across the membrane. The receptor can also transition to a ligand-bound, non-conducting state known as the desensitized state.

Similar to GPCRs, ligand-gated ion channels are integral membrane proteins and are therefore difficult to crystallize. Until recently, only low-resolution cryo-EM structures of the torpedo nicotinic acetylcholine receptor[15,16] and high-resolution structures of acetylcholine binding protein[17], a soluble protein homologous to the extracellular ligand-binding domain of the full-length nAChRs, were available for structural information. However, in the last few years, a series of high-resolution prokaryotic and invertebrate ligand-gated ion channel crystal structures were reported, representing major advancements in the field of membrane protein crystallography[18-22]. Of these structures, GluClα, a homopentameric glutamate-gated chloride channel from *C. elegans*, represents the only Cys-loop receptor crystallized to date[21]. Therefore, despite this recent structural data, there are still no high-resolution crystal structures available of vertebrate Cys-loop receptors. And, also similar to GPCRs, arguments have been made about the physiological relevance of the captured states. As such, structure-function studies continue to be an important way to study and better understand the dynamic processes of ligand binding and receptor activation.

Unnatural amino acid mutagenesis

While conventional mutagenesis is limited to the 20 naturally occurring amino acids, unnatural amino acid mutagenesis affords the ability to incorporate a wide range of chemically modified amino acids allowing for a more subtle perturbation of a potentially important residue (Figure 1.5). These unnatural amino acids can be incorporated into a protein at a specific site using a method known as *in vivo* nonsense suppression (Figure 1.6)[23]. This method uses a nonsense (or stop) codon introduced by mutation of the codon encoding the amino acid of interest and a suppressor tRNA molecule charged with the

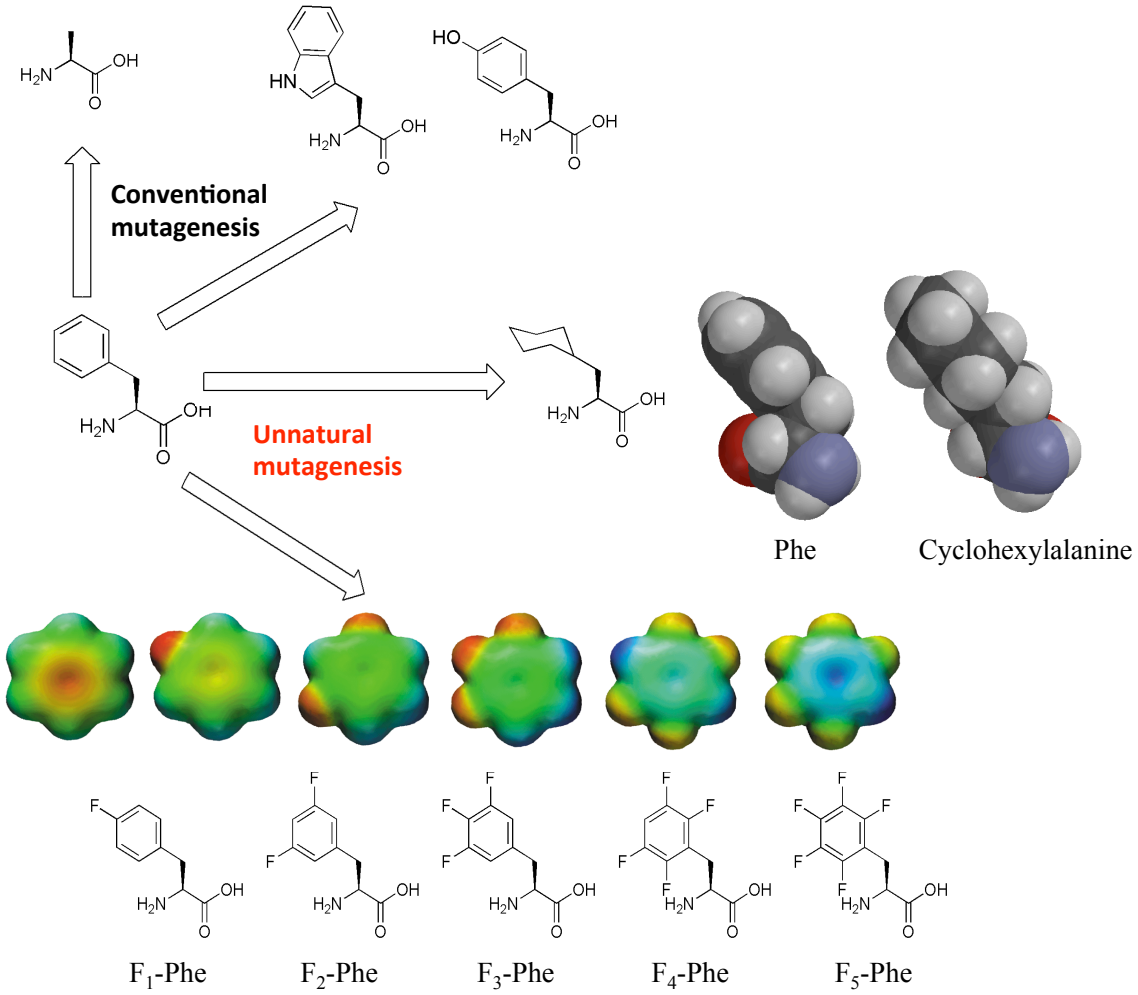

Figure 1.5. Diversity of side chain functionality made possible by unnatural amino acid mutagenesis.

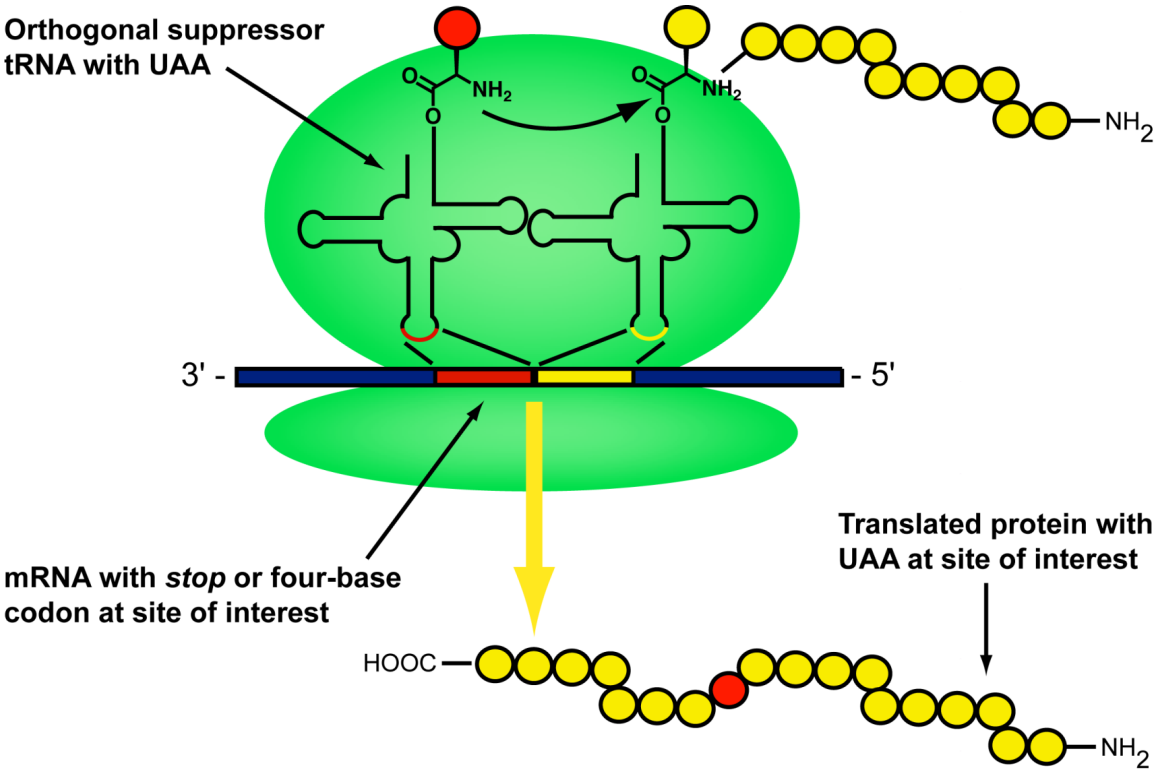

Figure 1.6. Schematic of site-specific incorporation of unnatural amino acids using nonsense suppression.

unnatural amino acid to be incorporated. Normally, the nonsense codon results in truncated protein due to premature termination of translation. However, in the presence of the suppressor tRNA (a tRNA with an anticodon engineered to recognize the TAG stop codon) a full-length protein containing the appropriate unnatural amino acid at the site of interest is produced. This is made possible by "hijacking" the cellular translational machinery, which causes the native polymerase to recognize the supplied suppressor tRNA and the stop codon as a match.

To determine the effect of unnatural amino acid mutagenesis of the receptor, mRNA encoding the TAG stop codon at the site for unnatural amino acid incorporation is co-injected with the appropriately charged tRNA into *Xenopus laevis* oocytes. Two-

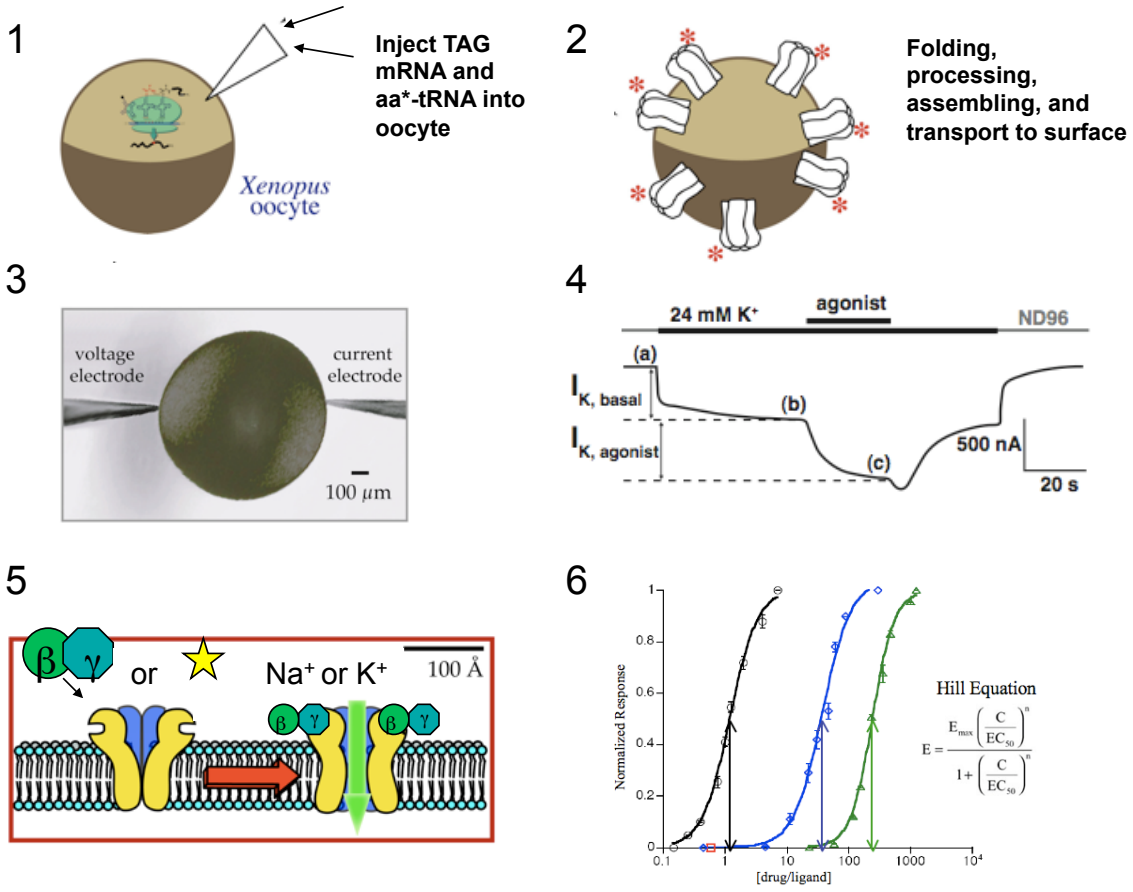

Figure 1.7: Electrophysiology of receptors containing unnatural amino acids. **(1)** Inject mRNA and unnatural amino acid charged tRNA into oocyte. **(2)** Oocyte uses cellular machinery to produce receptor with unnatural amino acid. **(3)** Two-electrode voltage clamp techniques are used to measure voltage across the membrane. **(4)** This is done using K^+-containing ND96 (for GPCRs) or Ca^{2+} free ND96 (LGICs) and an application of agonist. **(5)** Agonist application results in activation of the bound heterotrimeric G protein and release of $G_{\beta\gamma}$, which then bind to and activate GIRK channels or initiate direct ion movement through the ion-conducting pore. **(6)** The resulting outcome of a series of increasing agonist applications is an EC_{50} curve, which provides information about the effect of the mutation on agonist binding or function of the receptor[24].

electrode voltage clamp (TEVC) techniques are then used to measure the change in voltage across the oocyte membrane that results from the opening of the membrane-expressed ion channels upon agonist activation. In TEVC, the voltage electrode measures the membrane potential of the oocyte while the current electrode injects current into the oocyte equal to that passing through the open ion channels to maintain a

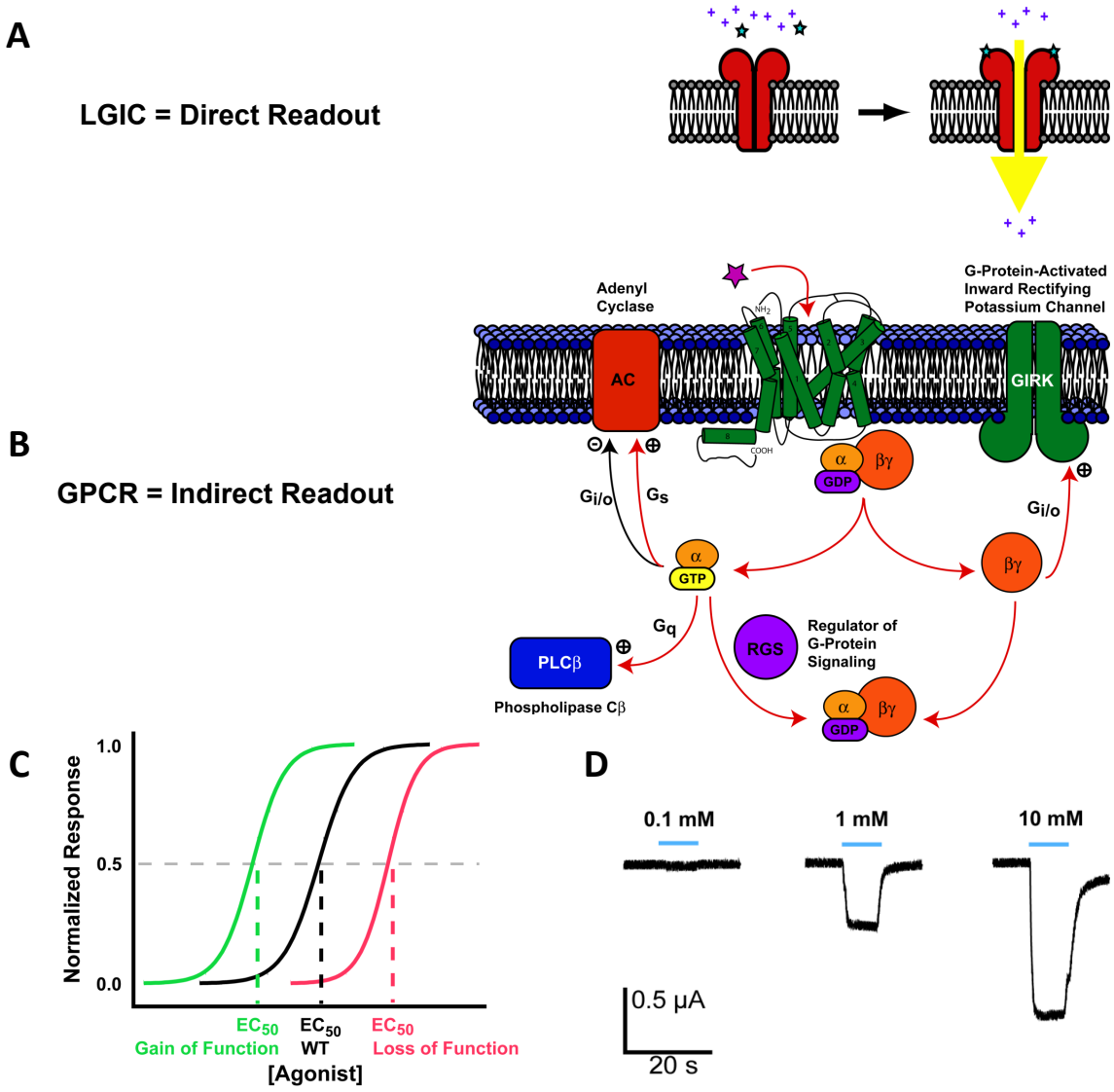

Figure 1.8. Using electrophysiology to quantify receptor functionality. **(A)** Activation of ligand-gated ion channels results in channel opening and passage of ions across the membrane. **(B)** Activation of $G_{\alpha i/o}$-coupled GPCRs leads to activation of associated GIRK channels through released $G_{\beta\gamma}$ subunits. **(C)** Dose-response data are fit to the Hill equation giving an EC_{50} measurement. Gain- and loss-of-function mutations are demonstrated by leftward or rightward shifts from wild type, respectively. **(D)** As increasing concentrations of agonist are applied higher currents across the membrane are observed. These data are fit to the Hill equation.

constant voltage across the membrane (Figure 1.7). The current applied through the current electrode is therefore a direct measure of the sum of currents through all ion channels in the membrane.

The function of the wild type and mutant receptors is assayed by applying increasing concentrations of agonist (Figure 1.8). As higher agonist concentrations are applied, more channels open. This results in dose-dependent increases in current across the membrane until this effect becomes saturated at sufficiently high doses. Any change in agonist binding or receptor activity due to incorporation of the unnatural amino acid can then be determined through the creation of an EC_{50} plot by fitting the data to the Hill equation. The EC_{50} value is the concentration required to elicit a half-maximal response and is an equilibrium measurement of agonist binding and channel opening. An increase in EC_{50} relative to wild type corresponds to a loss-of-function mutation, whereas a decrease in EC_{50} corresponds to a gain-of-function mutation.

In the case of ligand-gated ion channels, the observed current directly correlates to the activity of the channel. This occurs upon binding of an agonist to the ion channel, which causes the channel to open and allow ions to transverse the membrane. However, in the case of GPCRs, a direct output of receptor function cannot be determined by measuring the voltage across the membrane because GPCRs are not ion channels. Instead, a second messenger system involving G protein-coupled inward-rectifying potassium channels (GIRK) is used. When GPCRs are activated by an agonist, the $G_{\beta\gamma}$ dimeric subunit is released from the membrane[4-6]. The $G_{\beta\gamma}$ subunit is then free to interact with other molecules, and in the case of $G_{\alpha i/o}$-associated GPCRs results in the opening of GIRK channels[2,3]. TEVC can therefore be used to measure GPCR activation through movement of potassium ions across the membrane through the GIRK channels.

Dissertation work

In this dissertation, conventional and unnatural amino acid mutagenesis is used to study the function of two distinct classes of neuroreceptors, GPCRs and Cys-loop receptor ligand-gated ion channels. Traditional group suppression methodology was used for unnatural amino acid incorporation into *X. laevis* oocytes and TEVC electrophysiology was used as the assay. The receptors primarily targeted for structure-function study were the D2 and D4 dopamine receptors (GPCRs), the M2 muscarinic receptor (GPCR), and the GluCl receptors (LGICs). The 5-HT_{3A} receptor was used for attempted suppression in mammalian cells.

Chapter 2 describes research investigating the role of a conserved aromatic microdomain found in the core of the D2-like (D2, D3, and D4) dopamine receptors. This was assayed through conventional and unnatural amino acid mutagenesis of these aromatic residues and expected interaction partners. Double mutant cycle analysis was used to confirm electrostatic interactions between receptor side chains.

Chapter 3 details our attempts at unnatural amino acid suppression in mammalian cells. This chapter outlines our optimization of transfection conditions in HEK293T cells as progress toward this goal. While no suppression was observed with transfected acylated tRNA, expression using an *in vitro* transcribed human serine amber suppressor tRNA was observed, indicating the potential for success if transfection conditions can be further optimized. These optimization studies should provide a starting point for future researchers attempting to solve this problem.

Chapters 4 and 5 are dedicated to the study of GluCl receptors. In Chapter 4, the glutamate-receptor interactions are examined using conventional and unnatural amino

acid mutagenesis. Suppression in the GluClβ receptor proved difficult because of low receptor expression levels and a high wild type EC_{50}. Pore mutations and GluClα/GluClβ chimeras were made to minimize these difficulties. Chapter 5 describes the effects of GluClα/GluClβ chimeras on coupling of ligand binding and receptor activation.

Short appendices are included describing studies on the light-induced effects of Ru(bpy) functionalized poly-unsaturated fatty acids on a voltage-gated ion channel and screening of physostigmine analogs synthesized by the Reisman group against a variety of neuroreceptors.

References

1. Oldham, W.M. and Hamm, H.E., Heterotrimeric G protein activation by G-protein-coupled receptors. *Nat Rev Mol Cell Biol*, **2008**. *9*(1): p. 60-71.
2. Chan, K.W., Langan, M.N., Sui, J.L., Kozak, J.A., Pabon, A., Ladias, J.A., and Logothetis, D.E., A recombinant inwardly rectifying potassium channel coupled to GTP-binding proteins. *J Gen Physiol*, **1996**. *107*(3): p. 381-397.
3. Reuveny, E., Slesinger, P.A., Inglese, J., Morales, J.M., Iniguez-Lluhi, J.A., Lefkowitz, R.J., Bourne, H.R., Jan, Y.N., and Jan, L.Y., Activation of the cloned muscarinic potassium channel by G protein beta gamma subunits. *Nature*, **1994**. *370*(6485): p. 143-146.
4. Kofuji, P., Davidson, N., and Lester, H.A., Evidence that neuronal G-protein-gated inwardly rectifying K+ channels are activated by G beta gamma subunits and function as heteromultimers. *Proc Natl Acad Sci U S A*, **1995**. *92*(14): p. 6542-6546.
5. Krapivinsky, G., Krapivinsky, L., Wickman, K., and Clapham, D.E., G beta gamma binds directly to the G protein-gated K+ channel, IKACh. *J Biol Chem*, **1995**. *270*(49): p. 29059-29062.
6. Mark, M.D. and Herlitze, S., G-protein mediated gating of inward-rectifier K+ channels. *Eur J Biochem*, **2000**. *267*(19): p. 5830-5836.
7. Chien, E.Y., Liu, W., Zhao, Q., Katritch, V., Han, G.W., Hanson, M.A., Shi, L., Newman, A.H., Javitch, J.A., Cherezov, V., and Stevens, R.C., Structure of the human dopamine D3 receptor in complex with a D2/D3 selective antagonist. *Science*, **2010**. *330*(6007): p. 1091-1095.
8. Li, J., Edwards, P.C., Burghammer, M., Villa, C., and Schertler, G.F., Structure of bovine rhodopsin in a trigonal crystal form. *J Mol Biol*, **2004**. *343*(5): p. 1409-1438.

9. Cherezov, V., Rosenbaum, D.M., Hanson, M.A., Rasmussen, S.G., Thian, F.S., Kobilka, T.S., Choi, H.J., Kuhn, P., Weis, W.I., Kobilka, B.K., and Stevens, R.C., High-resolution crystal structure of an engineered human beta2-adrenergic G protein-coupled receptor. *Science*, **2007**. *318*(5854): p. 1258-1265.
10. Rasmussen, S.G., Choi, H.J., Fung, J.J., Pardon, E., Casarosa, P., Chae, P.S., Devree, B.T., Rosenbaum, D.M., Thian, F.S., Kobilka, T.S., Schnapp, A., Konetzki, I., Sunahara, R.K., Gellman, S.H., Pautsch, A., Steyaert, J., Weis, W.I., and Kobilka, B.K., Structure of a nanobody-stabilized active state of the beta(2) adrenoceptor. *Nature*, **2011**. *469*(7329): p. 175-180.
11. Rasmussen, S.G., DeVree, B.T., Zou, Y., Kruse, A.C., Chung, K.Y., Kobilka, T.S., Thian, F.S., Chae, P.S., Pardon, E., Calinski, D., Mathiesen, J.M., Shah, S.T., Lyons, J.A., Caffrey, M., Gellman, S.H., Steyaert, J., Skiniotis, G., Weis, W.I., Sunahara, R.K., and Kobilka, B.K., Crystal structure of the beta2 adrenergic receptor-Gs protein complex. *Nature*, **2011**. *477*(7366): p. 549-555.
12. Xu, F., Wu, H.X., Katritch, V., Han, G.W., Jacobson, K.A., Gao, Z.G., Cherezov, V., and Stevens, R.C., Structure of an Agonist-Bound Human A(2A) Adenosine Receptor. *Science*, **2011**. *332*(6027): p. 322-327.
13. Deupi, X., Edwards, P., Singhal, A., Nickle, B., Oprian, D., Schertler, G., and Standfuss, J., Stabilized G protein binding site in the structure of constitutively active metarhodopsin-II. *Proc Natl Acad Sci U S A*, **2012**. *109*(1): p. 119-124.
14. Rosenbaum, D.M., Zhang, C., Lyons, J.A., Holl, R., Aragao, D., Arlow, D.H., Rasmussen, S.G.F., Choi, H.J., DeVree, B.T., Sunahara, R.K., Chae, P.S., Gellman, S.H., Dror, R.O., Shaw, D.E., Weis, W.I., Caffrey, M., Gmeiner, P., and Kobilka, B.K., Structure and function of an irreversible agonist-beta(2) adrenoceptor complex. *Nature*, **2011**. *469*(7329): p. 236-240.
15. Miyazawa, A., Fujiyoshi, Y., Stowell, M., and Unwin, N., Nicotinic acetylcholine receptor at 4.6 A resolution: transverse tunnels in the channel wall. *J Mol Biol*, **1999**. *288*(4): p. 765-786.
16. Unwin, N., Refined structure of the nicotinic acetylcholine receptor at 4A resolution. *J Mol Biol*, **2005**. *346*(4): p. 967-989.
17. Brejc, K., van Dijk, W.J., Klaassen, R.V., Schuurmans, M., van Der Oost, J., Smit, A.B., and Sixma, T.K., Crystal structure of an ACh-binding protein reveals the ligand-binding domain of nicotinic receptors. *Nature*, **2001**. *411*(6835): p. 269-276.
18. Hilf, R.J. and Dutzler, R., X-ray structure of a prokaryotic pentameric ligand-gated ion channel. *Nature*, **2008**. *452*(7185): p. 375-379.
19. Bocquet, N., Nury, H., Baaden, M., Le Poupon, C., Changeux, J.P., Delarue, M., and Corringer, P.J., X-ray structure of a pentameric ligand-gated ion channel in an apparently open conformation. *Nature*, **2009**. *457*(7225): p. 111-114.
20. Hilf, R.J. and Dutzler, R., Structure of a potentially open state of a proton-activated pentameric ligand-gated ion channel. *Nature*, **2009**. *457*(7225): p. 115-118.
21. Hibbs, R.E. and Gouaux, E., Principles of activation and permeation in an anion-selective Cys-loop receptor. *Nature*, **2011**. *474*(7349): p. 54-80.
22. Nury, H., Van Renterghem, C., Weng, Y., Tran, A., Baaden, M., Dufresne, V., Changeux, J.P., Sonner, J.M., Delarue, M., and Corringer, P.J., X-ray structures of

general anaesthetics bound to a pentameric ligand-gated ion channel. *Nature*, **2011**. *469*(7330): p. 428-431.

23. Nowak, M.W., Gallivan, J.P., Silverman, S.K., Labarca, C.G., Dougherty, D.A., and Lester, H.A., In vivo incorporation of unnatural amino acids into ion channels in Xenopus oocyte expression system. *Methods Enzymol*, **1998**. *293*: p. 504-529.
24. Torrice, M.M., Bower, K.S., Lester, H.A., and Dougherty, D.A., Probing the role of the cation-pi interaction in the binding sites of GPCRs using unnatural amino acids. *Proc Natl Acad Sci U S A*, **2009**. *106*(29): p. 11919-11924.

Chapter 2

Functionally important aromatic-aromatic and sulfur-pi interactions in the D2 dopamine receptor

Reproduced with permission from:
Kristina N.-M. Daeffler, Henry A. Lester, and Dennis A. Dougherty
J. Am. Chem. Soc., **2012**, *134* (36), pp 14890–14896

Abstract

The recently published crystal structure of the D3 dopamine receptor shows a tightly packed region of aromatic residues on helices 5 and 6 in the space bridging the binding site and what is thought to be the origin of intracellular helical motion. This highly conserved region also makes contacts with residues on helix 3, and here we use double mutant cycle analysis and unnatural amino acid mutagenesis to probe the functional role of several residues in this region of the closely related D2 dopamine receptor. Of the eight mutant pairs examined, all show significant functional coupling ($\Omega > 2$), with the largest coupling coefficients observed between residues on different helices, C3.36/W6.48, T3.37/S5.46 and F5.47/F6.52. Additionally, three aromatic residues examined, F5.47, Y5.48, and F5.51 show consistent trends upon progressive fluorination of the aromatic side chain. These trends are indicative of a functionally important electrostatic interaction with the face of the aromatic residue examined, which is likely attributed to aromatic-aromatic interactions between residues in this microdomain. We also propose that the previously determined fluorination trend at W6.48 is likely due to a sulfur-π interaction with the side chain of C3.36. We conclude

that these residues form a tightly packed structural microdomain that connects helices 3, 5, and 6, thus forming a barrier that prevents dopamine from binding further toward the intracellular surface. Upon activation, these residues likely do not change their relative conformation, but rather act to translate agonist binding at the extracellular surface into the large intracellular movements that characterize receptor activation.

Introduction

G protein-coupled receptors (GPCRs) comprise a large class of integral membrane proteins activated by a wide range of agonists, including small molecule neurotransmitters, peptides, and light, leading to initiation of a wide range of downstream signaling cascades. Much research has been done on this class of molecules to elucidate the nature of receptor activation, i.e., how such a wide variety of agonists acts on hundreds of different receptors to induce activation of a small family of G proteins[1]. The recent publication of multiple GPCR crystal structures in both the inactive and active-like states complements decades of structure-function studies, resulting in a wealth of information about the function of these receptors[2-6]. However, much remains unknown about the nature of the specific events that cause large conformational changes in the cytoplasmic region of the receptor, resulting in activation.

The recently published high-resolution crystal structure of the human D3 dopamine receptor (D3R) offers a detailed snapshot of the receptor locked in an inactive, antagonist bound conformation[4]. This crystal structure shows a tightly packed hydrophobic core region of conserved residues that includes a cluster of six aromatic amino acids on helices 5 and 6. Aromatic residues are traditionally over-represented at

binding sites, and in the aminergic GPCRs, an important role in agonist binding and/or receptor activation has been proposed for residues in this microdomain[7-9]. In another family of ligand-activated receptors, the Cys-loop (pentameric) family of neurotransmitter-gated ion channels, a cluster of aromatics defines much of the agonist binding site, usually involving an important cation-π interaction to a protonated amine of the agonist[10-12]. In the aminergic GPCRs, the protonated amine has long been assumed to make a strong ionic interaction with the highly conserved D3.32, and recent crystal structures confirm this[4,13,14]. A complementary cation-π interaction to the cationic portion of agonists is still possible, but in the GPCR crystal structures reported to date, the aromatic residues in this microdomain do not seem to interact with any cationic center of agonists or antagonists. Instead, a majority of the aromatic residues in this region are located away from the binding site and appear to form a network of aromatic-aromatic interactions.

Aromatic-aromatic interactions are an important class of noncovalent interactions that participate in ligand-protein interactions, active site tuning, and protein stability[15-17]. For example, double mutant cycle analysis of two Tyr residues in the bacterial ribonuclease barnase demonstrated an important T-shaped aromatic-aromatic interaction that contributed -1.3 kcal/mol of interaction energy toward protein stability[18]. Similar interactions that demonstrate comparable interaction strengths have been observed in other proteins[19-21]. In addition to aromatic-aromatic dimers, higher order arrangements (trimers, tetramers, and larger) of aromatic residues have been observed with high frequency in proteins deposited in the Protein Data Bank[22]. This indicates a role for added stability through long-range interactions that bridge distant regions of the protein.

In addition to aromatic-aromatic interactions, the D3R crystal structure suggests a putative sulfur-π interaction with one of the aromatic residues in this region, as well as a hydrogen bond conserved across the family. The sulfur-π interaction has been probed in biological and model systems, and it has been estimated to contribute between 0.5 and 2 kcal/mol to binding/stability[23], although experimental studies in proteins are limited. Studies of hydrogen bonding also indicate a contribution of between 0.5-2 kcal/mol to protein stability, however interaction energy data between two polar uncharged residue side chains are lacking[24,25]. It has also been shown that the strength of a hydrogen bond is largely dependent on the polarity of its environment, with hydrogen bonds in the hydrophobic interior of proteins up to 1.2 kcal/mol stronger than solvent exposed interactions[26].

Given their location and conservation, it seems likely that the residues in this region have both an important structural and functional role in receptor activation. In the D3R crystal structure, the residues considered here are located at an important interfacial region between helices 3, 5, and 6, which likely serves as a connector domain that translates agonist binding in the extracellular region into intracellular helical motion and receptor activation. This region also likely forms the intracellular "floor" of the agonist/antagonist binding site and prevents these molecules from binding "lower" in the receptor, toward the intracellular space. In the present work we investigate the importance and nature of these noncovalent interactions using double mutant cycle analysis and unnatural amino acid mutagenesis in the closely related D2 and D4 dopamine receptors.

Methods

Molecular Biology. The human constructs of the DRD2 long form, DRD4 (Missouri S&T), and M2 receptors were subcloned into the pGEMhe vector, and GIRK1 and GIRK4 were in the pBSMXT plasmid. Mutagenesis of the DRD2 and M2 receptors was performed using Stratagene's QuikChange protocol, and mutagenesis of the DRD4 was performed using Herculase II Fusion polymerase (Stratagene) because of the high GC content of the cDNA. For nonsense suppression experiments, a TAG codon was mutated into the site of interest. The cDNA was linearized using the appropriate restriction enzyme (SbfI for DRD2, DRD4, and M2 and SalI for GIRK1 and GIRK4). mRNA was produced from the linearized plasmids by using the T7 mMessage Machine kit (Ambion) for DRD2, DRD4, and M2 and the T3 kit (Ambion) for GIRK1 and GIRK4.

74mer THG73 tRNA was synthesized from a DNA oligonucleotide template containing two 5' methoxy (C2' position) nucleotides to truncate transcription using Ambion's T7 MEGAshortscript kit[27]. Amino acids chemically appended to dCA were ligated to the end of the 74mer tRNA using methods previously described[28]. Acylation of tRNA was confirmed using MALDI mass spectrometry using a 3-hydroxypicolinic acid matrix. The NVOC protecting group on the amino acid was removed through a 5-minute irradiation step using a 1 kW Xenon lamp with WG-335 and UG-11 filters.

Oocyte Preparation and RNA Injection. Stage V-VI *Xenopus laevis* oocytes were harvested and injected with RNA as previously described[28]. For nonsense suppression experiments, 20 ng of receptor mRNA was coinjected with 10 ng each of GIRK1 and GIRK4 mRNA and an equal volume of deprotected ~1 μg/μL tRNA solution 48 hours

before recording. For conventional mutagenesis, 1-5 ng of receptor mRNA was coinjected with 10 ng each of GIRK1 and GIRK4 mRNA 48 hours before recording. For some low expressing mutants, receptor and GIRK1/4 mRNA and tRNA (if applicable) were injected a second time 24 hours before recording. Wild type recovery and wild type experiments used half the amount of receptor mRNA. As a negative control, all nonsense suppression sites were tested with a full length 76mer tRNA lacking an attached amino acid. In all cases, no significant expression was observed.

Electrophysiology. All oocyte experiments were performed on an OpusXpress 6000A (Axon Instruments) using two-electrode voltage clamp mode. Recording buffers were ND96 (96 mM NaCl, 2 mM KCl, 1 mM $MgCl_2$, 5 mM HEPES, 1.8 mM $CaCl_2$, pH 7.5) and high K^+ ringer (72 mM NaCl, 24 mM KCl, 1 mM $MgCl_2$, 5 mM HEPES, 1.8 mM $CaCl_2$, pH7.5). Solution flow rates were 2 mL/min., drug application flow rates were 2.5 mL/min. for DRD2 and DRD4 and 4 ml/min. for M2. Initial holding potential was -60 mV. Data were sampled at 125 Hz and filtered at 50 Hz. An ND96 prewash was applied for 10 s followed by high K^+ for 50 s to establish basal current and then application of agonist in high K^+ for 25 s. Agonist was then washed out with high K^+ buffer for 45 s and subsequently ND96 for 90 s. Agonist-induced currents were measured using the basal current as the baseline as described previously (Figure 2.1)[29]. Acetylcholine and dopamine (Sigma-Aldrich) dose solutions were made in high K^+ buffer from 1 M stock solutions. A minimum of 8 agonist doses were applied to each cell and a minimum of three batches of oocytes were used to give the final data.

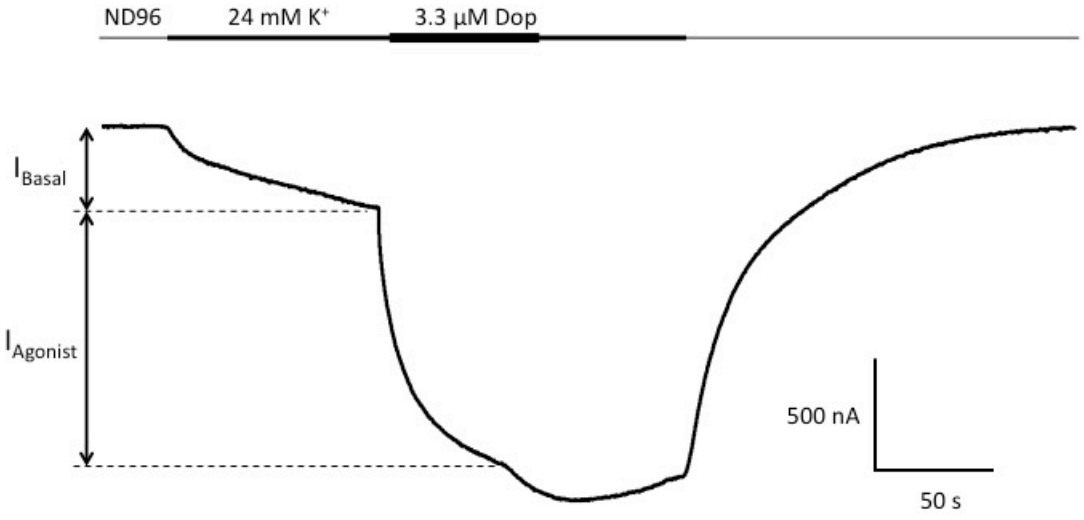

Figure 2.1. Sample trace of D2R wild type receptors expressed in *Xenopus laevis* oocytes with a 3.3 µM dopamine application. An EC_{50} curve was created by measuring the current ($I_{agonist}$) at varied dopamine concentrations, normalizing these values to the maximum $I_{agonist}$ value, and fitting the data to the Hill equation. Basal currents are caused by free $G_{\beta\gamma}$ in the cell activating the GIRK1/4 channels and were not included in data analysis.

Data Analysis. Data were fit to the Hill equation, $I_{norm} = 1/(1 + (EC_{50}/A))\ n_H$, where I_{norm} is the normalized current peak at [agonist] = A, EC_{50} is the concentration of agonist that elicits a half-maximum response, and n_H is the Hill coefficient. EC_{50} values were obtained by averaging the I_{norm} values for each agonist concentration and fitting those values to the Hill equation. Ω values were calculated using the equation: $[EC_{50}(mut_{1,2})*EC_{50}(WT)]/[EC_{50}(mut_1)*EC_{50}(mut_2)]$.

Results

Mutation Studies of D2R. As noted above, a microdomain of conserved residues on helices 3, 5, and 6, important for both agonist binding and receptor activation, has been

proposed to exist near the binding site of dopamine in the D2-like dopamine receptors (D2R, D3R, and D4R). The recently published crystal structure of D3R shows a tightly packed region of aromatic side chains on helices 5 and 6, along with a key cysteine and threonine on helix 3 (Figure 2.2). For the most part these residues do not directly contact the antagonist eticlopride, but rather they appear to form a connector domain between the agonist binding site and the intracellular domain of the receptor. In other GPCR structures, aligning aromatic residues are also not in contact with bound agonists/antagonists.

Although GPCRs are not ion channels, we are able to measure an electrophysiological readout of receptor activation through G protein-coupled inward-rectifying K^+ (GIRK) channels. GIRK channels are activated by the binding of $G_{\beta\gamma}$ subunits released from $G_{\alpha i/o}$-coupled GPCRs upon GPCR activation[30-32]. This assay has been described previously for the D2 and M2 muscarinic receptors and provides a sensitive readout of $G_{\alpha i/o}$-coupled GPCRs expressed in *Xenopus laevis* oocytes[29].

The assay we use is not applicable to D3R because the receptor has a high binding affinity for dopamine and thus prevents adequate washing off of agonist between drug applications[33]. The residues of interest are however highly conserved across the $G_{\alpha i/o}$-coupled D2-like family with only substitutions of phenylalanine for tyrosine at 5.48 and cysteine for phenylalanine at 5.51 in the D4R. Guided by the D3R crystal structure, we evaluated putative pairwise interactions between residues in this microdomain to determine whether these residues are functionally coupled using double mutant cycle analysis. We have primarily investigated the closely related D2R, but we have also considered the more distantly related D4R.

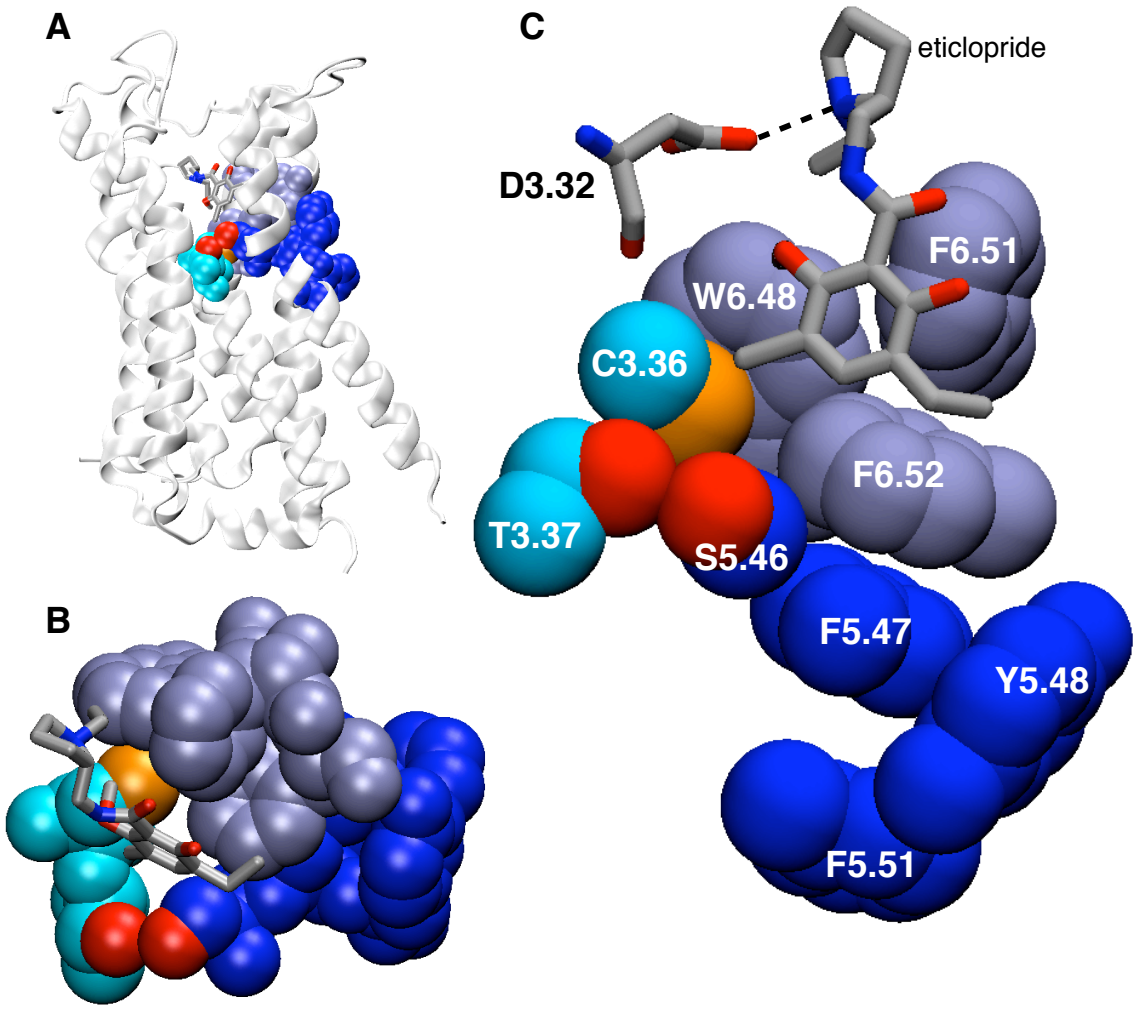

Figure 2.2: Space filling model of residues in the aromatic microdomain of the D3R (PDB 3PBL). Shown are both a side view (A) to position the domain of interest with respect to the receptor as a whole, and a top-down view (B). Protein residues are shown as space-filling, while the bound antagonist eticlopride is shown as a stick figure. (C) Enlarged view showing the residues considered here. Residues are color-coded according to their respective helices. Eticlopride and the highly conserved D3.32 are shown for reference.

Table 2.1: Conventional mutagenesis of residues in the aromatic microdomain of D2R

Mutant	EC_{50} (μM)	Hill	n	Mutant	EC_{50} (μM)	Hill	n
WT	0.020 ± 0.001	1.2 ± 0.1	15	F6.51A	> 100		10
C3.36A	0.49 ± 0.03	1.1 ± 0.1	16	F6.52A	0.071 ±0.003	1.4 ± 0.1	19
T3.37A	1.9 ± 0.2	1.0 ± 0.1	13	C3.36S	0.67 ± 0.04	1.1 ± 0.1	17
S5.46A	No Response			T3.37C	2.1 ± 0.1	1.1 ± 0.1	13
F5.47A	1.6 ± 0.2	0.9 ± 0.1	14	T3.37V	No Response		
Y5.48A	0.50 ± 0.02	1.1 ± 0.1	17	S5.46C	2.4 ± 0.1	1.0 ± 0.1	14
F5.51A	0.47 ± 0.02	1.1 ± 0.1	11	W6.48F	3.4 ± 0.1	1.0 ± 0.1	16
W6.48A	No Response			W6.48Y	0.65 ± 0.04	1.0 ± 0.1	17

Residues of interest were mutated to alanine to determine whether the receptor would function in the absence of each side chain (Table 2.1). Most alanine mutants were able to activate GIRK1/4 channels upon exposure to viable concentrations of dopamine (< 100 μM), generally with quite substantial shifts in EC_{50}. However, S5.46A, W6.48A, and F6.51A did not produce sufficient responses to applied dopamine. The more subtle mutations S5.46C, W6.48F, and W6.48Y did produce functional receptors, with large but measurable shifts in EC_{50}. F6.51Y did not display a significant shift in EC_{50} and F6.51W did not functionally express, and therefore this site was not examined further (Table 2.2).

To evaluate potential functional coupling of these residues, double mutant cycle analysis was performed using the mutants described in Table 2.1 (Figure 2.3, Table 2.3). Mutant cycle analysis is a standard technique used to determine whether the perturbing effects of two single mutants are functionally coupled or act independently. This is done by calculating a coupling coefficient ($\Omega = [EC_{50}(mut_{1,2})*EC_{50}(WT)]/[EC_{50}(mut_1)*EC_{50}(mut_2)]$). If the two mutations are independent of each other, $\Omega \sim 1$.

Table 2.2: Conventional mutagenesis of D2R

Mutant (D2R)	EC50 (μM)	Hill	n	Fold Shift
Wild type	0.020 +/- 0.001	1.2 +/- 0.1	15	-
C3.36A	0.49 +/- 0.03	1.1 +/- 0.1	16	25
C3.36K		No response		
C3.36L		No response		
C3.36M		No response		
C3.36S	0.67 +/- 0.04	1.1 +/- 0.1	17	34
T3.37A	1.9 +/- 0.2	1.0 +/- 0.1	13	95
T3.37C	2.1 +/- 0.1	1.1 +/- 0.1	13	105
T3.37S	0.0050 +/- 0.0003	1.1 +/- 0.1	21	1/4
T3.37V		No response		
S5.46A		No response		
S5.46C	2.4 +/- 0.1	1.1 +/- 0.1	14	120
F5.47A	1.6 +/- 0.2	0.9 +/- 0.1	14	80
F5.47W	0.34 +/- 0.01	1.3 +/- 0.1	12	17
F5.47Y	0.051 +/- 0.004	1.3 +/- 0.1	10	3
Y5.48A	0.50 +/- 0.02	1.1 +/- 0.1	17	25
Y5.48F	0.020 +/- 0.001	1.0 +/- 0.1	4	1
Y5.48W		No response		
F5.51A	0.47 +/- 0.02	1.1 +/- 0.1	11	24
F5.51W	0.045 +/- 0.003	1.2 +/- 0.1	12	23
F5.51Y	0.0051 +/- 0.0007	1.1 +/- 0.1	9	1/4
F6.44A	0.018 +/- 0.002	1.3 +/- 0.1	6	1/1.1
W6.48A		No response		
W6.48F	3.4 +/- 0.1	1.0 +/- 0.1	16	170
W6.48Y	0.65 +/- 0.04	1.0 +/- 0.1	17	33
F6.51A	> 100		10	>5000
F6.51W		No response		
F6.51Y	0.11 +/- 0.01	1.2 +/- 0.1	10	6
F6.52A	0.071 +/- 0.003	1.4 +/- 0.1	19	4
F6.52W	160 +/- 7	0.9 +/- 0.1	12	8000
F6.52Y	2.6 +/- 0.9	0.9 +/- 0.1	15	130
C3.36S/F5.47A	12 +/- 1	1.2 +/- 0.1	14	600
C3.36S/W6.48F	8.1 +/- 0.4	1.0 +/- 0.1	18	405
C3.36S/W6.48Y	2.1 +/- 0.1	1.0 +/- 0.1	15	105

T3.37C/S5.46C	2.0 +/- 0.1	1.1 +/- 0.1	17	100
F5.47A/Y5.48A	18 +/- 1	1.2 +/- 0.1	12	900
F5.47A/F5.51A	5.7 +/- 0.2	1.0 +/- 0.1	11	285
F5.47A/F6.52A	125 +/- 9	1.3 +/- 0.1	18	6250
F5.51A/F6.52A	4.6 +/- 0.1	1.1 +/- 0.1	16	230

Mutant cycles using EC_{50} values have been reported for multiple receptors to signify important protein-ligand and residue side chain interactions[34-38]. We appreciate, however, that the EC_{50} values presented here result from a complex signaling process, and so care must be taken in interpreting the results. As such, we have rejected the common practice of converting Ω values to ΔΔG values (=-RTln(Ω)), as this could be pushing the analysis too far. In the present case, an $\Omega > 1$ indicates that the double mutant is less functional than predicted from the single mutants, and an $\Omega < 1$ indicates that the double mutant is more functional than predicted. We do not think it is meaningful to distinguish these two cases, and simply conclude that if Ω deviates from unity by more than a factor of 2, the residues interact significantly. To facilitate comparisons we report Ω values < 1 as fractions, such that a mutant pair with an Ω of 1/5 would have the same interaction strength as a mutant pair with an Ω of 5.

In the D3R crystal structure, the side chain of C3.36 points directly into the face of the aromatic ring of W6.48. Mutant cycle analysis suggests a functionally important interaction between the two, with Ω values of 1/14 and 1/10 for the C3.36S/W6.48F and C3.36S/W6.48Y pairs, respectively (Table 2.3). C3.36S was used in place of C3.36A due to higher receptor expression levels of the single and double mutants.

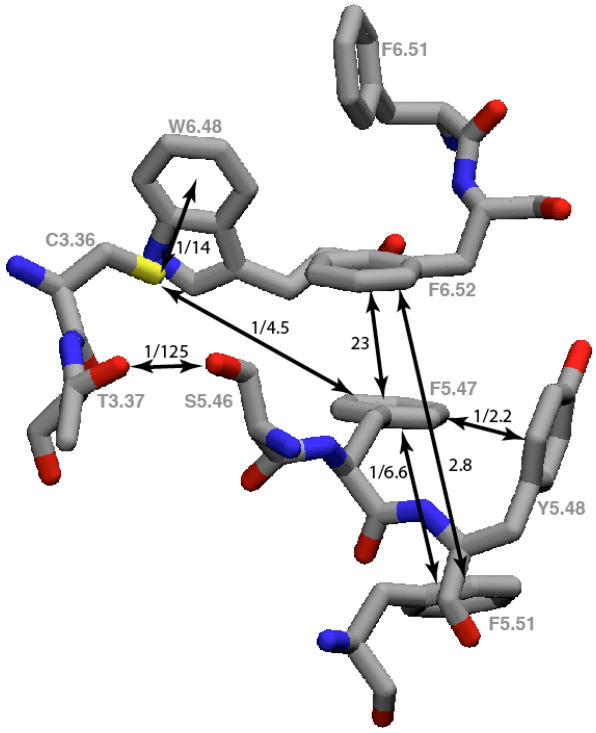

Figure 2.3: Mutant cycle analysis of the residues examined in this study. The strongest coupling values are observed between residues on different helices. The Ω values between residues are indicated.

Table 2.3: Mutant cycle analysis of putative pairwise interactions in the D2R

Mutant	EC_{50} (μM)	Hill	n	Ω
T3.37C/S5.46C	2.0 ± 0.1	1.0 ± 0.1	17	1/125
F5.47A/F6.52A	125 ± 9	1.3 ± 0.1	18	23
C3.36S/W6.48F	8.1 ± 0.4	1.0 ± 0.1	18	1/14
C3.36S/W6.48Y	2.1 ± 0.1	1.0 ± 0.1	15	1/10
F5.47A/F5.51A	5.7 ± 0.2	1.0 ± 0.1	11	1/6.6
C3.36S/F5.47A	12 ± 1	1.2 ± 0.1	14	1/4.5
F5.51A/F6.52A	4.6 ± 0.1	1.1 ± 0.1	16	2.8
F5.47A/Y5.48A	18 ± 1	1.2 ± 0.1	12	1/2.2

Other strong side chain couplings were observed between F5.47/F6.52 and F5.47/F5.51, indicating the presence of important aromatic-aromatic interactions in this region. The strongest interaction was observed between the putative hydrogen bond pair T3.37/S5.46. We recognize the potential complication of using cysteine mutants to probe this interaction, in that a disulfide bond could form and this could impact the mutant cycle analysis. However, the cysteine mutants were the only ones that expressed adequately to allow mutant cycle analysis. Treatment with DTT was inconclusive, presumably because of the presence of an important disulfide on the extracellular surface between helix 3 and extracellular loop 2. We are confident however that a hydrogen bond exists between these residues due to the overlapping electron density of the oxygen atoms of both side chains in the crystal structure. Both T3.37 and S5.46 were individually sensitive to mutation, and no other double mutant of T3.37/S5.46 functionally expressed. Weaker coupling energies were observed for the F5.51/F6.52 and F5.47/Y5.48 pairs, but there is still evidence for a meaningful interaction.

Nonsense suppression experiments. To further examine the nature of the interactions identified through mutant cycle analysis, unnatural amino acid mutagenesis was performed. Mutation of a residue to an unnatural analog can produce a more subtle perturbation, avoiding the potential issues that mutating large bulky aromatic residues to alanine can cause, such as forming destabilizing cavities. In the past we have used progressive fluorination of aromatic amino acid side chains to especially good effect. The surface of the aromatic side chains of Phe, Tyr, and Trp contains a build-up of negative electrostatic potential that leads to significant noncovalent interactions that are

not possible with simple hydrophobic residues such as Leu, Ile, and Val. Successive fluorination of the aromatic ring diminishes the negative electrostatic potential and thus weakens noncovalent interactions. The strongest of the noncovalent interactions involving aromatics is the cation-π interaction, in which a full positive charge is attracted to the negative electrostatic potential of the ring[39,40]. Fluorination studies have revealed over 20 cation-π interactions across a wide range of proteins[10-12]. The negative electrostatic potential of simple aromatics also gives rise to a number of so-called "polar-π" interactions, in which the positive end of a bond dipole interacts with the face of the ring[41]. NH and OH bonds of amines and alcohols/water can interact significantly with aromatics[42]. The CH bonds of aromatics are also polarized ($C^{\delta-}$••• $H^{\delta+}$), and this gives

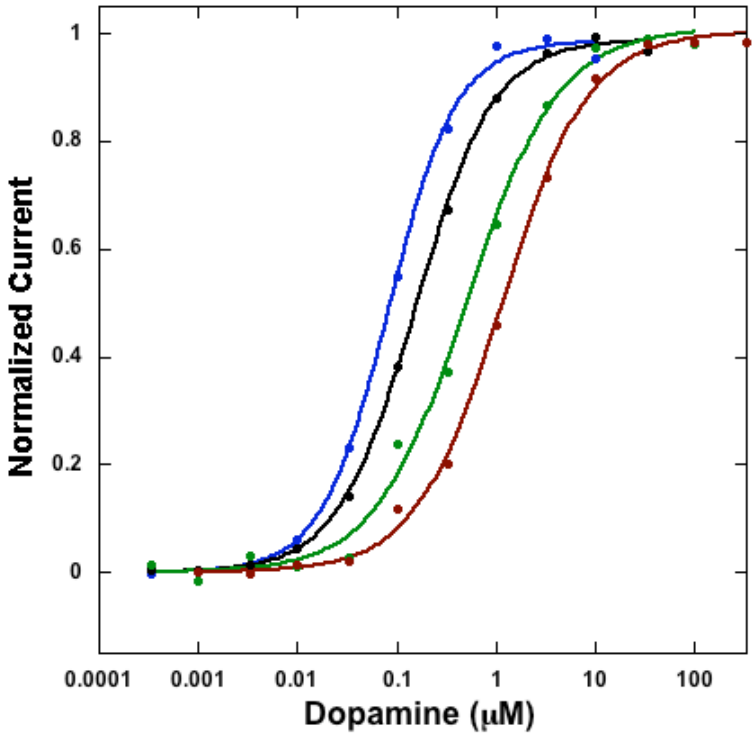

Figure 2.4: EC_{50} curves for D2R Y5.48Phe, F_1Phe, F_2Phe, and F_3Phe, respectively. Data was fit using the Hill equation.

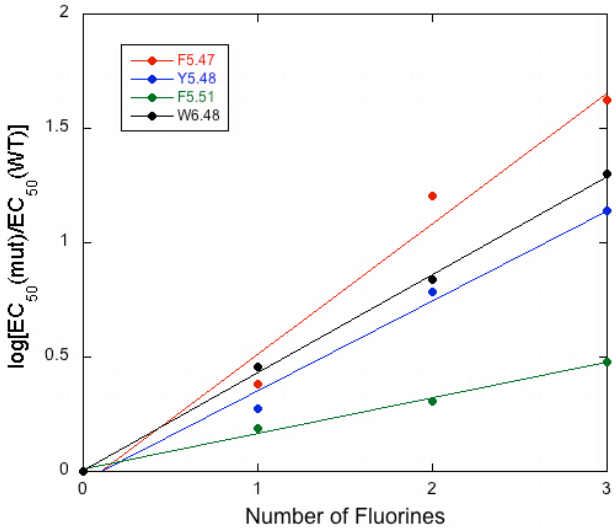

Figure 2.5. Fluorination trends of aromatic residues found in the aromatic microdomain of the D2R. A linear trend indicates the existence of an electrostatic interaction with the face of the residue examined.

Table 2.4: Unnatural amino acid mutagenesis of aromatic residues in the D2R

Site	Mutant	EC_{50} (μM)	Hill	n	Fold Shift
F5.47	Phe	0.026 ± 0.001	1.1 ± 0.1	19	-
	F_1Phe	0.087 ± 0.006	1.1 ± 0.1	8	3
	F_2Phe	1.0 ± 0.1	1.0 ± 0.1	9	39
	F_3Phe	1.3 ± 0.1	1.0 ± 0.1	12	49
	Me_2Phe	0.35 ± 0.02	1.3 ± 0.1	7	13
Y5.48	Phe	0.085 ± 0.004	1.3 ± 0.1	13	-
	F_1Phe	0.16 ± 0.01	1.1 ± 0.1	9	1.9
	F_2Phe	0.52 ± 0.06	0.9 ± 0.1	6	6.1
	F_3Phe	1.2 ± 0.1	1.0 ± 0.1	13	14
F5.51	Phe	0.024 ± 0.001	1.2 ± 0.1	18	-
	F_1Phe	0.045 ± 0.003	1.5 ± 0.1	9	1.6
	F_2Phe	0.059 ± 0.003	1.4 ± 0.1	13	2.0
	F_3Phe	0.087 ± 0.003	1.2 ± 0.1	12	2.8
W6.48	Trp	0.042 ± 0.004	1.0 ± 0.1	15	-
	F_1Trp	0.12 ± 0.01	1.0 ± 0.1	14	3
	F_2Trp	0.29 ± 0.03	1.0 ± 0.1	11	7
	F_3Trp	0.84 ± 0.06	0.9 ± 0.1	13	20
	F_4Trp	1.8 ± 0.3	0.8 ± 0.1	16	43

rise to the familiar aromatic-aromatic interactions, in which the positive periphery of aromatic systems and the negative center of aromatics interact in either T-shaped or parallel-displaced geometries[16,17]. Progressive fluorination should modulate these polar-π interactions just as it does a cation-π interaction.

Fluorination of residues F5.47, Y5.48, and F5.51 resulted in a linear fluorination trend upon incorporation of Phe analogs containing 1, 2, or 3 fluorines (Figure 2.4, Figure 2.5, and Table 2.4). As in previous studies, Y5.48 was probed with fluorinated Phe analogues, as fluorinating a tyrosine introduces the complicating feature of modulating the pK_a of the OH. The Y5.48F mutation produced only a slight deviation from wild type and therefore it is expected that Phe analogs should produce relevant data (Table 2.2). These results are indicative of an electrostatic interaction involving the face of the residue being fluorinated because fluorination should only significantly diminish the electrostatic component of interaction.

F5.47Cha was previously reported to exhibit a near-wild type EC_{50}[29]. This is inconsistent with the interpretation that the fluorination trend shown here is a result of an electrostatic interaction with the face of this side chain, as substituting cyclohexylalanine for phenylalanine should eliminate the electrostatic effect observed at this site. We have found considerable inconsistency in the expression of the F5.47Cha mutant, such that we have been unable to reproduce the previously reported results. As such, we conclude that there is a functionally important electrostatic interaction occurring with the face of F5.47. We have also previously reported a similar fluorination trend for W6.48 (reproduced here in Figure 2.5 and Table 2.4). Previous fluorination studies of F6.51 and F6.52 in the D2R receptor were inconclusive, in part due to complications from steric effects[29].

D4R. Fluorination studies in the D4 receptor produced results similar to what was observed in the D2R receptor, with the exception of F5.48, where no fluorination trend was observed (Table 2.6 and Figure 2.6). This is surprising, given the homology between the receptors, and the fact that all the aromatic residues examined except 5.51 (Cys in D4R) are conserved between the two receptors. It is also interesting to note that C3.36 and W6.48 show no functional coupling in the D4R receptor, despite the observed fluorination trend at W6.48 (Table 2.5). These data indicate that although the receptors show considerable sequence conservation, significant structural/functional differences between the two receptors do exist. This is also supported by the difference in homology and pharmacology patterns between receptors. D2R and D3R display higher sequence identity to each other (52%) than either do to D4R (39% and 41%, respectively)[43], and studies show that the pharmacologies of D2R and D3R are more similar than either are to D4R[44]. It is therefore likely that the D3R crystal structure provides a less accurate depiction of the D4R receptor than it does for the D2R receptor.

M2. The M2 muscarinic acetylcholine receptor contains a conserved aromatic residue at positions 5.47(F), 5.48(Y), 6.48(W), and 6.51(Y). It was previously determined that the M2 receptor did not show evidence of an electrostatic interaction at W6.48[29]. In this study we show that the M2 receptor also does not exhibit an electrostatic interaction at F5.47. This is not surprising, because the M2 receptor does not have an aromatic residue at the 5.51(V) or 6.52(N) positions, providing no aromatic residues to interact with the face of F5.47. We have also done a preliminary evaluation of several other residues that contribute to the aromatic cage of the M2 receptor (Y6.51, Y7.39, and Y7.43), but we

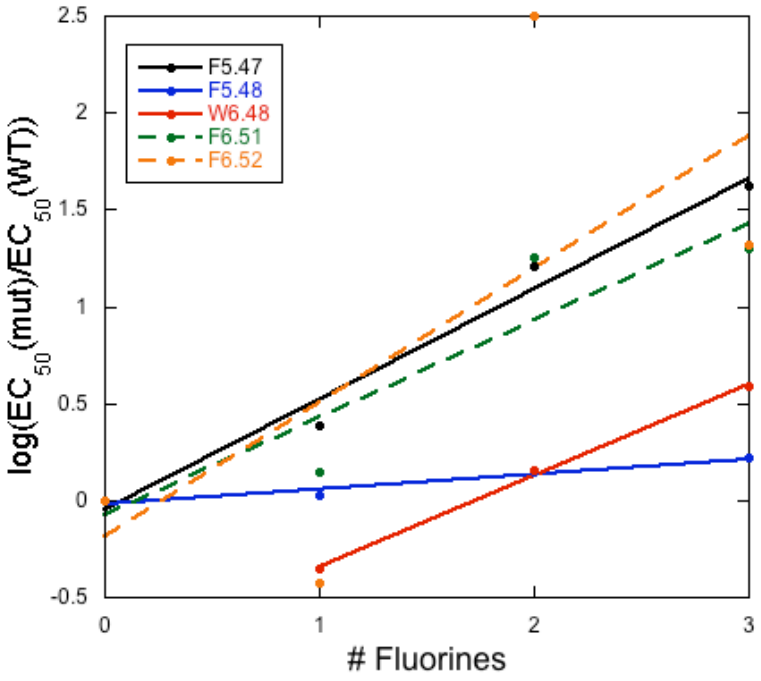

Figure 2.6: Fluorination trends of aromatic residues in the D4R. Solid lines represent residues showing a linear fluorination trend, dotted lines indicate poor fitting to a linear equation.

Table 2.5: Conventional mutagenesis of D4R

Mutant (D4R)	EC50 (μM)	Hill	n	Fold shift	Ω
Wild type	0.028 +/- 0.001	1.4 +/- 0.1	17	-	
F5.48A	0.016 +/- 0.001	1.4 +/- 0.1	12	1/1.7	
C5.51F	0.023 +/- 0.002	1.5 +/- 0.1	14	1/1.3	
C3.36S	0.017 +/- 0.001	1.4 +/- 0.1	13	1/1.7	
W6.48F	0.37 +/- 0.01	1.3 +/- 0.1	12	13	
W6.48Y	0.40 +/- 0.01	1.1 +/- 0.1	15	14	
C3.36S/W6.48F	0.28 +/- 0.01	1.3 +/- 0.1	13	10	1.2
C3.36S/W6.48Y	0.51 +/- 0.03	1.2 +/- 0.1	12	18	2.1
D3.32E	2.7 +/- 0.1	0.9 +/- 0.1	13	100	
D3.32N	230 +/- 14	1.2 +/- 0.1	10	8200	

Table 2.6: Unnatural amino acid mutagenesis of related aminergic receptors

Receptor/Site	Mutant	EC_{50} (μM)	Hill	n	Fold Shift
D4R F5.47	Phe	0.017 ± 0.002	1.3 ± 0.1	19	-
	F_1Phe	0.041 ± 0.005	1.2 ± 0.1	14	2.4
	F_2Phe	0.27 ± 0.01	1.0 ± 0.1	19	16
	F_3Phe	0.72 ± 0.04	1.0 ± 0.1	14	42
	Cha	0.55 ± 0.04	0.9 ± 0.1	12	32
	MePhe	0.031 ± 0.003	1.1 ± 0.1	4	1.8
	Me_2Phe	0.10 ± 0.01	1.1 ± 0.1	13	6
F5.48	Phe	0.018 ± 0.001	1.4 ± 0.1	20	-
	F_1Phe	0.019 ± 0.001	1.4 ± 0.1	12	1.1
	F_2Phe	0.025 ± 0.002	1.7 ± 0.2	13	1.4
	F_3Phe	0.030 ± 0.002	2.0 ± 0.2	12	1.7
	Cha	0.029 ± 0.002	1.4 ± 0.1	19	1.6
W6.48	Trp	0.018 ± 0.001	1.3 ± 0.1	32	-
	F_1Trp	0.0080 ± 0.0006	1.2 ± 0.1	20	1/5
	F_2Trp	0.026 ± 0.001	1.2 ± 0.1	21	1.4
	F_3Trp	0.070 ± 0.010	1.0 ± 0.1	18	3.7
	F_4Trp	0.13 ± 0.01	1.3 ± 0.1	11	5.5
	Nap	0.024 ± 0.002	1.4 ± 0.1	16	1.3
	MeTrp	0.0078 ± 0.0015	1.1 ± 0.2	4	1/2.5
F6.51	Phe	0.018 ± 0.001	1.1 ± 0.1	20	-
	BrPhe	0.093 ± 0.006	1.0 ± 0.1	10	5.5
	CNPhe	0.16 ± 0.01	1.2 ± 0.1	11	10
	F_1Phe	0.025 ± 0.002	1.2 ± 0.1	14	1.5
	F_2Phe	0.32 ± 0.01	1.1 ± 0.1	16	18
	F_3Phe	0.36 ± 0.02	1.1 ± 0.1	13	20
	Cha	0.39 ± 0.04	1.1 ± 0.1	13	21
	Me_2Phe	55 ± 7	1.0 ± 0.1	5	3000
F6.52	Phe	0.019 ± 0.001	1.1 ± 0.1	25	-
	BrPhe	0.039 ± 0.003	1.2 ± 0.1	12	2
	CNPhe	0.025 ± 0.002	1.3 ± 0.1	13	1.3
	F_1Phe	0.0072 ± 0.0004	1.4 ± 0.1	14	1/2.5
	F_2Phe	6.0 ± 0.3	0.7 ± 0.1	6	310
	F_3Phe	0.40 ± 0.02	0.9 ± 0.1	12	21

M2 F5.47	Phe	0.25 ± 0.02	1.2 ± 0.1	12	-
	F_3Phe	0.31 ± 0.02	1.0 ± 0.1	18	1.2
	Cha	0.97 ± 0.04	1.0 ± 0.1	13	3.9

have found these residues to be very sensitive to even subtle mutations such as Tyr-to-Phe, and so we have been unable to evaluate them in ways that parallel the work described here.

Discussion

It has long been appreciated that there are a number of conserved aromatic amino acids in class A GPCRs, and many studies have proposed that these residues play a crucial role in binding agonists/antagonists. We have previously probed some of these aromatics in the D2R and produced evidence that one highly conserved residue, W6.48, makes a direct binding interaction to dopamine. Our model also proposed a rotation of the side chain of W6.48 to facilitate dopamine binding, and indeed this residue has long been proposed to play the role of a "rotamer toggle switch" in GPCR activation. However, as more and more GPCR crystal structures with agonists/antagonists bound have appeared, a pattern has emerged in which drugs bind relatively "high up" (toward the extracellular space) in the receptor, at a location where many of the residues of this aromatic microdomain cannot directly contact the drug. Certainly in the D3R structure, which serves as the foundation for the present study, W6.48 and other contributors to the aromatic microdomain do not directly contact the bound antagonist eticlopride, and the side chain of W6.48 has not rotated. Many other structures of GPCRs show a similar conformation for the aligning residue, although in the recent structures of opioid

receptors W6.48 does contact bound drug. Also, in a recent structure of the M2 receptor with the antagonist QNB bound, the drug is bound more deeply in the receptor crevice, where 5 aromatic amino acids form an "aromatic cage" around the cationic end of the drug, as has been seen in a number of ACh binding sites. However, W6.48 is the only residue of the aromatic microdomain considered here that contributes to the aromatic cage. It is interesting, however, that in order to form the aromatic cage of the M2 receptor, the side chain of W6.48 has rotated to a position not seen in most other GPCR crystal structures, but that is similar to what we had previously proposed for D2R.

Returning to the D3 structure, a cluster of aromatic residues is evident, but it is unclear what its functional role might be. The present work was undertaken with a goal of evaluating the functional significance of this microdomain in the dopamine receptor, with an emphasis on evaluating possible functional interactions that are implied by the structure. As noted above, our assay system is not compatible with the D3R, and so we have investigated the closely related D2R, while also performing more limited studies on the more distantly related D4R and M2 receptor.

Residue coupling through mutant cycle analysis. We considered various pairwise interactions involving residues C3.36, T3.37, S5.46, F5.47, Y5.48, F5.51, W6.48, and F6.52 (Figure 2.3). Of the eight pairs considered, six produced clearly meaningful interactions ($\Omega \geq 4.5$), while two others were smaller, but still significant ($\Omega > 2$). Especially large coupling coefficients are seen with T3.37C/S5.46C, C3.36S/W6.48F, and F5.47A/F6.52A, providing evidence for strong functional coupling between residues that directly connect helices 3, 5, and 6. The notion that this cluster of residues functions

as a unit is supported by the long-range coupling seen between F5.51/F6.52 and C3.36/F5.47.

Probing aromatic-aromatic interactions using unnatural amino acid mutagenesis. While mutant cycle analysis and fluorination of aromatic residues have been previously used to examine aromatic-aromatic interactions in proteins[45,46], to our knowledge this is the first example of using unnatural amino acid mutagenesis to examine the electrostatic component of these interactions. We have successfully incorporated fluorinated phenylalanine and tryptophan derivatives at a number of conserved residues in this aromatic microdomain of the D2 dopamine receptor.

We noted above the previously reported strong and consistent response of W6.48 to fluorination and our earlier interpretation of this as indicating a cation-π interaction. However, this interpretation was called into question by the D3R structure. In that structure, W6.48 is not in a position to contact the amine of drugs or other atoms that may bear a large partial positive charge, but rather experiences a van der Waals contact with the side chain of C3.36, in which the sulfur of the cysteine points directly into the face of the Trp side chain. Mutant cycle analysis establishes a strong coupling between W6.48 and C3.36, indicating that this interaction is functionally significant. In the D3R crystal structure, W6.48 does make a weak hydrophobic contact with the bound drug eticlopride, and so we cannot completely rule out a direct interaction between dopamine and W6.48 in the activated receptor. However, it would be difficult to see how such an interaction could produce the linear fluorination trend of Figure 2.5, and so we feel that an interaction between W6.48 and C3.36 is the more plausible interpretation.

Sulfur-arene interactions are in fact quite common in protein crystal structures. For example, Met is as likely as Phe or Trp to be near another Trp, with the majority of the interactions being to the face of the ring[47,48]. While the nature of the interaction is primarily dispersive, there is generally considered to be a significant electrostatic component as well[49].

We propose that the fluorination of W6.48 is probing this sulfur-arene interaction, and removing electron density from the aromatic diminishes the magnitude of the interaction. In addition to a lack of hydrogen atom resolution in the crystal structure, computational studies disagree whether the face of aromatic side chains preferentially interact with the lone pairs of the sulfur atom or through an SH-π interaction[47,49,50]. Our fluorination experiments are unable to distinguish between the two scenarios because both occur through an electrostatic interaction with the face of W6.48. Progressive fluorination may also impact the dispersion component of the interaction, as F is the least polarizable of the elements. The fact that fluorination of W6.48 in the M2 receptor does not produce a comparable trend is consistent with this analysis, as residue 3.36 is valine in the M2 receptor, and so no sulfur-arene interaction is possible. To our knowledge, this is the first example of evaluating a sulfur-arene interaction by modulating the electrostatic surface of the arene. Note that the magnitude of the sulfur-arene interaction appears to be considerable. Tetrafluorination of W6.48 (which essentially makes the aromatic surface electrostatically neutral) results in a 300-fold shift in EC_{50}.

We also see linear fluorination plots for residues F5.47, Y5.48, and F5.51, indicating noncovalent electrostatic interactions with the faces of these residues. Given the crystallographic results, we propose that fluorination is probing various arene-arene

interactions in the D2 receptor. We emphasize that our assay is a functional one, indicating that the noncovalent interactions involving these residues play a significant functional role. In the past we have considered the relative slopes of such fluorination plots to be indicative of the magnitude of the electrostatic component of the relevant noncovalent interaction. Here, the relative values of the slopes are F5.47 > W6.48 > Y5.48 > F5.51. These would appear to be consistent with expectations from the D3R crystal structure. F5.47 is at the heart of the aromatic region of this microdomain, and it makes a parallel stacking interaction with F6.52 and F5.51 and a T-shaped interaction with Y5.48. Y5.48 only makes the single interaction to F5.47. F5.51 is further away from the other aromatics, and the slope associated with it is the smallest we have seen for a fluorination plot. We propose that it makes a weak parallel stacking interaction with F5.47. In our mutant cycle analyses, we paired F5.47 with both Y5.48 and F5.51, and the latter produced a larger coupling energy than the former, opposite to the fluorination trend. We are inclined to accept the conclusion from fluorination that the Y5.48•••F5.47 interaction is stronger than the F5.51•••F5.47 interaction because of the much more subtle perturbation introduced by fluorination vs. the highly perturbing arene-to-alanine mutation.

The major interactions probed here, involving residues on helices 3, 5 and 6 suggest a network of interactions that form a belt in the center of the receptor (C3.36/W6.48, F5.47/F6.52, and T3.37/S5.46). This belt is located between the binding site and what is thought to be the origin of intracellular helical motion. The relative orientations of these residues as well as residues in the binding site do not change much between the active and inactive structures in the homologous β2 adrenergic receptor.

However, a large movement of the side chain of F6.44 past I3.40 as well as the appearance of a large bulge at P5.50 are observed, all of which are located one helix turn toward the intracellular side of this proposed belt region[3]. We therefore propose that the residues examined play an important structural role in the activation process, specifically serving as a rigid structural unit that prevents dopamine from binding further toward the intracellular surface and translates agonist binding into the large intracellular helical movement of helices 5 and 6 that occur upon agonist binding.

Conservation in Other Receptors. While the residues in the transmembrane domain of GPCRs are highly conserved, it seems that the functional significance of many residues varies from receptor to receptor. Even within the same receptor family, such as D2R vs. D4R, aligning residues studied here do not always respond to functional probes in the same way. This is even more true for the less closely related M2 receptor. It appears that considerable caution is in order when making predictions about a GPCR based on structural or functional data from even a close relative of the receptor.

Conclusions

Using the D3R crystal structure as a model, we identified a conserved domain located between the agonist binding site and what is thought to be the origin of intracellular helical motion. Residues in this microdomain in the related D2R were examined using mutant cycle analysis and unnatural amino acid mutagenesis to determine whether putative interactions between residues side chains were functionally important. In this study, we demonstrate 7 functionally important noncovalent

interactions between residues on helices 3, 5, and 6. These interactions include aromatic-aromatic, sulfur-π, hydrogen bond, and long range interactions, which support the notion that this microdomain functions as a unit. We also show that the largest coupling coefficients are observed between residues on different helices, indicating an important region of helix connectivity.

References

1. Rosenbaum, D.M., Rasmussen, S.G., and Kobilka, B.K., The structure and function of G-protein-coupled receptors. *Nature*, **2009**. *459*(7245): p. 356-363.
2. Rasmussen, S.G., DeVree, B.T., Zou, Y., Kruse, A.C., Chung, K.Y., Kobilka, T.S., Thian, F.S., Chae, P.S., Pardon, E., Calinski, D., Mathiesen, J.M., Shah, S.T., Lyons, J.A., Caffrey, M., Gellman, S.H., Steyaert, J., Skiniotis, G., Weis, W.I., Sunahara, R.K., and Kobilka, B.K., Crystal structure of the beta2 adrenergic receptor-Gs protein complex. *Nature*, **2011**. *477*(7366): p. 549-555.
3. Rasmussen, S.G., Choi, H.J., Fung, J.J., Pardon, E., Casarosa, P., Chae, P.S., Devree, B.T., Rosenbaum, D.M., Thian, F.S., Kobilka, T.S., Schnapp, A., Konetzki, I., Sunahara, R.K., Gellman, S.H., Pautsch, A., Steyaert, J., Weis, W.I., and Kobilka, B.K., Structure of a nanobody-stabilized active state of the beta(2) adrenoceptor. *Nature*, **2011**. *469*(7329): p. 175-180.
4. Chien, E.Y., Liu, W., Zhao, Q., Katritch, V., Han, G.W., Hanson, M.A., Shi, L., Newman, A.H., Javitch, J.A., Cherezov, V., and Stevens, R.C., Structure of the human dopamine D3 receptor in complex with a D2/D3 selective antagonist. *Science*, **2010**. *330*(6007): p. 1091-1095.
5. Rosenbaum, D.M., Zhang, C., Lyons, J.A., Holl, R., Aragao, D., Arlow, D.H., Rasmussen, S.G.F., Choi, H.J., DeVree, B.T., Sunahara, R.K., Chae, P.S., Gellman, S.H., Dror, R.O., Shaw, D.E., Weis, W.I., Caffrey, M., Gmeiner, P., and Kobilka, B.K., Structure and function of an irreversible agonist-beta(2) adrenoceptor complex. *Nature*, **2011**. *469*(7329): p. 236-240.
6. Xu, F., Wu, H.X., Katritch, V., Han, G.W., Jacobson, K.A., Gao, Z.G., Cherezov, V., and Stevens, R.C., Structure of an Agonist-Bound Human A(2A) Adenosine Receptor. *Science*, **2011**. *332*(6027): p. 322-327.
7. Cho, W., Taylor, L.P., Mansour, A., and Akil, H., Hydrophobic Residues of the D-2 Dopamine-Receptor Are Important for Binding and Signal-Transduction. *Journal of Neurochemistry*, **1995**. *65*(5): p. 2105-2115.
8. Javitch, J.A., Ballesteros, J.A., Weinstein, H., and Chen, J.Y., A cluster of aromatic residues in the sixth membrane-spanning segment of the dopamine D2 receptor is accessible in the binding-site crevice. *Biochemistry*, **1998**. *37*(4): p. 998-1006.

9. Javitch, J.A., Fu, D.Y., Chen, J.Y., and Karlin, A., Mapping the Binding-Site Crevice of the Dopamine D2 Receptor by the Substituted-Cysteine Accessibility Method. *Neuron*, **1995**. *14*(4): p. 825-831.
10. Beene, D.L., Brandt, G.S., Zhong, W., Zacharias, N.M., Lester, H.A., and Dougherty, D.A., Cation-pi interactions in ligand recognition by serotonergic (5-HT3A) and nicotinic acetylcholine receptors: the anomalous binding properties of nicotine. *Biochemistry*, **2002**. *41*(32): p. 10262-10269.
11. Lummis, S.C.R., Beene, D.L., Harrison, N.J., Lester, H.A., and Dougherty, D.A., A cation-pi binding interaction with a tyrosine in the binding site of the GABA(C) receptor. *Chemistry & Biology*, **2005**. *12*(9): p. 993-997.
12. Zhong, W.G., Gallivan, J.P., Zhang, Y.O., Li, L.T., Lester, H.A., and Dougherty, D.A., From ab initio quantum mechanics to molecular neurobiology: A cation-pi binding site in the nicotinic receptor. *Proceedings of the National Academy of Sciences of the United States of America*, **1998**. *95*(21): p. 12088-12093.
13. Neve, K.A., Cox, B.A., Henningsen, R.A., Spanoyannis, A., and Neve, R.L., Pivotal Role for Aspartate-80 in the Regulation of Dopamine-D2 Receptor Affinity for Drugs and Inhibition of Adenylyl Cyclase. *Molecular Pharmacology*, **1991**. *39*(6): p. 733-739.
14. Kristiansen, K., Kroeze, W.K., Willins, D.L., Gelber, E.I., Savage, J.E., Glennon, R.A., and Roth, B.L., A highly conserved aspartic acid (Asp-155) anchors the terminal amine moiety of tryptamines and is involved in membrane targeting of the 5-HT2A serotonin receptor but does not participate in activation via a "salt-bridge disruption" mechanism. *Journal of Pharmacology and Experimental Therapeutics*, **2000**. *293*(3): p. 735-746.
15. Burley, S.K. and Petsko, G.A., Aromatic-aromatic interaction: a mechanism of protein structure stabilization. *Science*, **1985**. *229*(4708): p. 23-28.
16. Meyer, E.A., Castellano, R.K., and Diederich, F., Interactions with aromatic rings in chemical and biological recognition. *Angew Chem Int Ed Engl*, **2003**. *42*(11): p. 1210-1250.
17. Salonen, L.M., Ellermann, M., and Diederich, F., Aromatic rings in chemical and biological recognition: energetics and structures. *Angew Chem Int Ed Engl*, **2011**. *50*(21): p. 4808-4842.
18. Serrano, L., Bycroft, M., and Fersht, A.R., Aromatic-aromatic interactions and protein stability. Investigation by double-mutant cycles. *J Mol Biol*, **1991**. *218*(2): p. 465-475.
19. Anderson, D.E., Hurley, J.H., Nicholson, H., Baase, W.A., and Matthews, B.W., Hydrophobic core repacking and aromatic-aromatic interaction in the thermostable mutant of T4 lysozyme Ser 117-->Phe. *Protein Sci*, **1993**. *2*(8): p. 1285-1290.
20. Hong, H., Park, S., Jimenez, R.H., Rinehart, D., and Tamm, L.K., Role of aromatic side chains in the folding and thermodynamic stability of integral membrane proteins. *J Am Chem Soc*, **2007**. *129*(26): p. 8320-8327.
21. Kong, F.R. and King, J., Contributions of aromatic pairs to the folding and stability of long-lived human gamma D-crystallin. *Protein Science*, **2011**. *20*(3): p. 513-528.

22. Lanzarotti, E., Biekofsky, R.R., Estrin, D.A., Marti, M.A., and Turjanski, A.G., Aromatic-aromatic interactions in proteins: beyond the dimer. *J Chem Inf Model*, **2011**. *51*(7): p. 1623-1633.
23. Viguera, A.R. and Serrano, L., Side-Chain Interactions between Sulfur-Containing Amino-Acids and Phenylalanine in Alpha-Helices. *Biochemistry*, **1995**. *34*(27): p. 8771-8779.
24. Fersht, A.R., The Hydrogen-Bond in Molecular Recognition. *Trends in Biochemical Sciences*, **1987**. *12*(8): p. 301-304.
25. Albeck, S., Unger, R., and Schreiber, G., Evaluation of direct and cooperative contributions towards the strength of buried hydrogen bonds and salt bridges. *Journal of Molecular Biology*, **2000**. *298*(3): p. 503-520.
26. Gao, J.M., Bosco, D.A., Powers, E.T., and Kelly, J.W., Localized thermodynamic coupling between hydrogen bonding and microenvironment polarity substantially stabilizes proteins. *Nature Structural & Molecular Biology*, **2009**. *16*(7): p. 684-690.
27. Kao, C., Zheng, M., and Rudisser, S., A simple and efficient method to reduce nontemplated nucleotide addition at the 3 ' terminus of RNAs transcribed by T7 RNA polymerase. *Rna-a Publication of the Rna Society*, **1999**. *5*(9): p. 1268-1272.
28. Nowak, M.W., Gallivan, J.P., Silverman, S.K., Labarca, C.G., Dougherty, D.A., and Lester, H.A., In vivo incorporation of unnatural amino acids into ion channels in Xenopus oocyte expression system. *Ion Channels, Pt B*, **1998**. *293*: p. 504-529.
29. Torrice, M.M., Bower, K.S., Lester, H.A., and Dougherty, D.A., Probing the role of the cation-pi interaction in the binding sites of GPCRs using unnatural amino acids. *Proc Natl Acad Sci U S A*, **2009**. *106*(29): p. 11919-11924.
30. Kofuji, P., Davidson, N., and Lester, H.A., Evidence that neuronal G-protein-gated inwardly rectifying K+ channels are activated by G beta gamma subunits and function as heteromultimers. *Proc Natl Acad Sci U S A*, **1995**. *92*(14): p. 6542-6546.
31. Krapivinsky, G., Krapivinsky, L., Wickman, K., and Clapham, D.E., G beta gamma binds directly to the G protein-gated K+ channel, IKACh. *J Biol Chem*, **1995**. *270*(49): p. 29059-29062.
32. Mark, M.D. and Herlitze, S., G-protein mediated gating of inward-rectifier K+ channels. *Eur J Biochem*, **2000**. *267*(19): p. 5830-5836.
33. Kuzhikandathil, E.V., Westrich, L., Bakhos, S., and Pasuit, J., Identification and characterization of novel properties of the human D3 dopamine receptor. *Molecular and Cellular Neuroscience*, **2004**. *26*(1): p. 144-155.
34. Venkatachalan, S.P. and Czajkowski, C., A conserved salt bridge critical for GABA(A) receptor function and loop C dynamics. *Proceedings of the National Academy of Sciences of the United States of America*, **2008**. *105*(36): p. 13604-13609.
35. Price, K.L., Millen, K.S., and Lummis, S.C.R., Transducing agonist binding to channel gating involves different interactions in 5-HT3 and GABA(C) receptors. *Journal of Biological Chemistry*, **2007**. *282*(35): p. 25623-25630.
36. Gleitsman, K.R., Kedrowski, S.M.A., Lester, H.A., and Dougherty, D.A., An Intersubunit Hydrogen Bond in the Nicotinic Acetylcholine Receptor That

Contributes to Channel Gating. *Journal of Biological Chemistry*, **2008**. *283*(51): p. 35638-35643.

37. Blum, A.P., Lester, H.A., and Dougherty, D.A., Nicotinic pharmacophore: The pyridine N of nicotine and carbonyl of acetylcholine hydrogen bond across a subunit interface to a backbone NH. *Proceedings of the National Academy of Sciences of the United States of America*, **2010**. *107*(30): p. 13206-13211.
38. Kash, T.L., Jenkins, A., Kelley, J.C., Trudell, J.R., and Harrison, N.L., Coupling of agonist binding to channel gating in the GABA(A) receptor. *Nature*, **2003**. *421*(6920): p. 272-275.
39. Ma, J.C. and Dougherty, D.A., The cation-pi interaction. *Chemical Reviews*, **1997**. *97*(5): p. 1303-1324.
40. Dougherty, D.A., Cation-pi interactions in chemistry and biology: A new view of benzene, Phe, Tyr, and Trp. *Science*, **1996**. *271*(5246): p. 163-168.
41. Cozzi, F., Cinquini, M., Annuziata, R., and Siegel, J.S., Dominance of Polar/Pi over Charge-Transfer Effects in Stacked Phenyl Interactions. *Journal of the American Chemical Society*, **1993**. *115*(12): p. 5330-5331.
42. Steiner, T. and Koellner, G., Hydrogen bonds with pi-acceptors in proteins: Frequencies and role in stabilizing local 3D structures. *Journal of Molecular Biology*, **2001**. *305*(3): p. 535-557.
43. Levant, B., The D-3 dopamine receptor: Neurobiology and potential clinical relevance. *Pharmacological Reviews*, **1997**. *49*(3): p. 231-252.
44. Vantol, H.H.M., Bunzow, J.R., Guan, H.C., Sunahara, R.K., Seeman, P., Niznik, H.B., and Civelli, O., Cloning of the Gene for a Human Dopamine D4-Receptor with High-Affinity for the Antipsychotic Clozapine. *Nature*, **1991**. *350*(6319): p. 610-614.
45. Woll, M.G., Hadley, E.B., Mecozzi, S., and Gellman, S.H., Stabilizing and destabilizing effects of phenylalanine -> F-5-phenylalanine mutations on the folding of a small protein. *Journal of the American Chemical Society*, **2006**. *128*(50): p. 15932-15933.
46. Zheng, H., Comeforo, K., and Gao, J.M., Expanding the Fluorous Arsenal: Tetrafluorinated Phenylalanines for Protein Design. *Journal of the American Chemical Society*, **2009**. *131*(1): p. 18-19.
47. Pal, D. and Chakrabarti, P., Non-hydrogen bond interactions involving the methionine sulfur atom. *Journal of Biomolecular Structure & Dynamics*, **2001**. *19*(1): p. 115-128.
48. Samanta, U., Pal, D., and Chakrabarti, P., Environment of tryptophan side chains in proteins. *Proteins-Structure Function and Genetics*, **2000**. *38*(3): p. 288-300.
49. Tauer, T.P., Derrick, M.E., and Sherrill, C.D., Estimates of the ab initio limit for sulfur-pi interactions: The H2S-benzene dimer. *Journal of Physical Chemistry A*, **2005**. *109*(1): p. 191-196.
50. Biswal, H.S. and Wategaonkar, S., Sulfur, Not Too Far Behind O, N, and C: SH center dot center dot center dot pi Hydrogen Bond. *Journal of Physical Chemistry A*, **2009**. *113*(46): p. 12774-12782.

Chapter 3

Optimization of DNA and *in vitro* transcribed tRNA cotransfection into mammalian cells for the expression of unnatural amino acids*

*Work done in collaboration with Nyssa Puskar

Abstract

Unnatural amino acid incorporation into proteins in mammalian cells would allow for a versatile way to subtly perturb and study mammalian proteins and signaling cascades in an endogenous environment. Unfortunately, the methodology used by this lab has not been applied to mammalian cells in a manner that rivals the robust signals observed through electrophysiology of ion channels heterologously expressed in *Xenopus laevis* oocytes. We therefore seek to improve transfection conditions in HEK293T cells to enhance protein expression using an *in vitro* transcribed and acylated tRNA as assayed with a membrane sensitive dye and the FlexStation3. Here, we describe optimized cotransfection conditions for *in vitro* transcribed tRNA and plasmid DNA. Both double transfection using the Neon electroporation system and single transfection with TransIT gave robust functional responses to agonist application for wild type and mutant proteins. Using these transfection methods we were able to observe functional expression of receptors containing a serine residue delivered from an *in vitro* transcribed human amber serine suppressor tRNA, indicating effective transfection of both tRNA and DNA. Experiments using *in vitro* transcribed and acylated tRNA did not result in functional responses, indicating further optimization is required for effective delivery of this stoichiometric reagent.

Introduction

Nonsense suppression with unnatural amino acids has been well established as a powerful tool to study the structural and functional properties of proteins. Unnatural amino acid mutagenesis enables the site-specific introduction of nearly any chemically synthesized amino acid that can pass through the ribosome. This allows for the introduction of much more subtle perturbations or novel functionalities not available in the 20 conventional amino acids. For example, fluorinated aromatic amino acids can be used to identify electrostatic interactions with the face of the aromatic side chain[1,2], proline analogs to measure *cis-trans* preference[3], or α-hydroxy amino acids to examine hydrogen bond interactions with the backbone carbonyl or amine[4].

Two major methods have been developed for the efficient incorporation of unnatural amino acids into proteins in a variety of cellular expression systems: *in vitro* tRNA synthesis/acylation[5,6] and engineering of an orthogonal tRNA/synthetase pair[7]. Both methods have their benefits and drawbacks, and are therefore used for different purposes. The orthogonal tRNA/synthetase pair method has been effectively used to incorporate amino acids into a variety of expression systems with the ability to synthesize higher amounts of protein[7-10], however the amino acid side chains that can be incorporated are limited by the evolution of a new synthetase for each novel side chain. As such, only a small subset of unnatural amino acids can be incorporated by this method. Some permissive synthetases have been developed that allow incorporation of a variety of structurally similar unnatural amino acids, for example the *p*CNF-RS, which enables incorporation of 18 phenylalanine derivatives[11], however this still represents a small amount of possible side chains. Conversely, the *in vitro* transcription/acylation of

tRNA allows the efficient incorporation of a wide variety of unnatural amino acids, limited only by synthetic ability and recognition by the ribosome. While this method is more versatile for side chain functionality, it is limited by both low protein synthesis yield and the expression system that can be used (*Xenopus laevis* oocytes).

The ability to functionally express unnatural amino acid-containing proteins in mammalian cells is an important goal because it would allow the study of mammalian proteins in a biologically relevant environment and enable the introduction of subtle perturbations into complete endogenous signaling networks. Despite the successes of the orthogonal synthetase/tRNA system to incorporate unnatural amino acids into mammalian cells[9], protein expression with transiently transfected *in vitro* transcribed/acylated tRNA has had limited success. Successful incorporation of an amino acid using an *in vitro* transcribed/acylated tRNA has been demonstrated using microelectroporation of CHO cells and cultured neurons[12] and chemical transfection (Effectene) of COS1 cells[13]. Using microelectroporation, only a small number of cells are transfected, which limits the detection methods that can be used. The chemical transfection method allowed detection of enzymatic activity in cell lysates, however only the wild type amino acid was introduced as a proof-of principle experiment. These examples show that transfection of *in vitro* transcribed/acylated tRNA in mammalian cells is feasible, however much work remains to enhance the robustness and versatility of this suppression methodology.

We therefore sought to further develop the suppression methodology to give higher protein expression in mammalian cells for easy detection in a 96-well plate format. Here we attempt to improve the efficiency of tRNA delivery to the intracellular

translation machinery using a variety of transfection reagents and conditions. Our ultimate goal is to functionally express ion channels in a mammalian cell line that have an unnatural amino acid incorporated using nonsense suppression with an *in vitro* transcribed and acylated tRNA.

Methods

Molecular Biology. The human 5-HT_{3A} receptor in the pcDNA3.1+ vector was purchased from Missouri S&T cDNA research center and was subcloned into the pGEMhe vector for mRNA transcription. The mouse α4, α4-GFP, and β2 genes were in the pciNEO vector and the mouse β4 gene was in the pcDNA3.1+ vector. These constructs were obtained from the Lester group. The mouse α1, β1, γ, δ subunits were in the pAMV vector and the human α7 and Ric3 genes were in the pcDNA3.1+ vector. The EGFP constructs used were discussed by Monahan et al.[12].

Amber (TAG) or Frameshift (GGGT) mutations were introduced at the site of interest using the QuickChange protocol (Stratagene). To make mRNA, the cDNA was linearized using the appropriate restriction enzyme (NheI for pcDNA3.1+ and NotI for pAMV). mRNA was transcribed from the linearized plasmids by using the T7 mMessage Machine kit (Ambion).

cDNA encoding the THG73, YFaFS, and HSAS tRNAs were in the pUC19 vector and have been described previously[12,14,15]. 74mer THG73 and YFaFS tRNAs were synthesized from a DNA oligonucleotide template containing two 5' methoxy (C2' position) nucleotides to truncate transcription using Ambion's T7 MEGAshortscript kit[16]. Commercially available amino acids chemically appended to dCA were ligated to the end

of the 74mer tRNA using methods previously described[17]. Acylation of tRNA was confirmed using MALDI mass spectrometry using a 3-hydroxypicolinic acid matrix. The NVOC protecting group on the amino acid was removed through a 5-minute irradiation using a 1 kW Xenon lamp with WG-335 and UG-11 filters. 74mer HSAS tRNA was synthesized by linearizing the pUC19 vector with FokI and transcribing as above with the MEGAshortscript kit (Ambion).

Cell Culture Technique. HEK293T cells were purchased from ATCC. Cells were grown using DMEM:F12 (1:1) media with GlutaMAX-I (Gibco), 10% heat-inactivated fetal bovine serum (FBS) (Sigma), and penicillin/streptomycin (Sigma) at 37 ^{o}C and 5% CO_2 in a humidified atmosphere. Cells were passaged before confluency reached 90% and were discarded after ~35 passages. Passaging and harvesting cells from 100 mm dishes was performed by removing the liquid media above the cells, washing with 5 mL of PBS, and applying 1 mL of TrypLE (Gibco) and incubating at 37^{o}C for 5 minutes to detach the cells from the plate. To inactivate the TrypLE, 9 mL of fresh media was applied and the cells were mixed by pipetting until homogeneous. Cells were counted using a hemocytometer before seeding to ensure reproducible transfections.

Conditions were optimized for cell seeding on 100 mm (Table 3.1) and 35 mm (Table 3.2) dishes so that the desired confluency would be obtained on the day of transfection. Optimal confluency and size of dish varied for the different transfection protocols. Our table should therefore serve as a guide for obtaining the correct confluency for the transfections described below, and for additional kits that are

developed in the future. Most kits generally required a confluency of 70-90% so those seeding conditions are highlighted in the tables below.

In all cases, approximately 5 x 10^4 cells were plated post-transfection per well in a 96-well plate. Poly-D-Lysine treated black 96-well plates with flat clear bottoms (BD

Table 3.1: Optimization of HEK293T cell seeding for 100 mm dishes

Dilution	Dilution Shorthand	24 hr	36 hr	48 hr	72 hr
10 million cells/dish	1:1	80%	N/A	N/A	N/A
7.5 million cells/dish	1:1.5	70%	-	100%	N/A
5 million cells/dish	1:2	70%	90%	N/A	N/A
3.3 million cells/dish	1:3	25-30%	-	60%	80-90%
2.5 million cells/dish	1:4	20-30%	-	50%	80-90%
2 million cells/dish	1:5	30%	-	70%	90%
1 million cells/dish	1:10	15%	-	30%	70%

Table 3.2: Optimization of HEK293T cell seeding for 35 mm dishes

Dilution	24 hr	48 hr	72 hr
100,000 cells/dish	5%	10%	40%
200,000 cells/dish	10%	20%	50%
300,000 cells/dish	15%	25%	70%
400,000 cells/dish	25%	30%	70%
500,000 cells/dish	35%	50%	100%
600,000 cells/dish	30%	70%	N/A
700,000 cells/dish	30%	80%	N/A
800,000 cells/dish	40%	90%	N/A
900,000 cells/dish	50%	100%	N/A
1,000,000 cells/dish	60%	100%	N/A
1,500,000 cells/dish	70-100%	N/A	N/A

Falcon) were used for optimal spectroscopic results. Transfected cells were grown on the 96-well plate for 24-48 hours before recording on the FlexStation3.

Counting Cells with a Hemocytometer. To achieve a desired confluency for transfection, cells were counted using a hemocytometer and the appropriate amount of cells were seeded 1-3 days in advance. A hemocytometer is a thick glass microscope slide with an indent on two sides that creates a chamber for the cells to be counted. A thin cover slide is placed over this section to ensure the volume of the cells remains constant for each counting. The flat area in this chamber contains an etched grid with nine 1 mm x 1 mm counting squares (Figure 3.1) that each have a volume of 100 nL at a coverslip height of 0.1 mm.

To determine the amount of cells in a 100 mm cell culture dish, the growth media is removed from the dish and the adhered cells are washed with 5 mL PBS and

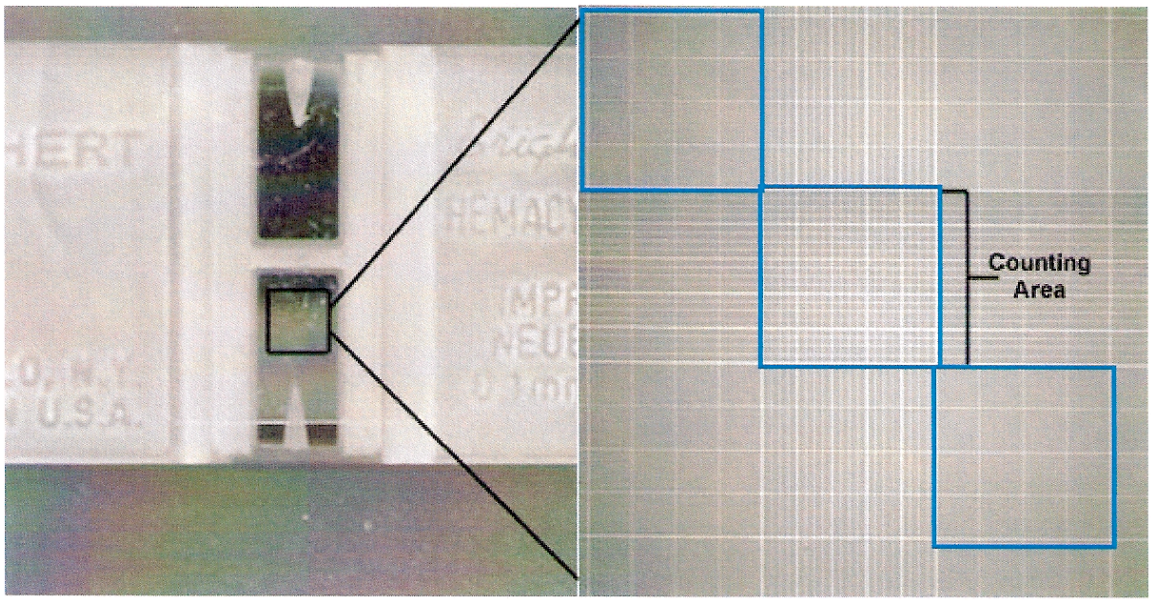

Figure 3.1: Hemocytometer

dissociated using 1 mL of TrypLE. To inactivate the TrypLE, 9 mL of growth media is added and the cells are resuspended until homogenous. From this cell solution, 10 uL are pipetted into the space created by the indent of the hemocytometer and the glass cover slip. The number of cells in each of three non-contiguous 1 mm x 1 mm squares in the homocytometer grid are then manually counted under a microscope and averaged together to determine the concentration of cells in the original mixture.

$$\left[\text{Conc. of cells } \left(\frac{\text{Cells}}{\text{mL}}\right)\right] = \left(\frac{\text{Average \# cells counted}}{0.1\ \text{mm}^3\ (100\ \text{nL})}\right)\left(\frac{10^6\ \text{nL}}{\text{mL}}\right) = \text{Avg. \# cells x } 10^4/\text{mL}$$

To plate 1,000,000 cells: $1{,}000{,}000\ \text{cells}\left(\frac{\text{mL}}{\text{Avg \# cells x } 10^4}\right)$ = mL of cells to seed plate

Transfections. A variety of transfections using different commercially available transfection reagents were performed to determine the conditions for optimal expression of DNA or mRNA and *in vitro* transcribed tRNA. Our optimized protocols are described below with some notes and their optimization data and relative efficiencies are further discussed in the results and discussion section.

PEI. Polyethylenimine (PEI) (Sigma-Aldrich) is a poly-cationic polymer that interacts with the negative charge of nucleic acids. During transfection, the net-positive complex interacts with negatively charged residues on the cell surface and allows the complex to pass across cell membranes through endocytosis. This method can be extremely cytotoxic and therefore low concentrations of PEI are used during transfection.

HEK293T cells were transfected with PEI in both 100 mm and 35 mm dishes. Transfections in 100 mm dishes were suitable for plating an entire 96-well plate while

transfections in 35 mm dishes were used for plating 3 columns in a 96-well plate. Transfections in 100 mm dishes were performed by adding 10 μg of DNA and 30 μL of a 1 mg/mL solution of PEI (prepared by dissolving PEI in acidified water and bringing to a final pH of 7.0 with NaOH) to 1 mL of DMEM:F12 media. The DNA/PEI mixture was then added to ~70% confluent plates with 9 mL of fresh DMEM:F12 + GlutaMax-I, FBS, and penicillin/streptomycin. After 24 hours, the media with the transfection reagent was removed and the cells were washed with 5 mL of PBS. The transfected cells were treated with 1 mL of TrypLE to detach the cells from the plate and incubated at 37^{o}C for 5 minutes. The cells were then resuspended in 9 mL of fresh media, transferred to a V-shaped plastic basin, and 100 μL of transfected cells were plated per well of the 96-well plate.

Transfections in a 35 mm dish were performed by adding 1.5 μL DNA and 9 μL of a 1 mg/mL solution of PEI to 0.3 mL of media. The DNA/PEI mixture was then added to the cell dish containing 2.7 mL of fresh media. After 24 hours the media with the transfection reagent was removed and the cells were washed with 3 mL of PBS. The transfected cells were treated with 0.3 mL of TrypLE and incubated at 37^{o}C for 5 minutes. The cells were then resuspended in 2.4 mL of fresh media and transferred to a V-shaped plastic basin. 100 μL of transfected cells were plated per well of the 96-well plate.

The PBS wash, TrypLE treatment, resuspension and plating steps were used for all transfections, regardless of the reagent used, to plate transfected cells. I will simply refer to it as plating in future sections. Additionally, fresh media will refer to

DMEM:F12 (1:1) + Glutamax-I, FBS, and penicillin/streptomycin unless otherwise specified.

ExpressFect. ExpressFect (Denville Scientific), formerly known as Hyfect, is also a poly-cationic transfection reagent that acts similarly to PEI. Denville Scientific claims that it shows increased transfection efficiency relative to other available transfection reagents and that it shows enhanced stability and resistance to serum (FBS) present in media. ExpressFect is also less cytotoxic than PEI. This reagent is sold in liquid form at a concentration of 5 mg/mL and is significantly more expensive than PEI.

ExpressFect transfections were performed on 35 mm dishes. A polymer solution and a DNA solution are made independently and combined before adding the complexes to the cells. The DNA solution contained 1-2 μg of DNA and 100 μL of DMEM:F12 (no FBS/antibiotics) and the polymer solution contained 4 μL of ExpressFect and 100 μL of DMEM:F12 (no FBS/antibiotics). The polymer solution was then added to the DNA solution and the mixture was incubated for 20 minutes at room temperature. During this time the media was changed with 1 mL of fresh media added to the 35 mm dish. The transfection mix was then added to the media over the cells (60-80% confluent) and the transfecting cells were incubated for 4 hours at 37^{o}C 5% CO_2. After 4 hours the cells were plated and incubated for 48 hours before recording on the FlexStation3. No severe cytotoxic effects were observed if the transfection reagents were left on the cells for 24 hours, and in some cases increased expression was observed.

***Trans*IT-mRNA.** *Trans*IT (Mirus Bio) is a broad spectrum, low toxicity transfection reagent. It is a non-liposomal reagent that is made up of a lipid/poly-cation mixture. The transfection reagent is supplied along with a "Boost Reagent" that is a proprietary compound solution required for successful transfection. Other transfection reagents in the *Trans*IT product line are available that are better suited for DNA or difficult to transfect cell lines. Our interest was to co-transfect plasmid DNA with *in vitro* transcribed and acylated tRNA. Because the tRNA is the limiting reagent and would likely prove more difficult to transfect than DNA, which formulations were originally optimized for, we chose the mRNA-optimized product. Other reagents in the *Trans*IT product line may be more successful, however they were not examined in this study. Many ratios of Boost:*Trans*IT and varied DNA and tRNA amounts were tested. Our optimized protocol for S61TAG 5-HT_{3A} expression when using HSAS is reported below. The optimization data are discussed in the results/discussion section later.

All *Trans*IT transfections were performed in 35 mm dishes. First, 2 μg of DNA was added to 250 μL of DMEM:F12 (no FBS or antibiotics). Then 3.75 μL of Boost Reagent was added to this mixture followed by 7.5 μL of *Trans*IT. The final mixture was incubated 2-5 minutes at room temperature while complex formation occurred. During the incubation step the media on the cells was changed and 2.5 mL of fresh media was added to the cells (60-90% confluent). The complexes were then added directly to the media and cells were incubated in the mammalian incubator for 24 hours. After 24 hours the cells were harvested and plated in 96-well plates and allowed to incubate for an additional 24 hours. In some cases we saw increased expression when a "double transfection" was performed. For a double transfection, after 24 hours instead of

harvesting and plating the cells, a fresh batch of transfection reagent and DNA and/or tRNA was added to fresh media. This second transfection was incubated in the mammalian incubator for 12 hours and then the cells were harvested and plated. Recording was still performed after 48 hours. In some cases, after the first transfection many of the cells on the edge of the 35 mm dish flaked off when removing the media, presumably due to cell death or poor cell health. In this case a PBS wash step was skipped.

TransMessenger. TransMessenger (Qiagen) is designed for transfection of cell lines with RNA. It is a lipid-based transfection reagent that is sold with an RNA-condensing enhancer and buffer optimized for transfection efficiency. This transfection method works by condensing the RNA and then coating it with the lipid-based transfection reagent. Suppression of S61TAG 5-HT_{3A} with HSAS was not very successful using this transfection reagent. Therefore, our optimized protocol described below includes the entire range of DNA and tRNA that was capable of eliciting any 5-HT response. The optimization of DNA and DNA+tRNA expression is described in the results and discussion section.

For transfection, 4 μL of Enhancer R and 0.5-2 μL of DNA + 2-4 μL of HSAS was diluted to a final volume of 100 μL with buffer EC-R. This mixture was incubated at room temperature for 5 minutes and then 8 μL of TransMessenger was added. The final mixture was incubated for an additional 10 minutes. After 10 minutes the media over the cells was removed and the cells were washed with PBS. Finally, 900 μL of DMEM:F12 (no FBS or antbiotics) was added to the transfection mixture and the total 1 mL of media

and transfection complexes were added directly to the cells (80-90% confluent). Cells were incubated with the transfection complexes for 3 hours after which they were washed with PBS and plated in a 96-well plate

Lipofectamine RNAiMAX. Lipofectamine RNAiMAX (Life Technologies) is a lipid-based transfection reagent optimized for transfection of cells with siRNA. Lipofectamine reagents function by forming liposomes, which are capable of delivering nucleic acids through lipofection. siRNA are small 20-25 nucleotide RNA primers, which we thought would more closely relate to tRNA (75-85 nucleotides) than reagents optimized for full length mRNA or DNA. Life Technologies sells other lipofectamine-based reagents optimized for DNA and difficult to transfect cell lines. No expression of S61TAG 5-HT_{3A} was observed when suppressed with HSAS. We therefore report the optimized procedure for transfection of DNA alone, recognizing that transfection of DNA is probably better suited for a different lipofectamine reagent that is optimized for DNA transfection.

RNAiMAX transfections were performed directly in the 96-well plate to be read using suspended cells harvested from 35 mm dishes. We did not try transfecting cells in the 35 mm dish as we had in the other transfection methods and suspect that would have provided better results. For the 96-well plate transfection, our best signal was achieved by mixing 2 μg of DNA in 600 μL of DMEM:F12 (no FBS or antibiotics) and aliquoting 25 μL of this mixture into each well in 3 columns (24 wells) of a 96-well plate. Then 0.3 μL of RNAiMAX was added per well and the final mixture was incubated for 10 minutes. During the 10-minute incubation period, cells from a 35 mm dish were

harvested (30-50% confluent) and resuspended in 6.5 mL of fresh media. After the 10-minute incubation step was complete, 100 μL of suspended cells were aliquoted into each well. Plates were read after 48 hours.

Mixing the RNAiMAX with the DNA/media mixture before aliquoting into the wells likely would have improved results. This would lead to more uniformity of RNAiMAX per well because of the error associated with pipetting such a small volume (0.3 μL), also fewer pipet tips would be used. Performing these transfections directly on adherent cells in the 35 mm dish also would have likely produced better results due to the better transfection efficiency of adherent cells versus suspended cells. These possibilities were not tested due to better results with other transfection reagents.

PolyFect. PolyFect (Qiagen) is an activated dendrimer system optimized for transfection of DNA into easy to transfect cell lines (HEK293, CHO, HeLa, and COS). The dendrimers are spherical shaped and have positively charged amino groups at the end of the branches. These positive charges interact with the negatively charged nucleic acids and compact the DNA, therefore allowing the complexes to pass across the membrane through endocytosis. None of the methods tested gave good expression of mouse muscle (β9'), therefore an optimized protocol is not reported here.

Neon. The Neon (Life Technologies) is an electroporation device that is designed to transfect all cell types by electrically creating small holes in the cell membrane and allowing the passage of nucleic acids across the membrane. We were inspired to try this method because of Sarah Monahan's success with microelectroporation of CHO cells[12],

and because all of the chemical transfection reagents used failed to result in expression of receptors that incorporated *in vitro* transcribed and acylated tRNAs.

For transfections to fill one 96-well plate, two 100 mm dishes of cells (60-90% confluent) were treated with 1 mL of TrypLE each and then resuspended in a total volume of 10 mL of DMEM:F12 (no FBS or antibiotics). The cells were added to a 15 mL Falcon tube and centrifuged for 5 minutes on setting 2 (slow) on the Lester lab centrifuge (in their cell culture room). The media was removed, 5 mL of PBS was added to the cells, and the cells were centrifuged for an additional 5 minutes. The PBS was then removed and the cells were resuspended in 50 μL of Buffer R (supplied with the Neon transfection kits).

Before transfection, 2.7 mL of fresh media was aliquoted into each of four V-shaped plastic basins. A clear plastic pipet stage was placed into the transfection system and was filled with 3 mL of electrolytic buffer, E buffer. 20 μL of resuspended cells were aliquoted into four 0.6 mL Eppendorf tubes and the DNA/tRNA mixture to be transfected for 3 columns in the 96-well plate was added to the cells. Our best results used 2 μg of DNA and 4 μg of HSAS for WT recovery and 8 μg for suppression at a sensitive site. It is important to dissolve tRNA in water instead of the 1 mM NaOAc normally used after ligations because of the effect it can have on the salt concentration of the transfection mixture. A salt concentration that is too high can cause arcing of the cells during transfection, which results in cell death.

Once the mixture of cells, DNA, and tRNA is created, 10 μL of cell mixture is pipetted into the transfection pipet using the gold tips provided in the Neon transfection kit. Note: 100 μL kits are available for larger scale transfections. It is important to avoid

any air bubbles in the pipet tip because of the potential for arcing. Once 10 μL are successfully pipetted, the tip is placed in the transfection system and the desired protocol is selected. We found that condition 7 (1200 V, 30 ms, 1 pulse) worked best for DNA and DNA+tRNA. In some cases a second transfection of tRNA only, was performed after 24 hours using condition 22 (1400 V, 10 ms, 3 pulses). After transfection the 10 μL of transfected cells were added to the media in the V-shaped basin. Another transfection using a second 10 μL of cells and nucleic acid mixture was performed using the same tip. In cases of a large volume of DNA and tRNA, a third transfection was performed using the remainder of the cell/nucleic acid mixture only if a full 10 μL of mixture remained. According to the manufacturer each tip can be used 3 times before it needs to be discarded, however we did not test whether the tips could be used more. New tips were always used for different mixtures of DNA/tRNA. After the transfections were complete, the cells were resuspended in the fresh media and 100 μL were plated into each well. The plates were read after 48 hours.

The optimal conditions were obtained by performing one 10 μL transfection for each of the 24 stock settings programed into the Neon. Each transfection was plated in one column on a 96-well plate resulting in two 96-well plates to read. This required 4 100 mm dishes of cells to transfect and the cells to be resuspended in a larger volume of Buffer R (240 μL). Plates were read after 48 hours and the columns with the largest RFU values were used for future experiments. Optimization experiments were performed for WT 5-HT_{3A} DNA only, S61TAG 5-HT_{3A} DNA + 74mer HSAS, and a second "double" transfection after 24 hours with 74mer HSAS only. These data can be found in the results and discussion section.

FlexStation3 recording of ion channels. The FlexStation3 (Molecular Devices) was used for all 96-well plate-based ion channel detection. To measure receptor function, HEK293T cells were transfected using one of the above described transfection methods. After a 48 hour incubation period the media above the cells was removed and the cells were washed with Flex Buffer (115 mM NaCl, 1 mM KCl, 1 mM $CaCl_2$, 1 mM $MgCl_2$, 10 mM D-glucose, and 10 mM HEPES at pH 7.5)[18]. The cells were then incubated with 100 μL/well of a 1:10 dilution (unless otherwise specified) of FLIPR Membrane Potential Assay Kit (blue) for 30 minutes at 37°C and 5% CO_2 and read using the FlexStation3. Wells were excited at 530 nm and fluorescence was recorded at 565 nm using a 550 nm filter at low photomultiplier tube (PMT) sensitivity after application of 100 μL of agonist to the wells. Fluorescence data were collected every 1.52 seconds for 180 seconds and data were analyzed using the SOFTmax Pro software (Molecular Devices) (Figure 3.2). The peak values for each well in a column of the 96-well plate were normalized to the maximum value and data were fit to the Hill equation to obtain the EC_{50} and Hill coefficient (n_H). The values from a minimum of 3 columns were averaged together to result in an EC_{50} curve with each column representing one n for statistical analysis.

Fluorescent dye experiments. Serial dilutions (1:1) of rhodamine B (Sigma) were made in a 96-well plate using water starting from a stock solution of 50 mM. The plate was assayed for peak fluorescence using the FlexStation3 by exciting the fluorophore at a wavelength of 540 nm and measuring the emission at 625 nm with a 610 nm cutoff filter. This experiment was performed using the low, medium, and high PMT settings. Similar

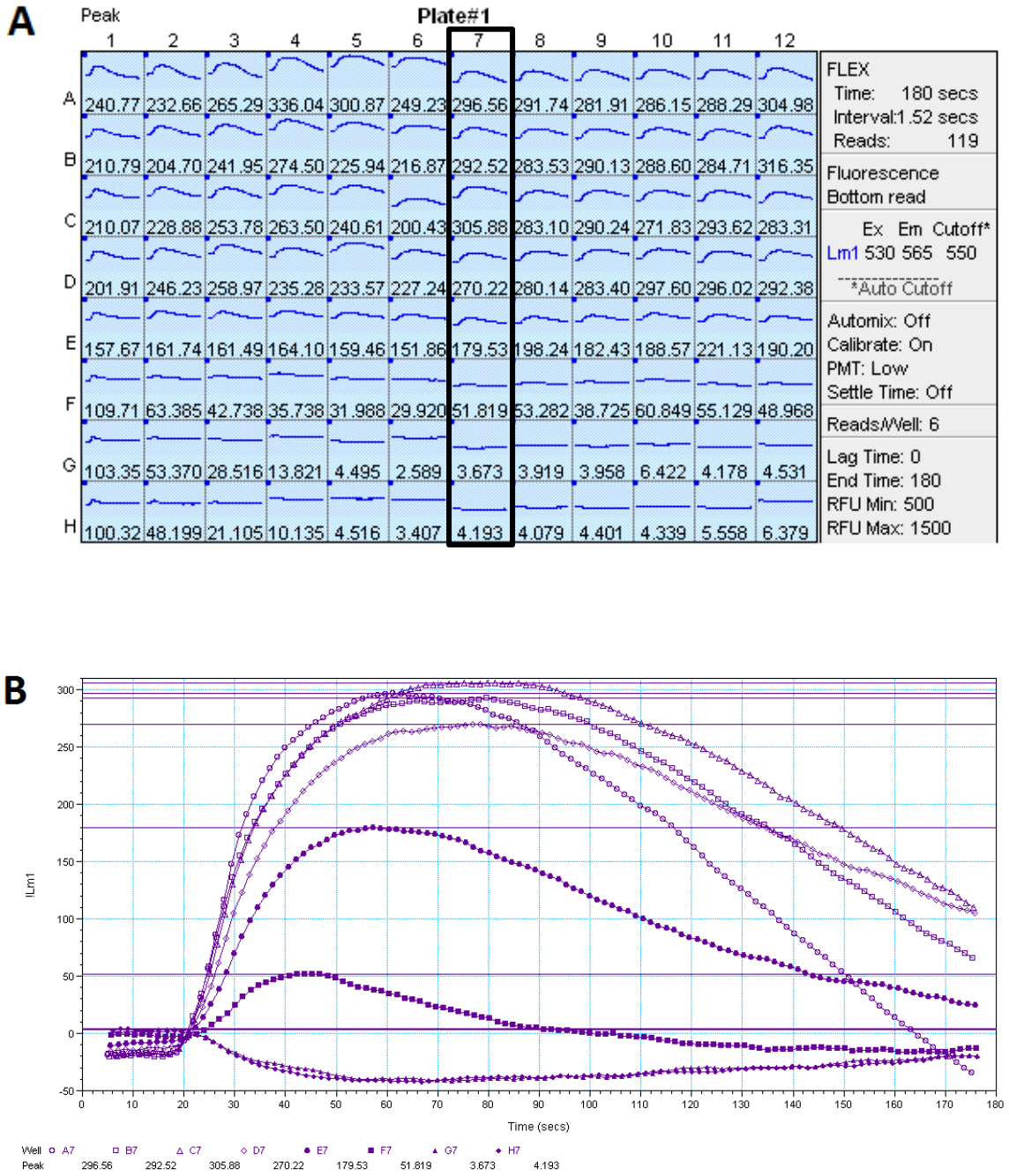

Figure 3.2: Typical FlexStation3 raw data for the 5-HT_{3A} receptor. **A)** 96-well plate of cells transfected with DNA. Wells were treated with 1:1 serial dilutions of agonist with decreasing concentration from row A-H. Peak RFUs are shown under the traces. **B)** Compiled fluorescence traces over time of the 8 wells in a single column (Column 7 from **A**) of the 96-well plate. The 8 wells represent responses to agonist concentrations that span the EC_{50} curve.

experiments were performed using eosin Y (City Chemical Company) and fluorescein (Sigma) using the low PMT setting.

Results and Discussion

Fluorescent dye experiments. While the SOFTmax Pro software will select the optimal PMT sensitivity for a variety of experiments, runs using the "Flex" tab in the instrument settings require the user to select between the high, medium, or low PMT sensitivity. When performing nonsense suppression in *Xenopus laevis* oocytes it is common to obtain a significantly weaker signal than when examining the wild type or mutant receptors created using conventional mutagenesis. Therefore, to obtain maximal responses for the unnatural amino acid mutagenesis experiments in HEK293T cells, it is important to optimize signal detection of the instrument to measure low changes in fluorescence.

To determine which PMT setting was optimal for our FlexStation3 experiments, we tested the response of the instrument over a range of small molecule fluorophore concentrations, from 6 nM to 50 mM of rhodamine B, eosin Y, and fluorescein. We found that when measuring moderate to large fluorophore concentrations, the PMT became saturated using both the high and medium sensitivity settings and reliable data could not be obtained. When using the high PMT sensitivity setting, the detector became saturated at 1.52 μM rhodamine B, which corresponded to a maximum instrument response of 300 relative fluorescence units (RFUs). The medium sensitivity setting allowed measurement of up to 49 μM rhodamine B and reached a maximum response before saturation of 6,500 RFUs. Decreasing the PMT sensitivity to low allowed measurement of up to 0.19 mM rhodamine B (10,000 RFUs) where self-quenching of the

fluorophore began to be observed. High concentrations of eosin y and fluorescein, which do not self-quench as strongly as rhodamine B, indicate that the instrument is capable of detecting fluorescence signals as high as 50,000 RFUs, well beyond the range of fluorescence expected in our membrane potential dye experiments (~500-5,000 RFUs).

In addition to testing the instrument at high fluorophore concentrations, we also measured the instrument response at very low concentrations. To determine the optimum

Table 3.3: Fluorescence read-out of rhodamine B solutions using the three PMT sensitivities: low, medium, and high.

Rhodamine B Concentration (μM)	Low PMT Setting	Medium PMT Setting	High PMT Setting
0.763	191.47	144.91	124.55
0.381	77.67	65.71	47.34
0.191	44.83	27.18	22.21
0.095	20.88	16.13	12.56
0.048	17.04	8.56	6.44
0.024	10.07	5.52	4.34
0.012	7.88	4.64	2.89
0.006	5.87	3.42	2.25

sensitivity setting for low fluorescence read-out, we assayed a 96 well plate with low concentrations of rhodamine B (< 1 μM) using the high, medium, and low PMT sensitivity settings (Table 3.3). The data from these experiments indicate that the low PMT setting provides the highest fluorescence read-out for low concentrations of fluorophore, and that this setting is optimal for both measuring high (detector saturation) and low (detector sensitivity) fluorescence. No advantage for using the medium or high

PMT setting was determined, therefore all experiments were performed using the low PMT sensitivity setting.

Optimization of mRNA transfections. For *X. laevis* oocyte experiments, receptor expression at the membrane is achieved through microinjection of receptor mRNA. To determine if transfection with mRNA would give larger responses than DNA in HEK293T cells, we examined the expression of three receptors, muscle type (β9'), α7 (with or without RIC3), and 5-HT_{3A} using the mRNA transfection kit, TransMessenger. Cells transfected with receptor mRNA showed an increase in fluorescence upon application of acetylcholine (ACh) to the muscle type receptor. The EC_{50} and Hill coefficient values measured by the FlexStation are similar to what are observed in *X. laevis* oocytes using the OpusXpress (Figure 3.3), however the responses were small (< 100 RFUs) and many data points had to be discarded to get a good fit. No fluorescence was observed in response to application of ACh to the α7 receptor or 5-hydroxytryptamine (5-HT) to the 5-HT_{3A} receptor. While *in vitro* poly-adenylation would likely improve mRNA stability and therefore receptor expression, producing mRNA is significantly more expensive than DNA and larger responses are elicited from DNA transfection experiments. This is especially true because the cell line we have chosen to use, HEK293T cells, is designed to amplify transfected plasmid DNA, which gives DNA transfection an additional benefit.

Optimization of DNA transfections – wild type. Before experiments with unnatural amino acids were attempted, we first sought to optimize transfection and incubation

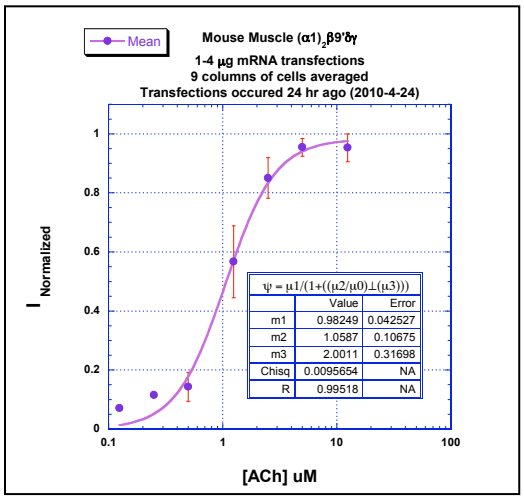

Figure 3.3: Data from TransMessenger transfection of the muscle type nAChR mRNA using the FlexStation fit to the Hill equation.

conditions for cells transfected with wild type DNA alone. We tested a variety of conditions using seven different commercially available transfection methods: PEI (Sigma-Aldrich), ExpressFect (Denville Scientific), *Trans*IT (Mirus Bio), RNAiMAX (Life Technologies) TransMessenger (Qiagen), Polyfect (Qiagen), and Neon (Life Technologies). We primarily focused on the 5-HT_{3A} receptor, because it is not known to have difficulties being transported from the endoplasmic reticulum to the membrane and because it has five identical subunits, which removes complications of stoichiometry changes. Some experiments however were performed using other Cys-loop receptors including the muscle type ($\alpha1_2\beta1\delta\gamma$) and neuronal α4β4, α4β2, and α7 nicotinic acetylcholine receptors (nAChRs). These experiments will be discussed first.

HEK293T cells transfected with α4β2, muscle type, and α7 nAChR DNA using PEI and ExpressFect resulted in no increase in fluorescence in response to application of ACh. It has been shown previously that the α4β2 nAChR is retained in the ER due to the lack of an ER export motif and the presence of an ER retention motif in the M3-M4 loop

region of the β2 receptor[19]. To test whether this was the case in our experiments we transfected cells with a 1:1 ratio of α4-GFP and either β2 or β4 (not retained in the ER). The expression pattern of the two receptors was visualized using confocal microscopy of the tagged green fluorescent protein (GFP) subunits (Figure 3.4). The images obtained

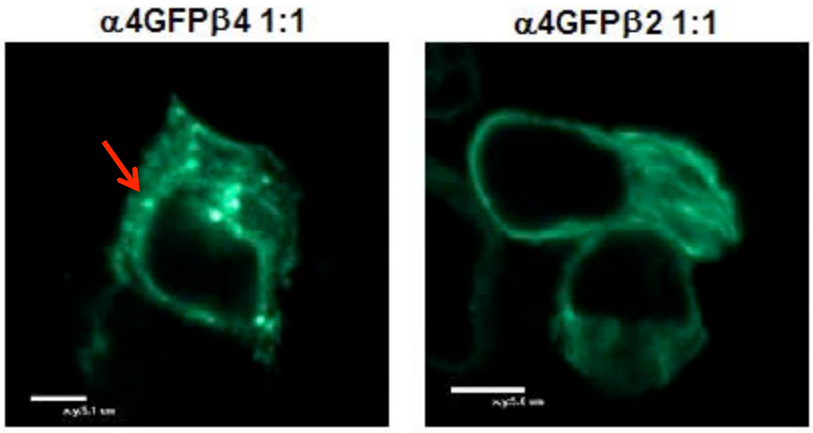

Figure 3.4: Confocal microscopy of α4-GFP/β2 and α4-GFP/β4 receptors in HEK293T cells transfected using ExpressFect. An ER exit site in the α4-GFP/β4 receptor is indicated by a red arrow.

show the α4β2 subunit heavily expressed in the ER whereas the α4β4 subunit is expressed both in the ER and at the membrane. GFP-tagged receptors can be observed exporting from the ER via ER exit sites (bright spots in the image).

We therefore concluded that our experimental results with the FlexStation agree with previously published data about the α4β2 neuronal receptor. We did not have GFP tagged constructs of the α7 and the muscle type receptors and therefore were not able to determine why these receptors did not exhibit functional expression using the FlexStation. Because the α4β4 receptor exhibited robust signals, we tested a variety of

Table 3.4: Functional data from the α4:β4 transfection ratios tested

α4:β4 Ratio	EC_{50} (μM)	Hill	n	Average Max RFU
2000:1	1.8 ± 0.2	1.2 ± 0.1	6	40.4
1000:1	1.5 ± 0.2	1.1 ± 0.2	5	52.9
500:1	0.75 ± 0.04	1.7 ± 0.1	17	104.4
200:1	0.70 ± 0.02	1.5 ± 0.1	17	106.2
100:1	0.72 ± 0.07	1.1 ± 0.1	20	144.6
50:1	0.70 ± 0.05	1.2 ± 0.1	20	155.4
30:1	0.65 ± 0.04	1.2 ± 0.1	20	163.8
10:1	0.66 ± 0.04	1.2 ± 0.1	21	125.0
3:1	0.75 ± 0.07	1.1 ± 0.1	19	80.1
1:1	3.1 ± 0.2	1.0 ± 0.1	23	67.0
1:3	5.5 ± 0.6	2.6 ± 0.5	2	47.3
1:10	7.5 ± 1.6	3.8 ± 3.2	2	16.1

transfection ratios of the two subunits to obtain pure populations of different stoichiometries (Table 3.4). It has previously been shown in *X. laevis* oocytes that pure populations of different stoichiometries can be obtained by biasing injection ratios of mRNA[20]. Here, we wanted to determine whether this principle held in mammalian cells and if we could detect changes in stoichiometries as well as the difference between pure and mixed populations using the FlexStation.

Interestingly, we found that the agonist sensitivities for the different stoichiometries are switched in the HEK293T cells relative to *X. laevis* oocytes. We see the formation of a low sensitivity stoichiometry when the transfection ratios were biased toward the β4 subunit (presumably $(\alpha4)_2(\beta4)_3$) and a higher sensitivity receptor when the transfection ratios are biased toward the α4 subunit (presumably $(\alpha4)_3(\beta4)_2$). Upon heavily biasing the transfection ratios toward α4 (≥ 1,000:1) we see the appearance of a

medium sensitivity receptor with a Hill coefficient of approximately 1.1, which is likely indicative of the formation of a third stoichiometry, the $(\alpha4)_4(\beta4)_1$ receptor. While we were able to bias the transfection ratios to make pure populations of what is likely the $(\alpha4)_3(\beta4)_2$ receptor, the transfection ratio needed to do so varied from batch to batch. The need to optimize our transfection conditions for every transfection batch indicated that the range needed to make a pure population was small. This would likely complicate both conventional and unnatural amino acid mutagenesis experiments in the future because of the need to optimize subunit bias for each mutant. We therefore sought to optimize expression conditions for a homopentameric receptor, the 5-HT_{3A} receptor, to avoid potential stoichiometry issues.

Since we anticipated a large loss of receptor expression when incorporating unnatural amino acids via nonsense suppression, we first wanted to optimize expression of the wild type receptor and cell health. To determine which transfection kit, transfection method, and incubation times were optimal for DNA transfection we tested a variety of conditions using seven different commercially available transfection kits. First, we tested the PEI and ExpressFect transfection reagents, because our collaborators in the Lummis and Lester labs had previously used them to successfully express membrane receptors in mammalian cells.

The PEI reagent was by far the most inexpensive reagent tested in these studies. Transfections with both PEI and ExpressFect gave comparable max RFU values as detected by the FlexStation (Figure 3.5) and the data obtained resulted in similar EC_{50} and Hill coefficient values when fit to the Hill equation (EC_{50} of 0.31 μM and n_H of 3.9

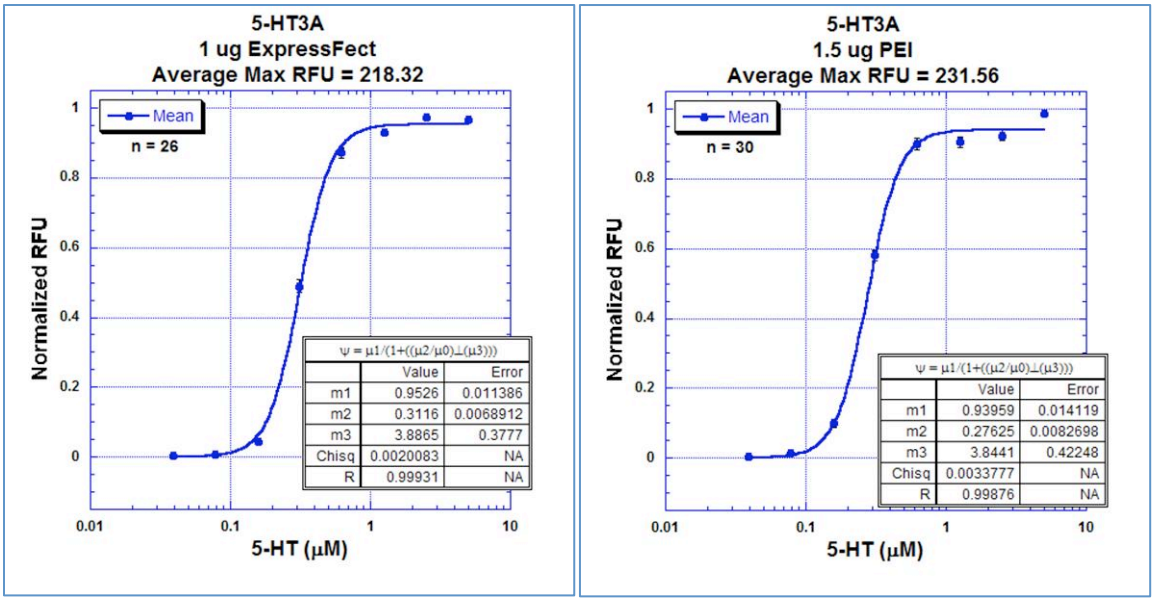

Figure 3.5: Data from 5-HT_{3A} transfections of HEK293T cells using ExpressFect (left) and PEI (right) fit to the Hill equation.

for cells transfected with ExpressFect and EC_{50} of 0.28 μM and n_H of 3.8 for cells transfected with PEI). These EC_{50} values are lower than what is observed using electrophysiology, however the data match well with published EC_{50} values for the 5-HT_{3A} receptor measured using fluorescent membrane potential dyes[21].

In addition to the PEI and ExpressFect transfection methods, we tested additional transfection kits to determine whether we could further enhance signals measured by the FlexStation. First, we sampled three different RNA transfection kits: TransMessenger, RNAiMAX, and *Trans*IT. Despite the fact we were looking to transfect DNA in these initial experiments, our final goal was to transfect DNA along with tRNA for suppression with unnatural amino acids. Unlike plasmid DNA, the tRNA is a stoichiometric reagent, and therefore efficient delivery of the tRNA in the future might be the limiting factor. The first step for optimizing DNA and tRNA cotransfections was to find the ideal

transfection and growth conditions for DNA alone using these three transfection kits (Tables 3.5-3.7).

Table 3.5: Transfection of HEK293T cells with 5-HT_{3A} DNA using the TransMessenger transfection reagent. Average Max RFUs were determined from three columns in a 96-well plate. The conditions for the highest RFU signal are highlighted in red.

WT DNA (µg)	TransMessenger (µL)	Avg Max RFU
0.1	8	207.6
0.5	8	366.0
2	8	346.8
2	4	No Response
2	8	376.0
2	16	287.5
4	8	310.0
4	16	361.7

Table 3.6: Transfection of HEK293T cells with 5-HT_{3A} DNA using the RNAiMAX transfection reagent. Average Max RFUs were determined from three columns in a 96-well plate. The conditions for the highest RFU signal are highlighted in red.

WT DNA (µg)	RNAiMAX (µL)	Avg Max RFU
Vary DNA, constant RNAiMAX		
0.02	7.5	82.3
0.1	7.5	141.5
0.5	7.5	209.1
2	7.5	270.6
Constant DNA, vary RNAiMAX		
2	2.5	162.0
2	7.5	146.1
2	15	163.3
2	30	42.9

Table 3.7: Transfection of HEK293T cells with 5-HT_{3A} DNA using the *Trans*IT transfection reagent. Average Max RFUs were determined from three columns in a 96-well plate. The conditions for the highest RFU signal are highlighted in red.

WT DNA (µg)	Boost Reagent (µL)	*Trans*IT (µL)	Avg Max RFU
0.02	5	7.5	No Response
0.1	5	7.5	107.0
0.5	5	7.5	308.9
2	5	7.5	467.6
2	1.25	2.5	408.1
2	3.75	7.5	497.8
2	7.5	15	541.8
2	15	30	563.5

From these optimization experiments it was determined that the highest transfection efficiency conditions for all three methods involved transfection of 2 µg of DNA. For both the TransMessenger and RNAiMAX transfection kits, a moderate amount of transfection reagents were found to give the highest signal, likely because of cell health issues at high concentrations of reagent. Conversely, expression using the *Trans*IT transfection kit continued to increase with higher concentrations of the transfection reagent, showing moderate expression increases with each doubling of the transfection reagent. For this particular reagent, cell health did not appear to be an issue. Of the three RNA transfection reagents tested, *Trans*IT gave the highest fluorescence signal overall (565 RFU vs. 376 RFU for TransMessenger and 270 RFU for RNAiMAX). Likewise, all three RNA transfection reagents gave higher average RFU signals than either ExpressFect or PEI (218 RFU and 232 RFU, respectively). It is important to note, however, that transfections with ExpressFect were done with 1 µg of DNA and PEI with

1.5 µg of DNA. Increasing DNA concentrations to 2 µg would likely give higher RFU signals, which could change the relative efficiencies of the transfection reagents.

The final chemical transfection reagent that we tested was the DNA transfection kit, PolyFect. We performed similar optimization experiments as for the mRNA transfection kits and were not able to find a transfection method that gave any fluorescence response to applied agonist. Most conditions tested resulted in massive cell death, and those with living cells resulted in no functional expression. The PolyFect kit was therefore not used in any further experiments.

In addition to the chemical transfection methods described above, we also tested transfection efficiencies by electroporation using the Neon Transfection System. The Neon software has 24 pre-programmed settings for cellular electroporation that vary the voltage delivered, time of voltage application, and number of voltage pulses. These 24 settings were applied to resuspended HEK293T cells + DNA and were each plated in a single column of a 96-well plate. Upon assaying the two 96-well plates from this experiment, it was shown that settings 6, 7, and 8 gave the highest RFUs upon application of agonist (Table 3.8). These settings correspond to a single 30 ms pulse length with a voltage application of between 1,100-1,300 V. Although the maximum RFU value was technically higher for transfection condition 6 (1,100 V, 1 pulse, 30 ms), we selected condition 7 (1,200 V, 1 pulse, 30 ms) as our optimum transfection method because it fell in the middle of three high signals. We thought that selecting this method might minimize potentially strong negative effects from batch-to-batch variability that could shift the optimal transfection setting in either direction. Next, using setting 7 on the Neon, we optimized expression levels for incubation time and amount of DNA

Table 3.8: Optimization of 5-HT_{3A} receptor expression using the Neon electroporation method. The best setting conditions are highlighted in red.

Condition	Voltage (V)	Width (ms)	# Pulses	Max RFU	Condition	Voltage (V)	Width (ms)	# Pulses	Max RFU
1	0	20	1	n/a	**13**	1100	20	2	242
2	1400	20	1	294	**14**	1200	20	2	311
3	1500	20	1	299	**15**	1300	20	2	280
4	1600	20	1	174	**16**	1400	20	2	115
5	1700	20	1	130	**17**	850	30	2	265
6	1100	30	1	342	**18**	950	30	2	254
7	1200	30	1	341	**19**	1050	30	2	301
8	1300	30	1	322	**20**	1150	30	2	238
9	1400	30	1	216	**21**	1300	10	3	265
10	1000	40	1	321	**22**	1400	10	3	273
11	1100	40	1	298	**23**	1500	10	3	270
12	1200	40	1	256	**24**	1600	10	3	87

Table 3.9: Optimization of DNA transfection conditions and incubation lengths. Amount of DNA transfected is for three columns in a 96-well plate.

DNA (µg)	1 Day Incubation, Avg Max RFU	2 Day Incubation, Avg Max RFU
1	145.0	232.0
2	300.1	359.7
4	137.4	309.3
8	185.1	304.5

transfected. We found that a two-day incubation resulted in higher expression levels for all DNA transfection amounts with 2 µg of DNA giving the highest signal (Table 3.9).

Conventional mutagenesis. After transfection conditions were optimized for the wild type 5-HT_{3A} receptor, we next attempted to assay conventional mutants. We were

interested in both the effect on expression upon introducing detrimental mutations and the ability of the FlexStation to measure shifts in EC_{50}. To introduce a large loss-of-function mutation, we sought to remove or modulate the side chain that participates in the crucial cation-π binding interaction (W183) with the agonist[22]. The W183A and W183Y mutations had been previously shown in HEK293 cells to give large loss-of-function fold shifts in the mouse 5-HT_{3A} receptor (166 and 22 fold, respectively)[23]. Using the human

Table 3.10: Data from conventional mutagenesis of both the human and mouse 5-HT_{3A} receptors. Mouse 5-HT_{3A} data was previously determined in a different study[23].

	Human $5HT_{3A}$			**Mouse $5HT_{3A}$**	
	EC_{50} (μM)	**Fold Shift**	**Hill**	**EC_{50} (μM)**	**Fold Shift**
Wild Type	0.28 ± 0.01	-	3.84 ± 0.42	0.24	-
W183A	180 ± 7	652	2.47 ± 0.21	39.8	166
W183Y	34.5 ± 1.9	125	2.49 ± 0.25	5.25	22

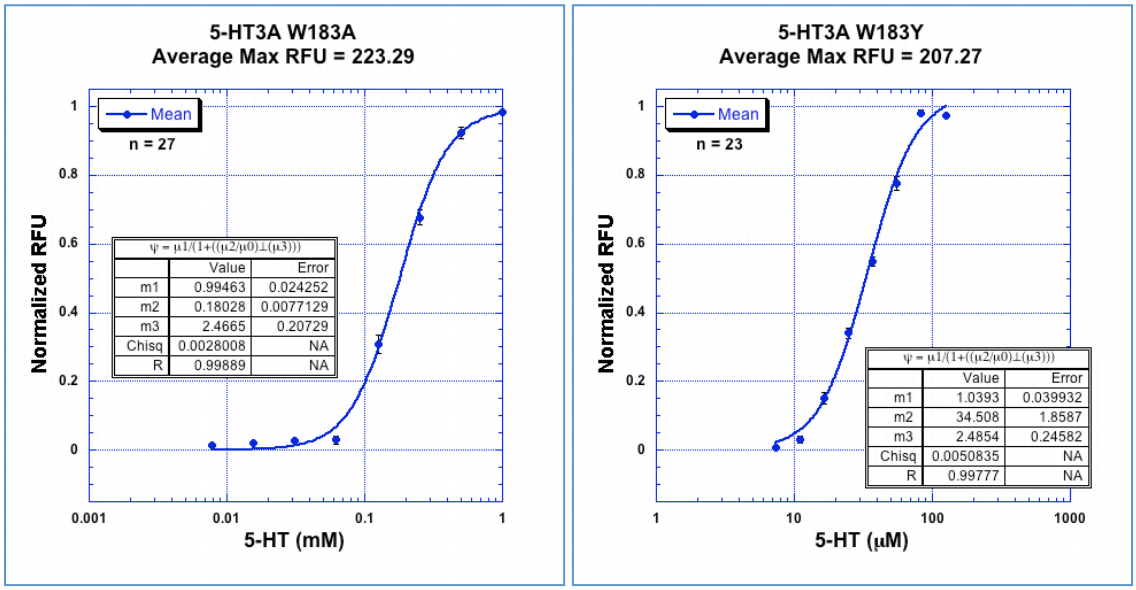

Figure 3.6: Data from 5-HT_{3A} mutant receptors (W183A and W183Y) fit to the Hill equation.

5-HT_{3A} construct we observed larger (652 and 125, respectively) fold shifts with data that fit well to the Hill equation (Table 3.10, Figure 3.6). These data indicated that we were able to measure large fold shifts using our transfection methods and assay. Interestingly, we did not observe a significant loss of signal amplitude at saturating agonist doses. The maximum RFUs given for the W183A and W183Y mutants were 223 and 207 RFUs, respectively compared to 218 RFUs for the wild type receptor using the ExpressFect transfection reagent.

Optimization of DNA and tRNA cotransfections: suppression with the human serine amber suppressor. To optimize DNA and tRNA cotransfection into HEK293T cells, we first began by finding ideal transfection conditions for a model DNA/tRNA suppression pair. The human serine amber suppressor (HSAS) is the endogenous serine tRNA found in human cells, however the anticodon has been mutated to recognize the amber stop codon (TAG). In the cell, this tRNA is recognized by the endogenous serine tRNA synthetase, which charges the unacylated tRNA with the natural amino acid serine. The HSAS tRNA is expected to give significantly higher receptor expression than the orthogonal acylated tRNAs commonly used for unnatural amino acid mutagenesis because it is recognized by the cellular machinery and is not a stoichiometric reagent. Therefore, to determine the ideal transfection conditions of DNA and tRNA, we began our optimizations with DNA and *in vitro* transcribed tRNA cotransfection using plasmid DNA with a TAG codon at the site of interest and the HSAS tRNA.

To examine whether an amino acid could be incorporated by this methodology, we first sought to visualize serine incorporation into enhanced green fluorescent protein

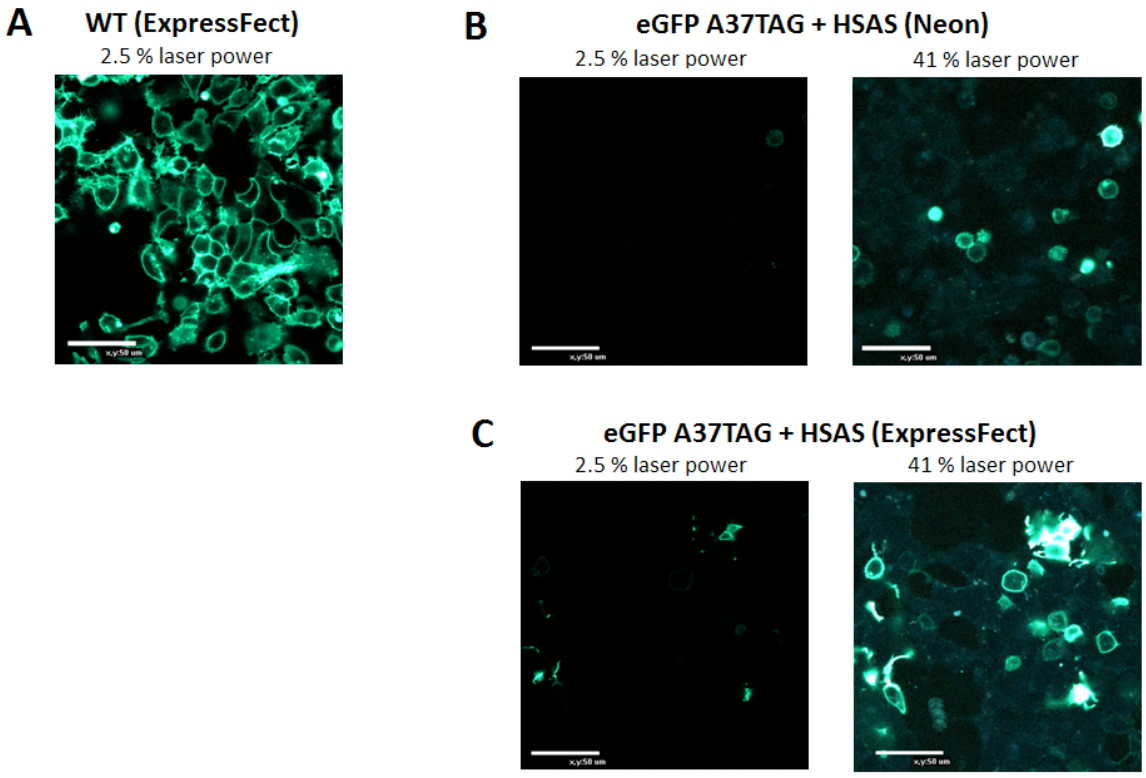

Figure 3.7: Confocal microscopy of serine suppression in eGFP using the HSAS tRNA. **A)** Wild type eGFP expression **B)** eGFP expression from HSAS suppression at A37TAG using the Neon transfection system. Confocal image is at both the laser power used to image wild type eGFP and a higher laser power to better image suppression efficiency **C)** Suppression of eGFP using ExpressFect.

(eGFP). We chose A37 as the site for suppression because it is located at the beginning of the protein before the residues that make up the GFP chromophore. Therefore, if the HSAS tRNA is transfected at a concentration lower than is required for sufficient protein synthesis or if the *in vitro* transcribed tRNA is not stable and/or recognized by host machinery, protein synthesis will be truncated before the chromophore can be formed and no fluorescence will be observed. We found that HEK293T cells cotransfected with HSAS and A37TAG eGFP plasmid resulted in observed fluorescence by confocal microscopy using both ExpressFect and the Neon. Although fluorescence was detected, indicating serine suppression at the A37 site, eGFP expression was significantly lower for

the suppression experiments than for wild type eGFP (approximately <1%) (Figure 3.7). Expression was slightly higher for the cells transfected using ExpressFect.

Once we were able to confirm that an amino acid could be incorporated into a high expressing protein using cotransfection of an *in vitro* transcribed tRNA and plasmid DNA, we next sought to test suppression efficiency in a neuroreceptor. First, we attempted to incorporate serine via wild type recovery at the S61 site in the 5-HT_{3A} receptor. Assuming 2 μg remains the ideal amount of DNA for maximal expression, we used a variety of transfection methods to determine which method gave the highest transfection efficiency and how much cotransfected tRNA was required (Table 3.11). No expression was observed when using PEI, indicating that this transfection method might not allow efficient transfection of RNA. Expression of 5-HT_{3A} was, however, observed when cells were transfected with ExpressFect and the Neon. Expression using ExpressFect was strongly variable from batch-to-batch, showing some expression with high concentrations of HSAS on some days and none on others. Expression using the Neon was more consistent, and expression was highest for transfection conditions using low amounts of HSAS. Response could be slightly increased by using a larger concentration of membrane potential dye (1:2 vs. 1:10) (Table 3.12). Maximum expression was approximately three-fold lower than the wild type signal, which is expected when using suppression. However, the ability to detect a signal and measure an EC_{50} value indicates potential viability using the suppression methodology.

We also tested the RNA transfection kits: TransMessenger, RNAiMAX, and *Trans*IT for their ability to cotransfect plasmid DNA and *in vitro* transcribed RNA. No expression was observed using RNAiMAX (Table 3.13). However, we did observe

functional 5-HT_{3A} receptor expression in cells transfected using TransMessenger (Table 3.14) and *Trans*IT (Table 3.15). The highest expressing transfection conditions using TransMessenger required more transfection reagent than *Trans*IT (16 µl vs. 7.5 µL per 35 mm dish) and gave lower wild type recovery signals (120 vs. 350 RFUs).

When using *Trans*IT, we observed higher wild type receptor expression with increasing concentrations of *Trans*IT (up to 30 µL), however in the presence of tRNA, higher *Trans*IT concentrations had the opposite effect. We therefore determined that

Table 3.11: 5-HT_{3A} expression of S61TAG DNA cotransfected with HSAS tRNA. Data is shown for three columns of cells transfected using PEI, ExpressFect, and Neon electroporation.

DNA (µg)	HSAS (µg)	Neon, Avg Max RFU	PEI, Avg Max RFU	ExpressFect, Avg Max RFU	ExpressFect, Avg Max RFU
		11/15/10	11/15/10	11/15/10	12/1/10
2 (WT)	0	297.1	195.7	320.5	309.5
2 (S61TAG)	2	93.8	No Response	No Response	No Response
2 (S61TAG)	4	37.7	No Response	80.9	No Response
2 (S61TAG)	8	No Response	No Response	78.3	No Response

Table 3.12: 5-HT3A receptor expression of S61TAG DNA cotransfected with HSAS tRNA using a 1:2 dye dilution.

DNA (µg)	HSAS (µg)	Neon, Avg Max RFU
2 (WT)	0	371.5
2 (S61TAG)	2	112.4
2 (S61TAG)	4	121.4
2 (S61TAG)	8	91.9

transfection conditions using 2 μg of DNA (and 4 μg of tRNA if applicable), 3.75 μL of Boost Reagent, and 7.5 μL of *Trans*IT were optimal for receptor expression in the case of wild type recovery and a balance of expression and cost effectiveness in the case of wild type. The *Trans*IT transfection reagent gave the highest overall wild type and wild type recovery signals of all methods and conditions tested. We therefore believe that this reagent is superior for both DNA transfection and RNA/DNA cotransfection.

In addition to wild type recovery, we also sought to incorporate a serine residue via suppression at a critical site in the receptor designed to perturb receptor function. For this we chose W183, the cation-π site crucial for ligand binding. We had previously shown using conventional mutagenesis that mutations at the W183 site (W183A and W183Y) resulted in a large loss-of-function mutations (652 and 125-fold, respectively), therefore we assumed a similar loss of function for the W183TAG(Ser) mutation. Using electroporation, we were able to obtain functional receptors with an EC_{50} of 370 μM 5-HT, which demonstrates a 1,200-fold shift relative to wild type. Expression of the mutant receptors was approximately three-fold lower than that for wild type recovery at S61 (Table 3.16). Introducing a functionally detrimental mutation in all of the five subunits can likely account for this loss of expression. No expression was observed using PEI, similar to what was observed for wild type recovery.

Optimization of DNA and tRNA cotransfections: unnatural amino acid mutagenesis. Using the transfection methods previously optimized for DNA and HSAS tRNA cotransfection, we next sought to incorporate an amino acid from an *in vitro* transcribed and acylated tRNA. Suppression with *in vitro* acylated tRNA has been

Table 3.13: Wild type recovery by cotransfection of HSAS and S61TAG plasmid DNA using RNAiMAX

DNA (µg)	HSAS (µg)	RNAiMAX (µL)	Avg Max RFU
2 (WT)	0	15	113.8
2 (S61TAG)	0	15	No Response
2 (S61TAG)	4	15	No Response
2 (S61TAG)	8	15	No Response

Table 3.14: Wild type recovery by cotransfection of HSAS and S61TAG plasmid DNA using TransMessenger

DNA (µg)	HSAS (µg)	TransMessenger (µL)	Avg Max RFU
Constant DNA, vary HSAS, constant TransMessenger			
2 (WT)	0	8	274.7
2 (S61TAG)	2	8	No Response
2 (S61TAG)	4	8	No Response
2 (S61TAG)	8	8	No Response
Vary DNA, constant HSAS, vary TransMessenger			
0.5 (S61TAG)	4	8	42.5
1 (S61TAG)	4	8	47.2
0.5 (S61TAG)	4	16	74.1
1 (S61TAG)	4	16	120.4
Constant DNA, vary HSAS, using 16 mL TransMessenger			
2 (WT)	0	16	208.4
2 (S61TAG)	2	16	63.8
2 (S61TAG)	4	16	No Response
2 (S61TAG)	8	16	No Response
Constant DNA, vary HSAS, using 32 mL TransMessenger			
2 (WT)	0	32	181.8
2 (S61TAG)	2	32	69.9
2 (S61TAG)	4	32	52.9
2 (S61TAG)	8	32	No Response

Table 3.15: Wild type recovery by cotransfection of HSAS and S61TAG plasmid DNA using *Trans*IT

$5HT_{3A}$ DNA (µg)	**HSAS (µg)**	**Boost Reagent (µL)**	***Trans*IT (µL)**	**Avg Max RFU**
		DNA constant, vary HSAS and Boost:TransIT		
2 (WT)	0	7.5	15	471.1
2 (S61TAG)	4	7.5	15	113.1
2 (S61TAG)	8	7.5	15	94.6
2 (S61TAG)	8	15	30	Cells Died
		Vary DNA, constant HSAS, vary Boost:TransIT		
0.5 (S61TAG)	4	3.75	7.5	95.2
1 (S61TAG)	4	3.75	7.5	91.1
0.5 (S61TAG)	4	7.5	15	44.8
1 (S61TAG)	4	7.5	15	73.2
		Constant DNA, vary HSAS, using 2.5 µL TransIT		
2 (WT)	0	1.25	2.5	167.7
2 (S61TAG)	2	1.25	2.5	No Response
2 (S61TAG)	4	1.25	2.5	37.4
2 (S61TAG)	8	1.25	2.5	33.5
		Constant DNA, vary HSAS, using 7.5 µL TransIT		
2 (WT)	0	3.75	7.5	489.0
2 (S61TAG)	2	3.75	7.5	162.9
2 (S61TAG)	4	3.75	7.5	353.5
2 (S61TAG)	8	3.75	7.5	340.0

Table 3.16: Conventional mutagenesis of the $5\text{-}HT_{3A}$ receptor using HSAS serine suppression at W183. Results are compared between PEI and electroporation.

DNA (µg)	**HSAS (µg)**	**Neon, Avg Max RFU**	**PEI, Avg Max RFU**
2 (WT)	0	180.6	73.9
2 (W183TAG)	0.5	No Response	No Response
2 (W183TAG)	2	14.9	No Response
2 (W183TAG)	4	33.5	No Response

effectively used to incorporate unnatural amino acids into receptors in *X. laevis* oocytes, and its implementation in mammalian cells is the ultimate goal of this project. To achieve sufficient nucleic acid delivery, we tested a variety of optimized transfection methods that have been previously described in this chapter.

Unlike the HSAS experiments where an endogenous tRNA was used to incorporate its cognate natural amino acid, suppression with unnatural amino acids requires the use of an orthogonal tRNA. For a tRNA to be orthogonal, it must not be reaminoacylated with its associated natural amino acid by the host synthetases after delivery of the desired unnatural amino acid. This prevents background expression of receptors lacking the unnatural amino acid and facilitates investigation of the desired mutation. Unfortunately, because the tRNA is not recharged with another amino acid *in vivo*, the unnatural amino acid-containing tRNA is a stoichiometric reagent. In *X. laevis* oocytes, this leads to lower expression levels of receptors containing an unnatural amino acid relative to wild type or conventional mutants.

To determine whether we could effectively incorporate an unnatural amino acid into receptors in HEK293T cells, we cotransfected cells with DNA and acylated tRNA previously developed for unnatural amino acid mutagenesis in *X. laevis* oocytes: *Tetrahymena thermophila* G73 (THG73) or the yeast phenylalanine frameshift suppressor (YFaFS)[15]. Orthogonal suppressor tRNAs are often derived from distantly related organisms and we believed that the tRNAs used in *X. laevis* oocytes would also be orthogonal in mammalian cells. We did not observe any response to applied agonist for cells transfected using any of the methods tested (Tables 3.17-3.19 for THG73-W at W183TAG and Table 3.20 for YFaFS-W at W183GGGT). Because suppression with

alpha-hydroxy amino acids often gives higher expression levels in *X. laevis* oocytes, likely due to reduced hydrolysis of the amino acid during incubation, we also attempted to suppress with tryptophan α-hydroxy (Wah) at the W183 site (Table 3.21) and Sah at the S61 site (data not shown). In both cases, no receptor expression was observed indicating that while hydrolysis may be a problem, other issues likely prevent adequate unnatural amino acid incorporation.

Although we were not able to measure functional expression of mutant 5-HT_{3A} receptors suppressed with *in vitro* acylated tRNA on the FlexStation, we wanted to determine visually whether any mutant protein was being produced. We therefore sought

Table 3.17: Attempted wild type recovery at W183 using *in vitro* transcribed THG73-W tRNA and W183TAG plasmid DNA. Cells were transfected by Neon electroporation.

W183TAG DNA (µg)	THG73-W tRNA (µg)	Avg Max RFU
	Constant DNA	
2	0	No Response
2	2 (THG73-76mer)	No Response
2	0.1	No Response
2	0.5	No Response
2	1	No Response
2	2	No Response
2	4	No Response
	Constant tRNA	
1	2	No Response
2	2	No Response
4	2	No Response
8	2	No Response
16	2	No Response
32	2	No Response

Table 3.18: Attempted wild type recovery at W183 using *in vitro* transcribed THG73-W tRNA and W183TAG plasmid DNA. Cells were transfected by ExpressFect.

W183TAG DNA (µg)	THG73-W (µg)	ExpressFect, Avg Max RFU
0.5	1.25	No Response
1	1.25	No Response
2	1.25	No Response
5	1.25	No Response

Table 3.19: Attempted wild type recovery at W183 using *in vitro* transcribed THG73-W tRNA and W183TAG plasmid DNA. Cells were transfected by PEI.

W183TAG DNA (µg)	THG73-W (µg)	PEI, Avg Max RFU
Vary DNA, wide range of tRNA		
0.5	0.5	No Response
1	0.5	No Response
1	2	No Response
1	3	No Response
tRNA constant (1 µg)		
0.25	1	No Response
0.5	1	No Response
1	1	No Response
2	1	No Response
Vary DNA and tRNA, but keep total nucleic acid constant (1 µg)		
0.25	0.75	No Response
0.75	0.25	No Response
0.1	0.9	No Response
0.9	0.1	No Response

Table 3.20: Attempted wild type recovery at W183 using *in vitro* transcribed YFaFS-W tRNA and W183GGGT plasmid DNA. Cells were transfected by Neon electroporation

Trial Date	W183GGGT DNA (µg)	YFaFS-W tRNA (µg)	Avg Max RFU
Trial 1	2 (WT)	0	572.6
	2	8 (YFaFS-76mer)	No Response
	2	8	No Response
Trial 2	2 (WT)	0	301.2
	2	8 (YFaFS-76mer)	No Response
	2	4	No Response
	2	8	No Response
Trial 3	2 (WT)	0	443.7
	2	8 (YFaFS-76mer)	No Response
	2	4	No Response
	2	8	No Response

Table 3.21: Attempted mutagenesis at W183 using an α-hydroxy acid. Cells were transfected with *in vitro* transcribed THG73-Wah tRNA and W183TAG plasmid DNA.

DNA (µg)	tRNA (µg)	Neon, Avg Max RFU	*Trans*IT, Avg Max RFU
2 (WT)	0	645.7	407.5
2 (W183TAG)	4	No Response	No Response
2 (W183TAG)	8	No Response	No Response
2 (W183TAG)	12	No Response	No Response

to incorporate an *in vitro* acylated amino acid into eGFP to avoid the need for suppression and assembly of five subunits per receptor and high surface expression of functional receptors for FlexStation analysis with the voltage-sensitive dye.

To visually observe suppression efficiency, we imaged HEK293T cells transiently transfected with mutant eGFP using confocal microscopy (Figure 3.8). Cells transfected with wild type eGFP showed robust fluorescence indicating efficient DNA transfection

and protein synthesis. Conversely, cells transfected with A37TAG eGFP DNA showed very low fluorescence indicating truncation of protein translation early during protein synthesis, which is expected for a nonsense mutation in cells that lack a corresponding suppressor tRNA. When cells were cotransfected with A37TAG eGFP DNA and an *in vitro* transcribed suppressor tRNA (76mer THG73), a slight increase in expression was observed. The increase in observed signal is indicative of a small amount of *in vivo* acylation and full-length protein synthesis, therefore providing evidence that both the DNA and tRNA are successfully cotransfected. Unfortunately, when cells were cotransfected with A37TAG eGFP DNA and THG73-Ala, no additional expression was observed. This suggests that the *in vitro* acylated amino acid is not being delivered to the growing peptide and is instead likely hydrolyzed during Neon electroporation or the 48 hour incubation period.

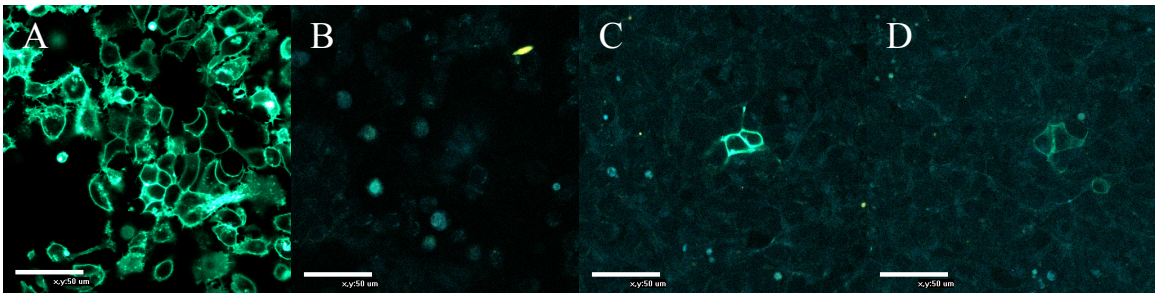

Figure 3.8: Confocal microscopy of HEK293T cells transfected with eGFP using Neon electroporation. **A)** Wild type eGFP, 2.5% laser power 90% saturation **B)** A37TAG DNA, 41% laser power 96% saturation **C)** A37TAG DNA with 76mer THG73 tRNA, 41% laser power 96% saturation **D)** A37TAG DNA with THG73-Ala, 41% laser power 96% saturation

Double transfections. To enhance expression, we sought to determine whether a second transfection 24 hours after the first led to better agonist responses, similar to what is performed in *X. laevis* oocytes for difficult-to-express mutants. For this, we tested our

two most successful DNA and tRNA cotransfection methods: *Trans*IT and Neon electroporation. For *Trans*IT double transfections, we tested the effect on expression of a second application of transfection reagents and either DNA and tRNA or tRNA only. We determined that a second transfection of DNA did not lead to enhanced expression because the expression of the wild type receptor was not changed compared to the singly transfected cells (Table 3.22). We did however observe an increase in receptor expression upon a second transfection of tRNA only for all S61TAG + HSAS conditions tested, further supporting that tRNA is the limiting reagent for suppression. While a three to six-fold increase in receptor expression was observed for serine incorporation at S61TAG, no expression was observed using the orthogonal THG73-W tRNA (Table 3.23). This indicates that while a second transfection increases the pool of intracellular tRNA without negatively affecting cell health, a larger acylated tRNA population is still required.

Next, to determine whether a second transfection using electroporation gave enhanced signals relative to the *Trans*IT transfection method, we performed a series of double transfections using the pre-programmed instrument settings. The first transfection

Table 3.22: Double *Trans*IT transfection of HEK293T cells with S61TAG DNA and HSAS tRNA. Both a second transfection with DNA and tRNA and tRNA only were performed.

DNA (µg)	HSAS (µg)	Boost Reagent (µL)	*Trans*IT (µL)	2X (DNA+HSAS) Avg Max RFU	2X (HSAS only) Avg Max RFU
2 (WT)	0	3.75	7.5	621.6	626.0
2 (S61TAG)	2	3.75	7.5	46.2	177.7
2 (S61TAG)	4	3.75	7.5	51.9	321.4
2 (S61TAG)	8	3.75	7.5	85.0	390.1

Table 3.23: Double *Trans*IT transfection of HEK293T cells with W183TAG DNA and THG73-W tRNA. Both a second transfection with DNA and tRNA and tRNA only were performed.

W183TAG DNA (µg)	tRNA (µg)	Boost Reagent (µL)	*Trans*IT (µL)	2X DNA+tRNA Avg Max RFU	2X tRNA only Avg Max RFU
2	8 (THG73-76mer)	3.75	7.5	No Response	No Response
2	2 (THG73-W)	3.75	7.5	No Response	No Response
2	4 (THG73-W)	3.75	7.5	No Response	No Response
2	8 (THG73-W)	3.75	7.5	No Response	No Response

Table 3.24: Optimization of Neon double transfection of S61TAG DNA and HSAS tRNA. Data represents cells first transfected using condition 7 and a second transfection 24 hours later using the specified instrument setting. Condition 1 represents singly transfected cells.

Condition	Max RFU	Condition	Max RFU
1 (single)	17.4	**13**	No Response
2	161.1	**14**	118.8
3	158.1	**15**	209.8
4	170.5	**16**	278.4
5	193.4	**17**	54.0
6	172.6	**18**	135.9
7	219.2	**19**	223.5
8	264.5	**20**	279.7
9	315.7	**21**	260.1
10	216.8	**22**	390.0
11	253.7	**23**	273.1
12	277.1	**24**	183.1

was performed as previously described using 2 µg of S61TAG DNA and 4 µg of HSAS tRNA and electroporation with condition 7. We found that a second transfection with 4 µg of tRNA after a 24 hour incubation gave enhanced agonist-induced signals for all

conditions tested, except condition 13, relative to cells transfected a single time (condition 1) (Table 3.24). The highest expressing second transfection condition was found to be condition 22 (1400 V, 10 ms, 3 pulses) as determined by maximum RFU. When the same double transfection conditions were applied to W183TAG DNA and THG73-W tRNA no expression was observed (Table 3.25).

Table 3.25: Neon double transfection of HEK293T cells with W183TAG DNA and THG73-W tRNA or tRNA only.

DNA (µg)	tRNA (µg)	Nucleic Acid Double Transfected	Avg Max RFU
2 (WT)	0	DNA only	Instrument disrupted, data lost
2 (W183TAG)	8 (THG73-76mer)	tRNA only	No Response
2 (W183TAG)	8 (THG73-W)	tRNA only	No Response
2 (W183TAG)	8 (THG73-W)	tRNA + DNA	No Response

tRNA stability. To determine whether the lack of suppression efficiency by *in vitro* acylated tRNA was due to significant hydrolysis of the amino acid upon transfection and/or incubation at 37^{o}C, stability tests were performed. The integrity of the acylated tRNA was examined by MALDI-TOF analysis before and after typical transfection conditions for the two most efficient methods: *Trans*IT and Neon electroporation. To ensure that MALDI-TOF analysis is sensitive enough to detect a mass loss in the range of an amino acid, we measured the mass of the tRNA before and after deprotection of the NVOC protecting group. Analysis shows a mass loss of 238, which corresponds to the expected 239 mass loss of the NVOC group (Figure 3.9). We are therefore confident that MALDI-TOF analysis would be sensitive enough to measure the mass loss of a large amino acid such as tryptophan (204 g/mol).

Next, we wanted to simulate the transfection conditions experienced by the deprotected tRNA in our above-described methods. For the simulated *Trans*IT transfection, tRNA was deprotected for 10 minutes and incubated in the presence of the *Trans*IT transfection reagents at 37^{o}C for 24 hours. A mass loss of 206 was observed between the non-deprotected untreated tRNA and the deprotected *Trans*IT-treated tRNA (Figure 3.10). This mass corresponds better to the NVOC protecting group than both the NVOC and W side chain (239 vs. 442) indicating that W is likely not hydrolyzed during transfection. Likewise, we subjected tRNA to a 10 minute deprotection step followed by Neon electroporation using protocols 7 and 22, to represent the Neon transfection conditions used in our experiments. MALDI-TOF analysis shows a mass loss of 195 and 305, respectively (Figure 3.11). Both of these mass values are closer to the mass of the NVOC protecting group, however the broadness of the peak may obscure definitive assignment. To increase the sharpness of the mass peak, the treated tRNA was subsequently run through a BD Biosciences CHROMA SPIN-30 DEPC-H_2O desalting column. Column purification resulted in a low concentration of purified tRNA and therefore no mass data was able to be obtained.

Dye optimization. To determine the concentration of membrane potential dye that elicited the largest fluorescence signal in response to applied agonist, a variety of dye dilutions were tested. The different dye concentrations were tested on the wild type 5-HT_{3A} receptor expressed by both PEI transfection of wild type DNA and Neon transfection of S61TAG DNA and *in vitro* transcribed HSAS tRNA (Table 3.26).

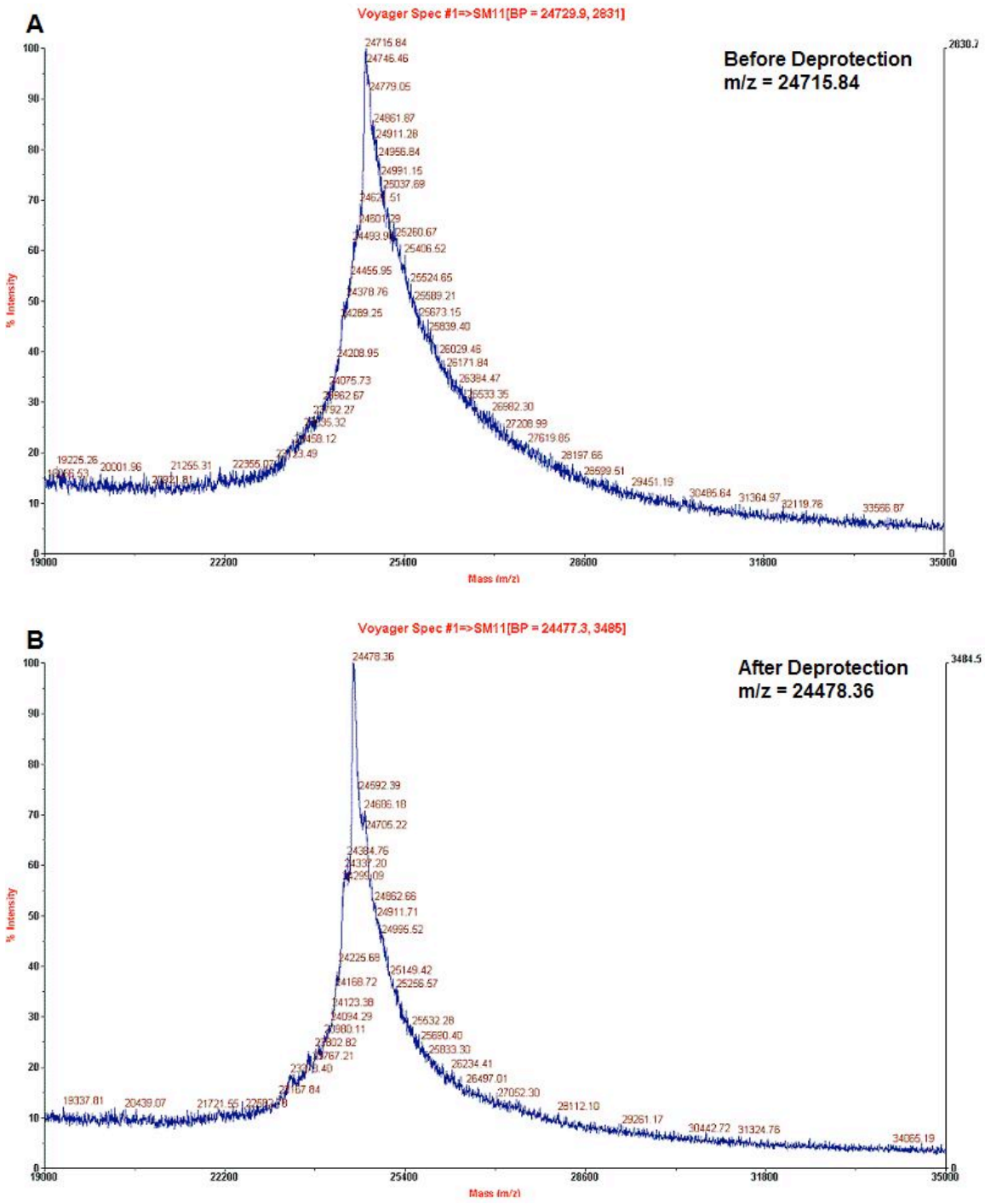

Figure 3.9: MALDI-TOF analysis of THG73-W tRNA **A)** before and **B)** after NVOC deprotection.

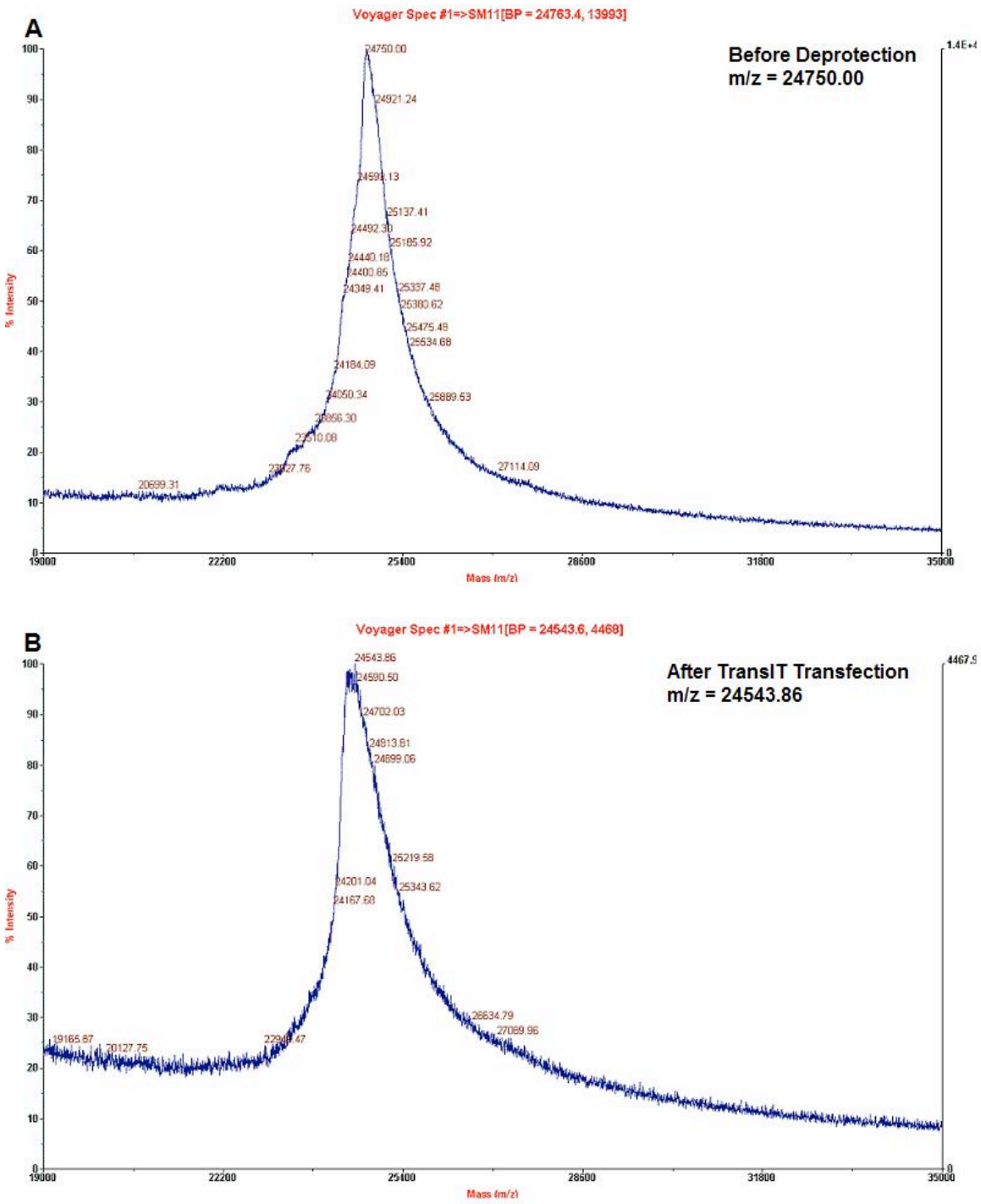

Figure 3.10: MALDI-TOF analysis of THG73-W incubated with *Trans*IT transfection reagents **A)** before NVOC deprotection and transfection and **B)** after transfection conditions.

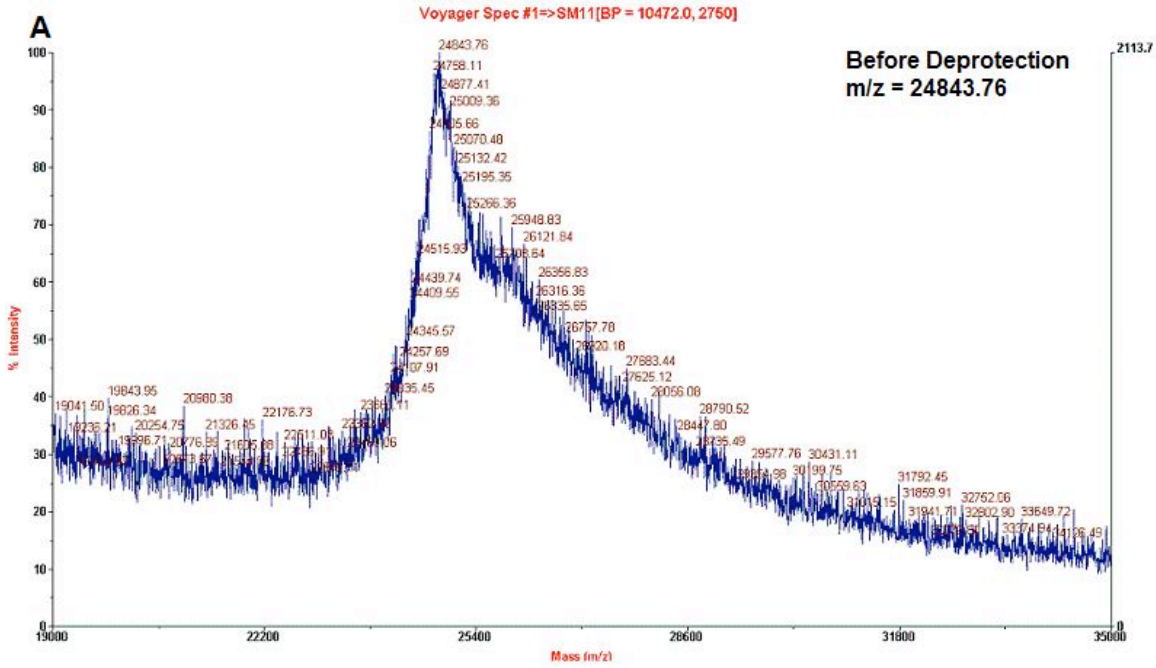
A
Voyager Spec #1=>SM11[BP = 10472.0, 2750]
Before Deprotection
m/z = 24843.76
% Intensity
Mass (m/z)

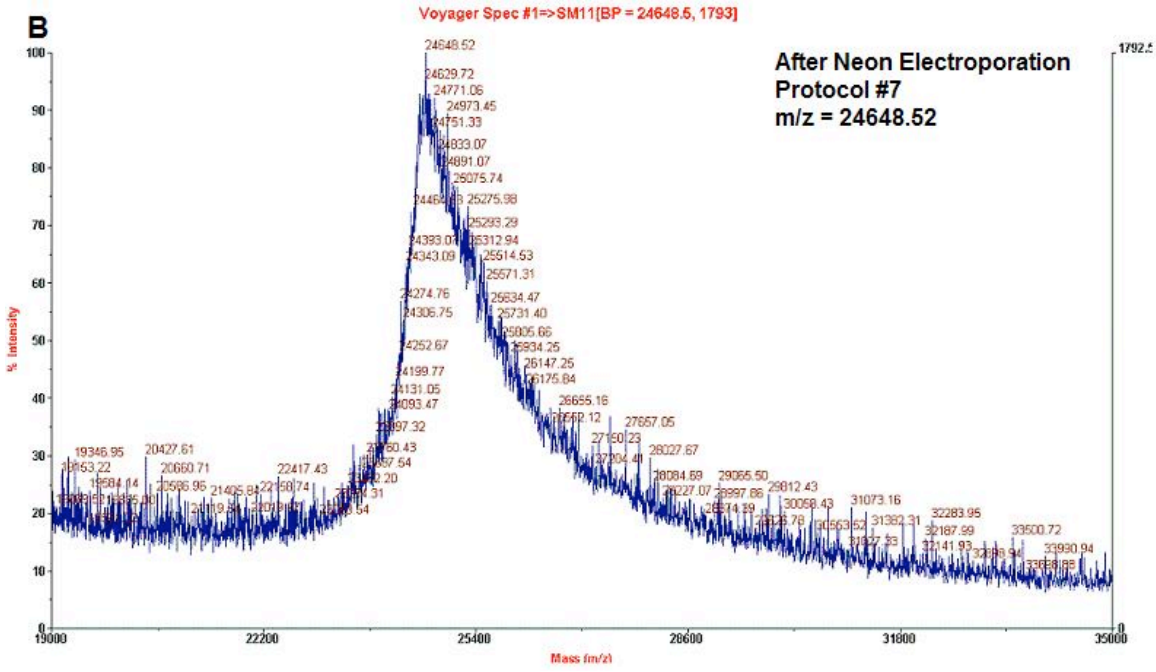
B
Voyager Spec #1=>SM11[BP = 24648.5, 1793]
After Neon Electroporation
Protocol #7
m/z = 24648.52
% Intensity
Mass (m/z)

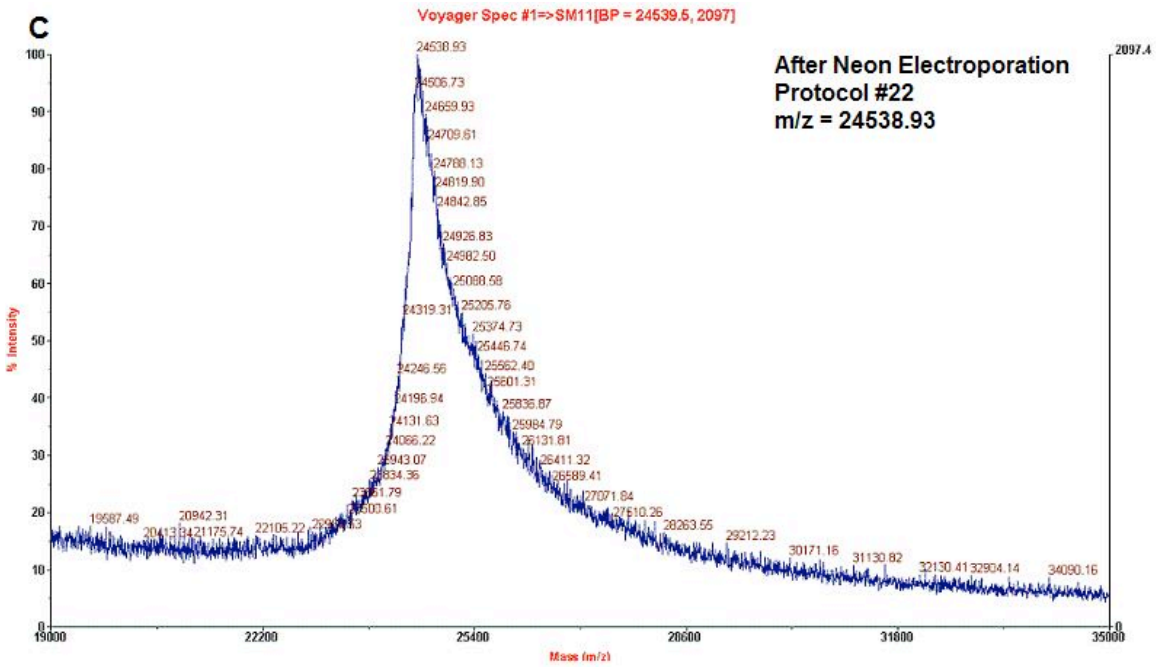

Figure 3.11: MALDI-TOF analysis of THG73-W electroporation with the Neon transfection system **A)** before NVOC deprotection and electroporation, **B)** after deprotection and electroporation with condition 7, and **C)** after deprotection and electroporation with condition 22.

Optimization of wild type and wild type recovery experiments was performed to determine the best dye dilutions for both high and low receptor signals.

It was found that the 1:2 dye dilution (5 mL of dye + 5 mL of Flex buffer), relative to the manufacturer's protocol, elicited the maximal response for both the high and low expressing receptor populations. Using the full-strength dye recommended by Molecular Devices elicited a comparable high signal relative to the 1:2 dilution, however it required twice as much dye, which is not cost effective. Therefore it was determined that using the 1:2 dilution of membrane potential dye was the optimal concentration for all experiments involving the 5-HT_{3A} receptor. For cost-effectiveness it is also possible to use lower concentrations of dye down to a 1:10 dilution (1 mL of dye + 9 mL Flex

Table 3.26: Optimization of membrane potential dye concentration for assaying 5-HT_{3A} receptors

Dye Dilution	5-HT_{3A} wild type Max RFU	5-HT_{3A} S61TAG + HSAS Max RFU
1:1	986.86	83.55
1:2	994.67	83.46
1:5	616.73	53.02
1:10	466.11	42.12

buffer) for high receptor expressing conditions such as experiments assaying wild type receptor function.

Conclusions and Future Directions

In conclusion, we were able to optimize cotransfection conditions for *in vitro* transcribed tRNA and plasmid DNA into HEK293T cells. We found that the highest expression of functional receptors was observed when cells were transfected with the *Trans*IT-mRNA transfection reagent or through a double transfection with the Neon electroporation system. Both conditions gave comparable results, however transfection with *Trans*IT required less total nucleic acid. Additionally, we found that transfection with plasmid DNA gave larger functional expression than transfection with mRNA. Coupled with the lower cost of making large quantities of DNA than mRNA, we believe that DNA is superior to mRNA for all mammalian cell experiments.

Cotransfection of HSAS tRNA and plasmid DNA gave robust signals for both wild type recovery and conventional mutagenesis experiments, indicating that *in vitro* transcribed tRNA is successfully transfected into cells. However, when using the stoichiometric, orthogonal, and acylated tRNAs (THG73 and YFaFS), we did not observe

any functional expression of receptors, indicating low protein synthesis. Therefore, despite our initial success with HSAS, further optimization and troubleshooting is required for the ultimate goal of unnatural amino acid mutagenesis in mammalian cells. Some possible issues that could be arising are listed and discussed below:

1) *Lack of tRNA post-transcriptional modifications:* The majority of *in vivo tRNA* processing steps are not required for an *in vitro* transcribed tRNA because a mature tRNA lacking leader, trailer, and intron sequences is initially synthesized and the terminal CA is added upon acylation with dCA-amino acid. The *in vitro* transcribed tRNA does however lack several conserved post-transcriptional modifications added by a variety of enzymes in the cell. These enzymes and their resulting modifications vary between species and tRNA molecules, however the modifications have been shown to be important for tRNA stability, anticodon recognition, and binding by host translational machinery[24]. While many of these modifications are conserved between species, it is likely that many human (or other mammalian) enzymes will not recognize bacterial, protozoan, or yeast tRNA due to variations in tRNA sequence and structure. Therefore, if crucial modifications are not introduced, the orthogonal tRNA may be recognized as foreign and degraded or not be tightly bound by elongation factor-1α (EF-1α) as a required preliminary step to ribosome delivery. Interestingly, the orthogonal synthetase/tRNAs evolved for use in mammalian cells employ a bacterial tRNA. These tRNAs bind their cognate synthetase, which is an early step in elongation factor recruitment. Therefore, these orthogonal tRNA molecules may either be modified appropriately by host machinery, can be directly handed off to EF-1α to

facilitate incorporation into the growing peptide, or may suggest that these modifications are not necessary during over-producing conditions.

2) *tRNA not recognized by elongation factors or the ribosome:* Prior to incorporation of an amino acid by an endogenous tRNA: the mature tRNA molecule binds its cognate synthetase, is acylated with its corresponding amino acid, is handed off to elongation factors, and is finally passed off to the ribosome by the elongation factor. Because the orthogonal tRNAs used in these studies cannot (by design) bind to any of the endogenous synthetases, it is possible that binding by the elongation factors is impaired. Without the synthetase to hand off the acylated orthogonal tRNA to the elongation factor, the tRNA may remain in solution long enough that the degradation rate is higher than the binding rate to the elongation factors. To overcome this issue, over-expressing the elongation factor EF-1α may allow for a larger population of acylated tRNA to be sequestered from degradation pathways and shuttled to the ribosome for incorporation. Alternatively, a "dummy" synthetase could be used that lacks enzymatic activity (cannot acylate the tRNA), but is capable of binding the tRNA and elongation factors for hand-off.

3) *Transfection/incubation temperature:* Mammalian cells are transfected/incubated at significantly different temperatures than *X. laevis* oocytes: 37^{o}C vs. 18^{o}C, respectively. The higher incubation temperature may lead to denaturing of the tRNA or an increase in the stringency for binding interactions. For example, although the orthogonal tRNAs bind elongation factors sufficiently well in *X. laevis* oocytes, the added temperature might provide enough energy to break the

non-ideal noncovalent interactions that hold together the exogenous tRNA/endogenous elongation factor complex, therefore decreasing translation efficiency.

4) *Hydrolysis of amino acid from the tRNA:* The increased incubation temperature of mammalian cells might also lead to increased hydrolysis of the *in vitro* acylated amino acid off of the tRNA. Similar to oocyte experiments, the amino acid is deprotected by UV irradiation before transfection. Once deprotected, the amino acid becomes a labile group that can be hydrolyzed in water. In addition to higher incubation temperatures, the transfection time is longer for mammalian cells than for oocytes. In an oocyte experiment, the tRNA is directly injected into the cell where it is can be rapidly bound by elongation factors and shuttled to the ribosome for incorporation into the growing peptide. Conversely, in mammalian cells, the tRNA is mixed with transfection reagent and applied externally to cells. Over a period of 24 hours the transfection reagent/DNA/tRNA complexes diffuse across the cell membrane delivering nucleic acid to the transcriptional/translational machinery. During these 24 hours, any tRNA that is external to the cell is not protected by elongation factors and is therefore susceptible to hydrolysis. Use of α-hydroxy acids and/or pre-incubation with purified EF-1α might lead to decreased hydrolysis rates.

5) *Low concentration of stoichiometric tRNA reagent:* Because the tRNA is applied external to cells rather than through direct injection, higher amounts of tRNA are required to achieve a comparable concentration of intracellular tRNA as we use in oocyte experiments. Unfortunately, a proportional increase in transfection

reagent is required for higher concentrations of nucleic acid, which leads to a decrease in cell viability. In a typical oocyte experiment, assuming 50 nL of 1 μg/μL tRNA is injected into an oocyte with a diameter of 1 mm, the concentration of tRNA inside the cell is 95.5 μg/mL. We were able to transfect a maximum of 8 μg of tRNA in a 35 mm dish with 3 mL of media over the cells, which amounts to 2.67 μg/mL of tRNA in solution. This concentration is approximately 35-fold less than that used in a typical oocyte experiment and is likely a major contribution to the lack of protein expression.

6) *Misfolded/denatured/hydrolyzed by transfection reagents:* It is possible that during complexation with the transfection reagent the tRNA is denatured or misfolded from its normal structure. Therefore, upon delivery to the cytoplasm, the single stranded unmodified RNA would likely appear as foreign to the cell and would be quickly degraded. Most transfection reagents are designed and optimized for nucleic acids without a defined structure such as: DNA, mRNA, or siRNA. It is possible that a new class of transfection reagents might be required to more effectively transport tRNA across the membrane.

Acknowledgements

I would like to thank Sarah Lummus, A.J. Thompson, and Shawna Frazier for teaching me all I know about cell culture and use of the FlexStation. I would also like to thank Crystal Dilworth for helping us with the confocal experiments.

References

1. Daeffler, K.N., Lester, H.A., and Dougherty, D.A., Functionally Important Aromatic-Aromatic and Sulfur-pi Interactions in the D2 Dopamine Receptor. *J Am Chem Soc*, **2012**. *134*(36): p. 14890-14896.
2. Zhong, W.G., Gallivan, J.P., Zhang, Y.O., Li, L.T., Lester, H.A., and Dougherty, D.A., From ab initio quantum mechanics to molecular neurobiology: A cation-pi binding site in the nicotinic receptor. *Proceedings of the National Academy of Sciences of the United States of America*, **1998**. *95*(21): p. 12088-12093.
3. Limapichat, W., Lester, H.A., and Dougherty, D.A., Chemical Scale Studies of the Phe-Pro Conserved Motif in the Cys Loop of Cys Loop Receptors. *Journal of Biological Chemistry*, **2010**. *285*(12): p. 8976-8984.
4. Xiu, X., Puskar, N.L., Shanata, J.A., Lester, H.A., and Dougherty, D.A., Nicotine binding to brain receptors requires a strong cation-pi interaction. *Nature*, **2009**. *458*(7237): p. 534-537.
5. Nowak, M.W., Gallivan, J.P., Silverman, S.K., Labarca, C.G., Dougherty, D.A., and Lester, H.A., In vivo incorporation of unnatural amino acids into ion channels in Xenopus oocyte expression system. *Methods Enzymol*, **1998**. *293*: p. 504-529.
6. Noren, C.J., Anthonycahill, S.J., Griffith, M.C., and Schultz, P.G., A General-Method for Site-Specific Incorporation of Unnatural Amino-Acids into Proteins. *Science*, **1989**. *244*(4901): p. 182-188.
7. Liu, C.C. and Schultz, P.G., Adding New Chemistries to the Genetic Code. *Annual Review of Biochemistry, Vol 79*, **2010**. *79*: p. 413-444.
8. Santoro, S.W., Wang, L., Herberich, B., King, D.S., and Schultz, P.G., An efficient system for the evolution of aminoacyl-tRNA synthetase specificity. *Nature Biotechnology*, **2002**. *20*(10): p. 1044-1048.
9. Liu, W.S., Brock, A., Chen, S., Chen, S.B., and Schultz, P.G., Genetic incorporation of unnatural amino acids into proteins in mammalian cells. *Nature Methods*, **2007**. *4*(3): p. 239-244.
10. Chin, J.W., Cropp, T.A., Anderson, J.C., Mukherji, M., Zhang, Z.W., and Schultz, P.G., An expanded eukaryotic genetic code. *Science*, **2003**. *301*(5635): p. 964-967.
11. Young, D.D., Young, T.S., Jahnz, M., Ahmad, I., Spraggon, G., and Schultz, P.G., An Evolved Aminoacyl-tRNA Synthetase with Atypical Polysubstrate Specificity. *Biochemistry*, **2011**. *50*(11): p. 1894-1900.
12. Monahan, S.L., Lester, H.A., and Dougherty, D.A., Site-specific incorporation of unnatural amino acids into receptors expressed in mammalian cells. *Chemistry & Biology*, **2003**. *10*(6): p. 573-580.
13. Kohrer, C., Xie, L., Kellerer, S., Varshney, U., and Rajbhandary, U.L., Import of amber and ochre suppressor tRNAs into mammalian cells: A general approach to site-specific insertion of amino acid analogues into proteins. *Proceedings of the National Academy of Sciences of the United States of America*, **2001**. *98*(25): p. 14310-14315.
14. Saks, M.E., Sampson, J.R., Nowak, M.W., Kearney, P.C., Du, F., Abelson, J.N., Lester, H.A., and Dougherty, D.A., An engineered Tetrahymena tRNAGln for in

vivo incorporation of unnatural amino acids into proteins by nonsense suppression. *J Biol Chem*, **1996**. *271*(38): p. 23169-23175.

15. Rodriguez, E.A., Lester, H.A., and Dougherty, D.A., In vivo incorporation of multiple unnatural amino acids through nonsense and frameshift suppression. *Proceedings of the National Academy of Sciences of the United States of America*, **2006**. *103*(23): p. 8650-8655.
16. Kao, C., Zheng, M., and Rudisser, S., A simple and efficient method to reduce nontemplated nucleotide addition at the 3 ' terminus of RNAs transcribed by T7 RNA polymerase. *Rna-a Publication of the Rna Society*, **1999**. *5*(9): p. 1268-1272.
17. Nowak, M.W., Gallivan, J.P., Silverman, S.K., Labarca, C.G., Dougherty, D.A., and Lester, H.A., In vivo incorporation of unnatural amino acids into ion channels in Xenopus oocyte expression system. *Ion Channels, Pt B*, **1998**. *293*: p. 504-529.
18. Lummis, S.C.R., Thompson, A.J., Bencherif, M., and Lester, H.A., Varenicline Is a Potent Agonist of the Human 5-Hydroxytryptamine(3) Receptor. *Journal of Pharmacology and Experimental Therapeutics*, **2011**. *339*(1): p. 125-131.
19. Srinivasan, R., Pantoja, R., Moss, F.J., Mackey, E.D.W., Son, C.D., Miwa, J., and Lester, H.A., Nicotine up-regulates alpha 4 beta 2 nicotinic receptors and ER exit sites via stoichiometry-dependent chaperoning. *Journal of General Physiology*, **2011**. *137*(1): p. 59-79.
20. Puskar, N.L., Xiu, X.A., Lester, H.A., and Dougherty, D.A., Two Neuronal Nicotinic Acetylcholine Receptors, alpha 4 beta 4 and alpha 7, Show Differential Agonist Binding Modes. *Journal of Biological Chemistry*, **2011**. *286*(16): p. 14618-14627.
21. Price, K.L. and Lummis, S.C.R., FlexStation examination of 5-HT3 receptor function using Ca2+ and membrane potential-sensitive dyes: Advantages and potential problems. *Journal of Neuroscience Methods*, **2005**. *149*(2): p. 172-177.
22. Beene, D.L., Brandt, G.S., Zhong, W., Zacharias, N.M., Lester, H.A., and Dougherty, D.A., Cation-pi interactions in ligand recognition by serotonergic (5-HT3A) and nicotinic acetylcholine receptors: the anomalous binding properties of nicotine. *Biochemistry*, **2002**. *41*(32): p. 10262-10269.
23. Thompson, A.J., Lochner, M., and Lummis, S.C.R., Loop B Is a Major Structural Component of the 5-HT(3) Receptor. *Biophysical Journal*, **2008**. *95*(12): p. 5728-5736.
24. Phizicky, E.M. and Hopper, A.K., tRNA biology charges to the front. *Genes & Development*, **2010**. *24*(17): p. 1832-1860.

Chapter 4

Functional Evaluation of Key Interactions Evident in the Structure of the Eukaryotic Cys-loop Receptor GluCl

Abstract

The publication of the first high-resolution crystal structure of a eukaryotic Cys-loop receptor, GluClα, has provided valuable structural information on this important class of ligand-gated ion channels (LGIC). However, limited functional data exists for the GluCl receptors. Before applying the structural insights from GluCl to mammalian Cys-loop receptors such as nicotinic acetylcholine and GABA receptors, it is important to establish that conserved functional features of this receptor class are present in the more distantly related GluCl receptors. Here, we seek to identify these ligand-binding interactions, including the frequently observed cation-π interaction. Our studies were performed in the homologous GluClβ receptor because GluClα is not activated by glutamate in *Xenopus laevis* oocytes. Mutagenesis of the signal peptide and pore lining helix was performed to enhance functional expression and sensitivity to applied ligand, respectively. Conventional and unnatural amino acid mutagenesis indicate a strong cation-π interaction between Y206 and the protonated amine of glutamate as well as other important ionic and hydrogen bond interactions between the ligand and the binding site, as predicted by the crystal structure.

Introduction

The Cys-loop receptors are a family of pentameric ligand-gated ion channels involved in fast synaptic transmission. They are the target of a variety of native neurotransmitters, along with therapeutics targeting, among others, Parkinson's disease, Alzheimer's disease, schizophrenia, pain, and nicotine addiction in humans[1-3]. Members of this family include the excitatory, cation-permeable, nicotinic acetylcholine receptors (nAChRs) and 5-HT_{3A} receptors, and the inhibitory, anion-permeable, $GABA_{A/C}$ and glycine receptors. These receptors possess conserved structural elements, including an extracellular ligand binding domain, four transmembrane helices of which one, M2, forms the channel pore, and the eponymous disulfide loop in the extracellular domain.

Until recently, structural models of Cys-loop receptors were based on the low resolution cryo-EM structures of the *Torpedo marmorata* nAChR[4,5] or the high resolution X-ray crystal structures of acetylcholine binding proteins[6], soluble proteins homologous to the extracellular, ligand-binding domain of the full length receptor. However, recent developments in membrane protein crystallography have led to a wealth of new high-resolution structures including two homologous bacterial ligand-gated ion channels, ELIC and GLIC[7-9], and most recently, GluClα, from *Caenorhabditis elegans*[10].

GluCl represents a true, eukaryotic Cys-loop receptor, although there is no mammalian homologue. It is an anion-permeable channel, and it displays 34% sequence identity to its closest human homolog, the α1 glycine receptor. The GluClα receptor was crystallized in the presence of the native orthosteric ligand, glutamate, as well as the positive allosteric modulator, ivermectin, a broad-spectrum antiparasitic clinically used for the treatment of river blindness in humans and animal parasites in veterinary

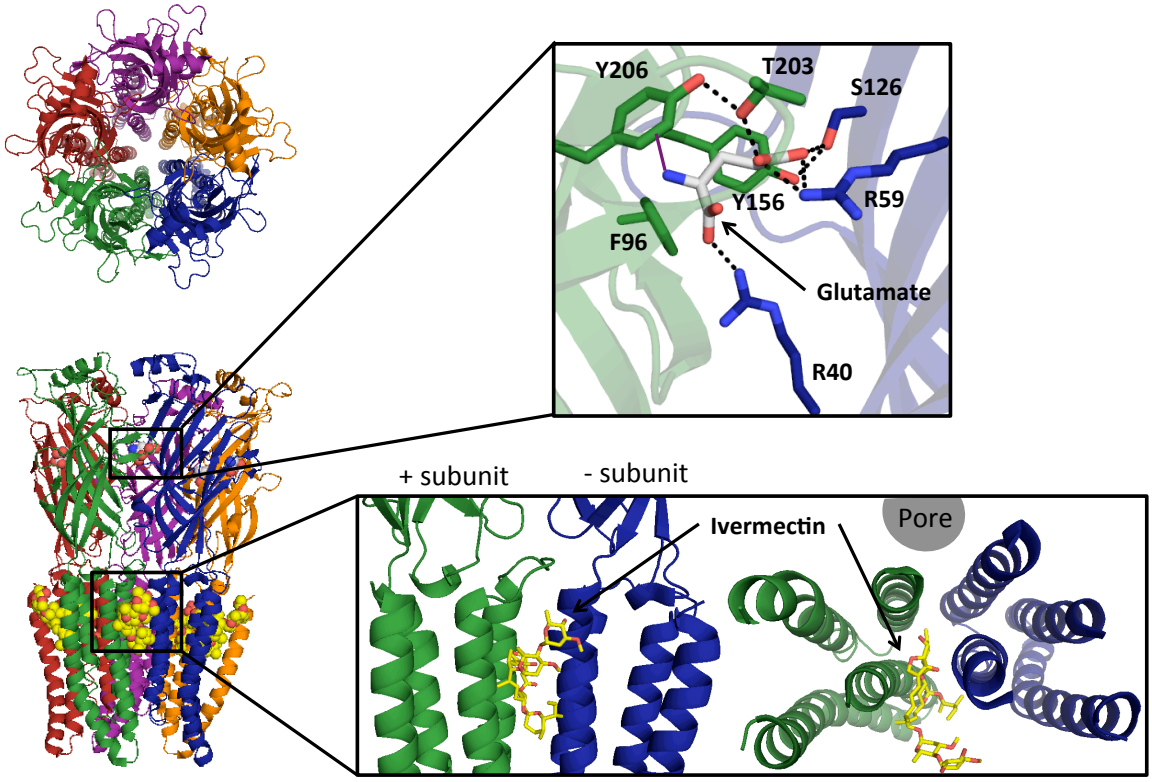

Figure 4.1. Crystal structure of GluClα crystallized in the presence of glutamate and ivermectin (PDB ID: 3RIF)[10]. Both ligands bind at the interface of two identical subunits with glutamate binding at the extracellular orthosteric ligand binding site and ivermectin at an allosteric site in the transmembrane region. The primary (+) and complementary (-) subunits are indicated in green and blue, respectively.

medicine[3,11-13] (Figure 4.1). Both ligands were shown to bind at the interface of two subunits of which the primary (+) subunit contributes loops A-C and the complementary (-) subunit loops D-F to the orthosteric glutamate binding site.

While the GluClα structure represents a milestone in the study of Cys-loop receptors, relatively few functional studies on this receptor have been reported. In contrast, a large number of wide-ranging functional studies of mammalian Cys-loop receptors have been reported[1,14,15]. In our own labs we have developed a series of functional probes based on unnatural amino acid mutagenesis that provide high precision information on drug-receptor interactions and protein structural features. These include a

cation-π interaction between the protonated amine of endogenous ligands and one of several conserved aromatic amino acids in the binding site, which has been demonstrated in all Cys-loop receptors studied to date[16]. In addition, several hydrogen bonding interactions, including hydrogen bonds to the protein backbone, have been established to be important in several Cys-loop receptors.

In the present work we set out to determine whether key structural features of the *C. elegans* GluClα receptor have functional consequences that parallel those seen in mammalian Cys-loop receptors. Mutagenesis was performed on the closely related GluClβ receptor because the GluClα receptor is not activated by glutamate in the absence of ivermectin in *Xenopus laevis* oocytes[17]. Every ligand-binding residue considered here is conserved in the two forms, however residues in the M2 helix vary between receptors. To facilitate these studies, the receptor had to be optimized for expression in *Xenopus* oocytes, by altering the signal peptide and by introducing a mutation in the pore-lining regions. Our studies find functional significance for many of the key features of the GluClα receptor structure, and also highlight the challenges of probing binding interactions in invertebrate receptors.

Methods

Molecular biology. The mammalian codon optimized GluClβ receptor from *C. elegans*[18] was subcloned into the pGEMhe vector and the stop codon of the receptor was mutated from TAG to TGA. Mutagenesis of the GluClβ receptor was performed using the QuikChange protocol (Stratagene), and for nonsense suppression experiments, a TAG codon was mutated into the site of interest. The cDNA was linearized using SbfI (New

England Biolabs) and mRNA was produced from the linearized plasmids by using the T7 mMessage Machine kit (Ambion).

74mer THG73 tRNA was *in vitro* transcribed from a DNA oligonucleotide template containing two 5' methoxy (C2' position) nucleotides to site-specifically truncate transcription by the T7 MEGAshortscript kit (Ambion)[19]. Amino acids chemically appended to dCA were ligated to the 74mer tRNA, resulting in full-length acylated tRNA, using methods previously described[20]. Acylation of tRNA was confirmed using MALDI mass spectrometry using a 3-hydroxypicolinic acid matrix. The NVOC protecting group on the amino acid was removed immediately prior to injection through a 5-minute irradiation step using a 1 kW Xenon lamp with WG-335 and UG-11 filters.

Chimeras. Chimeras were synthesized by mutating in an EcoRI restriction enzyme site (GAATTC) in both the GluClα and GluClβ receptors at the desired cut site. First, the inherent EcoRI site in the GluClα M3-M4 loop (AT**GAATTC**C) was removed using silent mutations (AT**GAACAG**C) to eliminate undesired cutting. The mutated receptors were then cut with EcoRI and HindIII (5' of the encoded gene) and the fragments separated by gel electrophoresis on a 1% agarose gel. The resulting bands were isolated and purified using a gel extraction kit (Qiagen) and the desired GluClα and GluClβ fragments were ligated together using DNA ligase. The engineered EcoRI restriction site was then mutated back to the wild type α/β or β/α sequence and mRNA was produced as described above.

Oocyte preparation and injection. Stage V-VI *Xenopus laevis* oocytes were harvested and injected with RNA as previously described[20]. For nonsense suppression experiments, 37.5 ng of receptor mRNA was coinjected with excess deprotected ~1 μg/μL tRNA solution both 48 hours and 24 hours before recording. For conventional mutagenesis, 12.5 ng of receptor mRNA was injected 48 hours before recording. As a negative control, all nonsense suppression sites were tested with a full length 76mer tRNA lacking an attached amino acid to ensure no read-through expression was observed.

Data Collection and analysis. All oocyte experiments were performed on an OpusXpress 6000A (Axon Instruments) using two-electrode voltage clamp mode. The recording buffer was calcium-free ND96 (96 mM NaCl, 2 mM KCl, 1 mM $MgCl_2$, and 5 mM HEPES, pH 7.5). The initial holding potential was -60 mV. Data were sampled at 125 Hz and filtered at 50 Hz. A calcium-free ND96 prewash was applied for 30 s (1 mL/min.) followed by application of agonist for 15 s (4 mL/min.). Agonist was then washed out with calcium-free ND96 buffer for 116 s (3 mL/min.). Agonist-induced currents were measured from the baseline. Glutamate dose solutions were made in calcium-free ND96 buffer from a 50 mM (pH 7.5) stock solution. The maximum dose of 100 mM glutamate was made from the glutamate-HCl salt in water and brought to a pH of 7.5.

Data were fit to the Hill equation, $I_{norm} = 1/(1 + (EC_{50}/A))\ n_H$, where I_{norm} is the normalized current peak at [agonist] = A, EC_{50} is the concentration of agonist that elicits a half-maximum response, and n_H is the Hill coefficient. EC_{50} values were obtained by averaging the I_{norm} values for each agonist concentration and fitting those values to the

Hill equation. $\Delta\Delta G$ values were calculated by the equation $\Delta\Delta G=-RT\ln\Omega$, where $\Omega=[EC_{50}(mut_{1,2})*EC_{50}(WT)]/[EC_{50}(mut_1)*EC_{50}(mut_2)]$.

Results and Discussion

Mutagenesis of pore lining residues to increase the sensitivity of GluClβ to glutamate. Mutation of the pore lining residues on the M2 helix of Cys-loop receptors has had dramatic effects on ligand sensitivity[21-23], open channel duration[21,24], and receptor desensitization[22,25]. Specifically, mutation of a conserved hydrophobic residue in the 9' position (i.e., the 9th residue from the N-terminus of helix M2, Figure 4.2) has been used in nicotinic acetylcholine receptors (nAChRs) to increase ligand sensitivity and current size, thereby facilitating measurement of low expressing and large loss-of-function mutations[26-28]. Similar to many nAChRs, the GluClβ homomeric receptor gives small current responses to applied glutamate and demonstrates a relatively high wild type EC_{50} of 0.35 mM (Table 4.1). The high EC_{50} value is problematic for measuring loss-of-function mutations for many reasons. Glutamate is not soluble at concentrations higher than 50 mM in buffered solution, and while a hydrochloride salt increases this solubility, it also dramatically increases the osmolarity of the solution to several times greater than the running buffer[29]. Also, at high concentrations of glutamate, currents are observed in uninjected oocytes, which may be due to non-specific activation of endogenous receptors or osmotic response. These currents, while small, complicate measurement of low-expressing mutants. Also, in high expressing mutants, rapid desensitization of GluClβ occurs at concentrations greater than 100 mM, prohibiting further measurements.

Therefore, to enable measurement of low expressing and large loss-of-function mutants, it is important to lower the EC_{50} of the wild type receptor.

Unlike 9' mutations in individual nAChR subunits, mutation of the L9' residue in GluClβ to either alanine or phenylalanine led to constitutive activation of the receptor, characterized by large baseline currents (>1 μA), and no additional response to applied glutamate. A similar increase in basal activation of GluClαβ heteromers was previously observed in GluClαL9'X-βWT receptors, along with a decrease in the amplitude of the ligand response in HEK293 cells[23]. An exception to this was the GluClαL9'F-βWT receptor, which demonstrated increased sensitivity to ivermectin and glutamate (not shown) with no loss of signal amplitude. The gain-of-function phenotype was not observed in GluClαL9'F homomers and is not observed here in GluClβL9'F homomers, indicating the effect may be specific to the heteromeric receptor. Similar observations have been reported in other Cys-loop receptors [21,29]. All receptors with 9' mutations that give large functional responses and an increase in ligand sensitivity are heteromeric receptors, where fewer than five individual subunits contained the

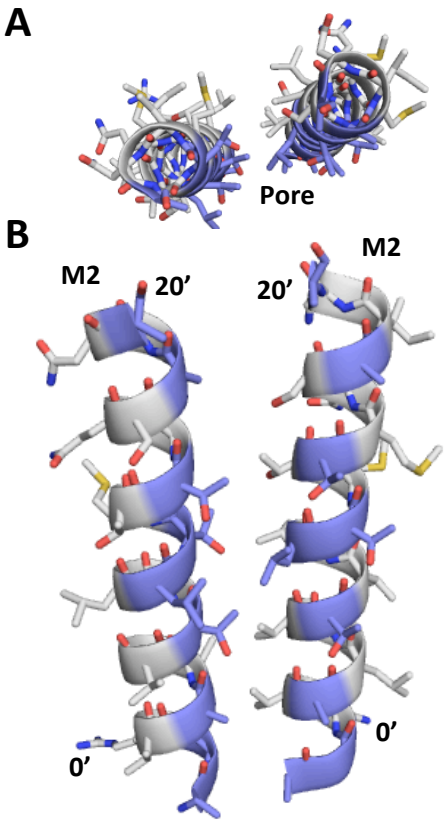

Figure 4.2. The M2 pore lining helix of GluClβ. View from (A) the top of the receptor and (B) from the side. Residues in the ion-conducting pore are highlighted in blue and the location of the 0' arginine and 20' alanine are indicated. Side chains of the GluClα crystal structure were mutated to the corresponding GluClβ side chains in PyMol.

9’ mutation. In the cases where all five subunits had 9’ mutations, either in homomeric or multiply mutated receptors, small ligand-induced responses and high resting currents were observed, indicative of receptor activation in the absence of agonist. Therefore, to create a receptor with increased sensitivity to glutamate and no significant loss of current amplitude, other pore-lining residues, potentially with a lesser effect on channel gating, were targeted for mutagenesis.

The GluClα crystal structure (PDB ID: 3RIF) indicates that the pore-lining residues are at the -2’, -1’, 2’, 6’, 9’, 10’, 13’, 17’, and 20’ positions in the M2 helix (Figure 4.2). These residues physically shape the channel and influence the conductance and the equilibrium between inactive and active conformations through the presence or

Table 4.1: GluClβ M2 helix mutations

Mutation	EC_{50} (mM)	Hill	n	I_{max} (μA)	Fold shift
WT	0.35 +/- 0.01	2.5 +/- 0.2	20	0.4-4	-
AG-2',-1'PA	0.46 +/- 0.01	1.8 +/- 0.1	10	12-66	1.3
A2'S	0.63 +/- 0.01	2.0 +/- 0.1	12	0.6-6	1.8
A2'T	No response				
T6'A	Very low response				
T6'S	0.0080 +/- 0.0005	2.4 +/- 0.3	27	0.06-8	1/44
L9'A	Constitutively active				
L9'F	Constitutively active				
L9'V	No response				
T10'A	0.013 +/- 0.001	2.8 +/- 0.1	14	2-28	1/27
T10'S	0.011 +/- 0.001	2.5 +/- 0.1	14	0.3-4	1/32
T13'A	0.038 +/- 0.001	2.8 +/- 0.1	11	0.1-6	1/9
T13'S	No response				
A17'G	>5		10		
A17'S	0.23 +/- 0.01	2.5 +/- 0.1	10	0.6-12	1/1.5
A17'T	0.058 +/- 0.001	2.8 +/- 0.1	13	0.3-13	1/6
A20'S	No response				
A20'T	0.11 +/- 0.02	1.7 +/- 0.1	14	0.5-48	1/3
T6'S/T10'S	Constitutive activity - some glutamate response				

absence of steric bulk and polarity of the side chains[30]. In this study, to modulate these properties of the receptor, the pore-lining residues were mutated to amino acids of varying size and polarity (Table 4.1). Constitutive activity was only observed in mutations at the 9' site, whereas mutations to the other residues had varied effects on receptor EC_{50} and current across the membrane. Of the mutations tested, the T6'S mutation led to the greatest increase in receptor sensitivity (44-fold), followed by mutation of the T10' residue to either alanine or serine (27 and 32-fold, respectively), and the T13'A mutation (9-fold). The T6'A and T13'S mutants were not functional. These results indicate that smaller residues near the pore constriction facilitate channel opening, and that while polarity of the 6' side chain is required, it is not important at the 10' or 13' positions. The double mutant T6'S/T10'S gave low agonist response and high leak currents indicative of agonist-independent openings as was observed in the L9'A and L9'F mutants.

To ensure that the T6'S mutation does not affect measurement of other side chain substitutions, a distal loss-of-function mutation was incorporated into the wild type and T6'S containing receptor for comparison. This mutation, Y206F, is located in the extracellular domain of the receptor at the glutamate binding site and disrupts an important hydrogen bond between itself and a nearby threonine side chain, T203 (see below). The loss-of-function observed in the T6'S/Y206F mutant was 12.5-fold compared to 12.3-fold in the single Y206F mutant. These values are not significantly different and therefore indicate that the T6'S mutation is multiplicative and should not affect measurement of binding site interactions (Table 4.2). No effect on signal amplitude was observed in T6'S-containing receptors. Because of the large increase in

glutamate sensitivity and a demonstrated lack of coupling between the T6'S mutation and the ligand binding site, it was determined that incorporation of T6'S as a background mutation is ideal for measuring large loss-of-function mutations to the GluClβ receptor.

Table 4.2. Multiplicative effect of the T6'S mutation

Mutation	EC_{50} (mM)	Hill	n	I_{max} (μA)	Fold Shift
WT	0.35 +/- 0.01	2.5 +/- 0.2	20	0.4-3.9	-
T6'S	0.0080 +/- 0.0005	2.4 +/- 0.3	27	0.06-8	-
Y206F	4.3 +/- 0.1	2.4 +/- 0.1	13	0.2-8	12.3
T6'S/Y206F	0.10 +/- 0.01	2.6 +/- 0.3	14	0.14-7	12.5

Of the other mutations tested, only small shifts in EC_{50} were observed. Mutagenesis of the -2' and -1' residues to be like the GluClα receptor (AG to PA) resulted in no shift of EC_{50}, but a large increase in current through the channel. It is also interesting to note that while the A2'S mutation had minimal effect on receptor function, the A2'T mutation abolished sensitivity of the receptor to glutamate. The converse mutation in GluClα, T2'A, was previously shown to restore glutamate sensitivity to an otherwise glutamate-insensitive channel[17]. It is therefore likely that the 2' residue plays an important role in the coupling of ligand binding to receptor activation.

Optimization of receptor expression. It has been shown previously that surface expression of the GluClβ homomeric receptor in HEK293 cells is low relative to the homomeric GluClα and the heteromeric GluClαβ receptors, because it is retained in the endoplasmic reticulum (ER) more so than other GluCl receptors[23]. We observe this functionally in *X. laevis* oocytes, with approximately 10-fold enhanced currents of the heteromer relative to the GluClβ homomeric receptor (data not shown). Data for the

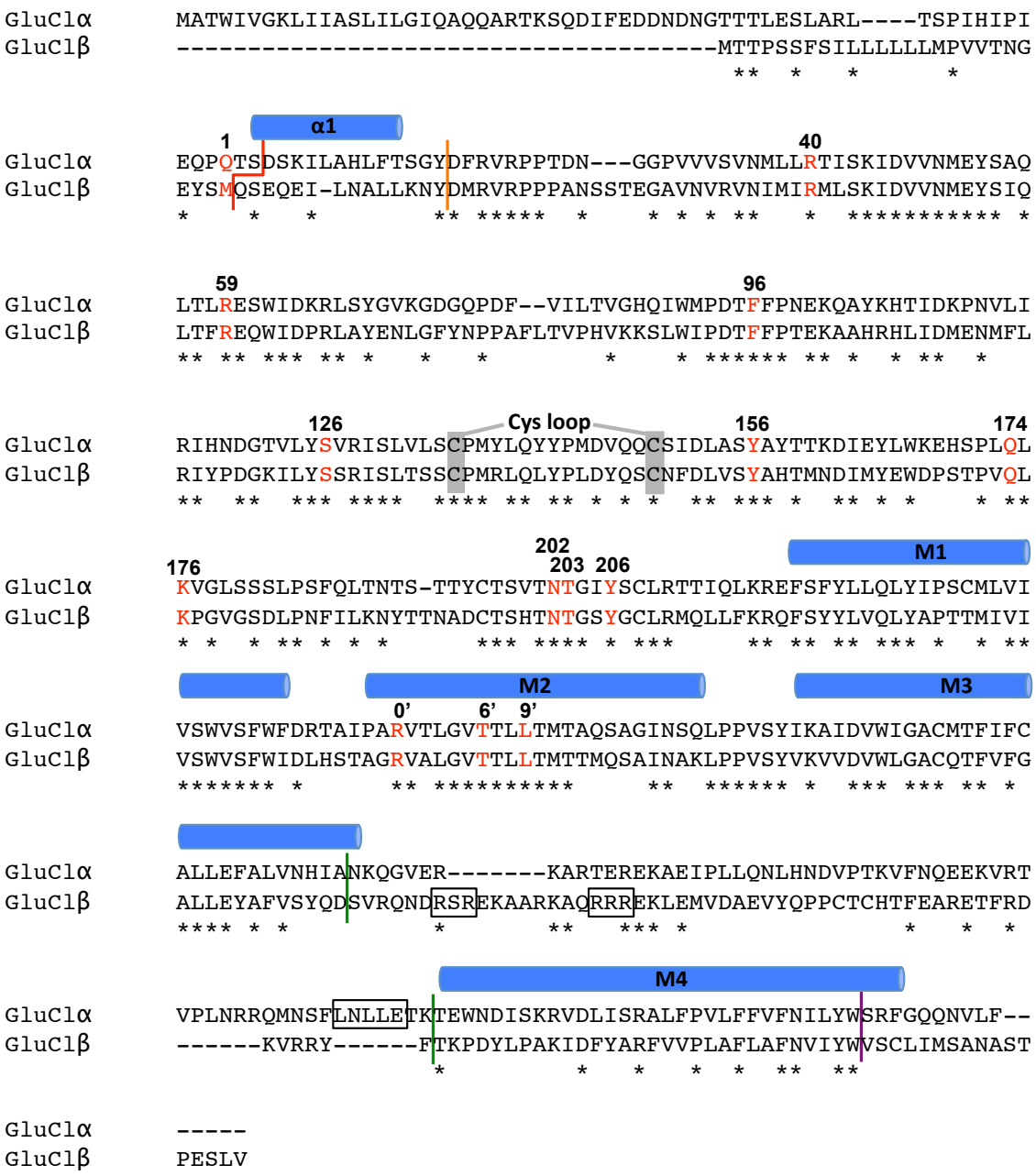

Figure 4.3. Sequence alignment of GluClα and GluClβ. Sites for chimera synthesis and receptor mutagenesis are indicated: α signaling peptide chimera spliced at red line, α signaling peptide + α1 helix spliced at orange line, M3-M4 loop spliced between green lines, C terminus spliced at purple line, and putative ER retention RxR motifs and ER export LxxLE motif are highlighted in black boxes. Sequence alignment was made using Clustal Omega.

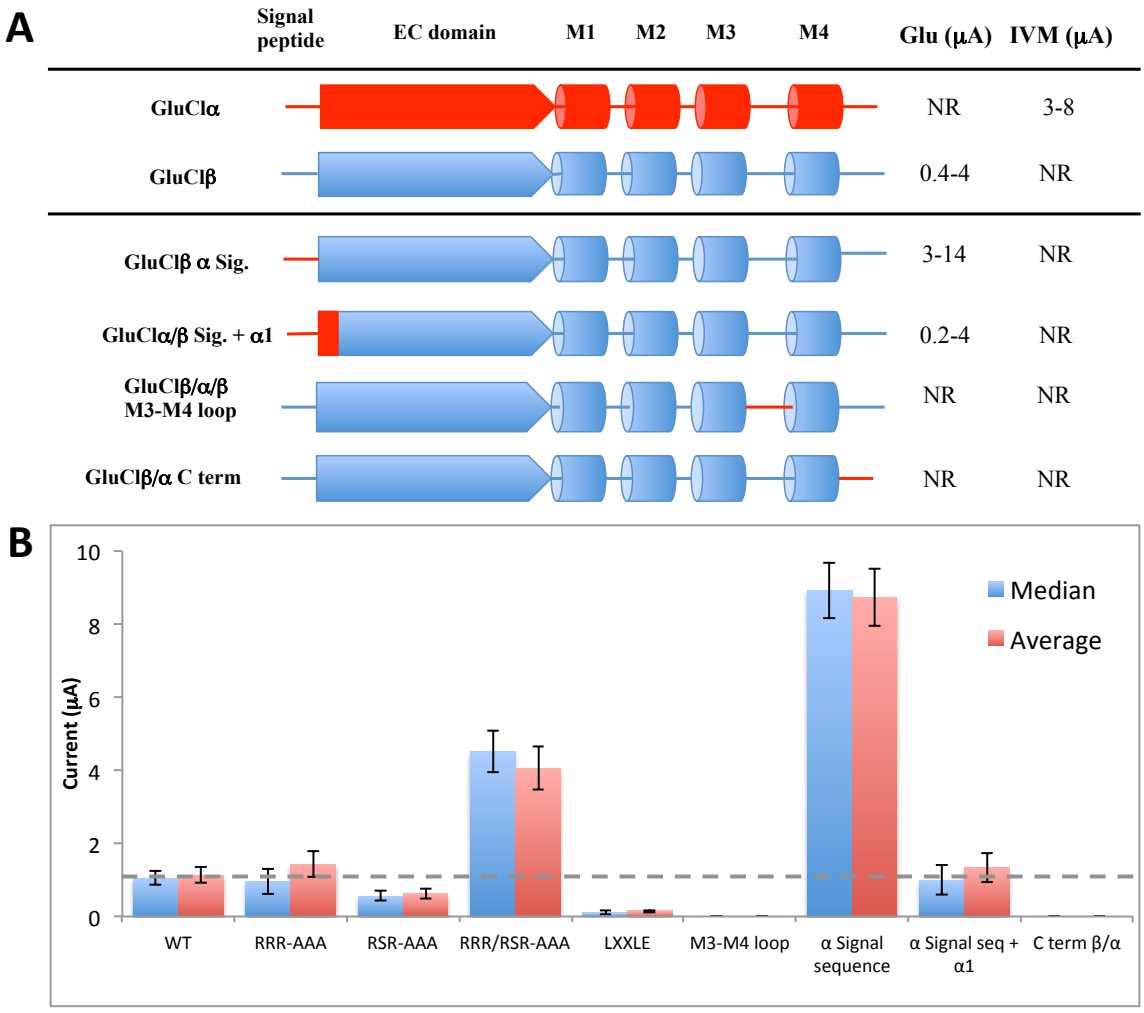

Figure 4.4. Effects of mutations and chimeras on GluClβ functional expression. **(A)** Schematic of chimeras examined and **(B)** average and median currents from *X. laevis* oocytes expressing the specified mutant receptor.

homomeric GluClα receptor are not available because this receptor is not gated by glutamate in *X. laevis* oocytes[17]. The relatively low receptor expression of GluClβ does not affect studies of wild type GluClβ or conventional mutants, however expression becomes an issue when attempting to incorporate unnatural amino acids by nonsense problematic to distinguish between a receptor that does not respond to the applied glutamate concentrations and a receptor that is expressed too poorly to detect. To avoid

Table 4.3: Effects of receptor mutagenesis on functional expression. All mutations have the T6'S mutation unless otherwise noted.

Mutation	EC_{50} (μM)	Hill	n	I_{max} (μA)	Median (μA)	Average (μA)	Fold Change Median	Fold Change Average
WT	11 +/- 1	3.0 +/- 0.1	19	0.1-4	1.1	1.1	-	-
RRR_AAA	14 +/- 1	2.8 +/- 0.1	15	0.1-4	1.0	1.4	1	1
RSR_AAA	14 +/- 1	2.6 +/- 0.1	15	0.1-3	0.6	0.6	-2	-2
RRR/RSR_AAA	15 +/- 1	2.8 +/- 0.1	20	0.8-10	4.5	4.1	4	4
LXXLE	14 +/- 1	3.2 +/- 0.1	12	0.02-0.23	0.1	0.15	-11	-8
M3-M4 loop	No response							
α signal peptide (no T6'S)	980 +/- 20	1.9 +/- 0.1	16	3-14	8.9	8.7	9	8
α signal peptide + α1 (no T6'S)	110 +/- 10	2.6 +/- 0.2	14	0.2-6	1.0	1.4	1	1
M4-C term β/α	No response							

this issue, we sought to increase receptor expression without affecting the receptor's function.

To enhance functional surface expression of GluClβ receptors, point mutants or chimeras with GluClα segments were made in regions of the receptor previously shown to affect Cys-loop receptor trafficking and expression levels (Figure 4.3)[31-37]. These regions include the signal peptide, the C-terminus, and the intracellular M3-M4 loop, which contains two RxR putative ER retention motifs in the GluClβ receptor. Chimeras were made with GluClα since it does not accumulate in the ER and because of the high similarity between the receptors, which minimizes the chance of affecting receptor function. Of the mutations and chimeras examined, only GluClβ with the α signal peptide and the RSR/RRR_AAA mutant (replacement of all six residues in the two ER retention motifs with alanine) gave enhanced expression relative to the wild type receptor (Figure 4.4 and Table 4.3). Conversely, introduction of a putative ER export motif (LxxLE) in the M3-M4 loop decreased expression, and the M3-M4 loop and α C-

terminus chimeras resulted in non-functional receptors. Mutation of either RxR motif singly to AAA had no effect on receptor expression and replacement of the GluClβ α1 helix with the corresponding segment from GluClα neutralized the increased expression observed upon introduction of the GluClα signal peptide. Removal of both RxR ER retention motifs enhanced expression approximately 4-fold whereas the α signal peptide chimera had approximately 8-fold enhanced expression. The α signal peptide chimera gave currents comparable to other Cys-loop receptors, and therefore mutant receptors not responding to glutamate at the applied concentrations are assumed to be non-functional rather than inadequately expressed. No shift in EC_{50} was observed for any of the chimeras or mutants examined, with the exception of a less than three-fold loss of function of the α signal peptide chimera.

Evaluating Potential Cation-π Interactions. A cation-π interaction between agonist and receptor is a universal feature of Cys-loop receptors. These binding sites are rich in aromatic residues, and in most nAChRs and the $5HT_{3A}$ receptor, a Trp on loop B provides the π system. Receptors for smaller agonists such as GABA and glycine do not typically have Trp residues, and the cation-π interaction is formed to a Phe or Tyr. Along with loop B, aromatics on loops A and C have been shown to make cation-π interactions to agonists.

To facilitate visualization of the discussed residues in the GluClα crystal structure, the residue identifier for the corresponding GluClα amino acid is included after the GluClβ number (ex. Y206(200) corresponds to Yβ(α)). The GluClα numbering is included for the first mention of the residue only. The glutamate-bound GluClα crystal structure suggests a strong cation-π interaction between Y206(200) on the C loop and the

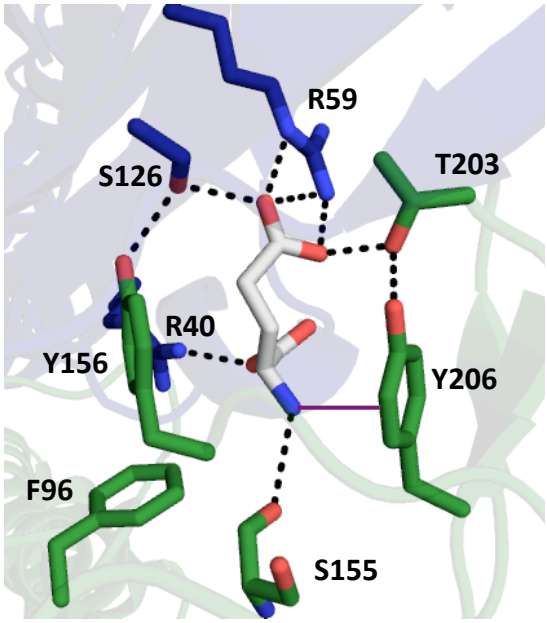

Figure 4.5. The glutamate binding site and predicted electrostatic interactions between the ligand and its surrounding amino acids. The primary subunit is colored in green and the complementary subunit in blue.

protonated amine of glutamate (Figure 4.5). The crystal structure also indicates the potential for a weaker, but still significant, electrostatic interaction between the α carbon of the ligand (which carries a substantial positive charge) and the face of Y156(151), located on the B loop. These aromatic residues are conserved among Cys-loop receptors and have been previously shown to participate in important cation-π interactions in other receptors with their corresponding ligands[26,38-41]. Additionally, a phenylalanine, F96(91), on loop A and a tryptophan on the D loop of the complementary face are conserved members of the aromatic binding box. However, these residues are not predicted to participate in an electrostatic interaction with the ligand or any other residue. A major difference between the GluCl receptors and other Cys-loop receptors is the absence of a second aromatic residue on the C loop (C1).

We have established a general protocol for evaluating cation-π interactions[16], in which the aromatic of interest is substituted with electron withdrawing groups that are known to diminish the cation-π binding ability of the ring (Figure 4.6). A clear correlation between cation-π binding ability and receptor function, as reported by EC_{50}, indicates a functionally significant cation-π interaction. An especially convenient system is a series of progressively fluorinated phenylalanine derivatives, which systematically

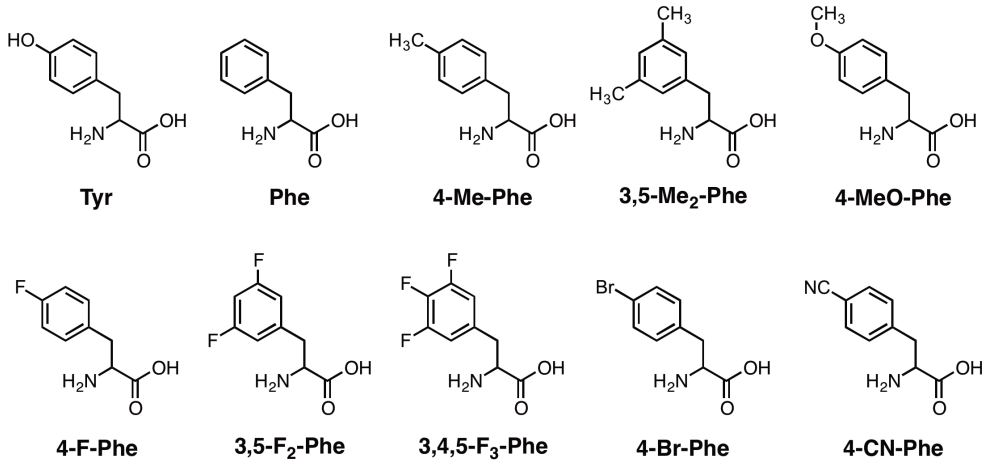

Figure 4.6. Chemical structures of amino acids used in this study.

Table 4.4. Unnatural amino acid mutagenesis of aromatic binding site residues. Data were obtained from a receptor containing the α signal peptide for enhanced functional expression. All mutants have the T6'S background mutation.

Mutation	EC_{50} (mM)	Hill	n	I_{max} (μA)	Fold Shift
WT	0.93 +/- 0.02	1.8 +/- 0.1	26	2-13	-
T6'S	0.013 +/- 0.001	2.7 +/- 0.2	17	2-13	-
F96TAG					
Phe	0.012 +/- 0.001	2.8 +/- 0.3	12	0.1-4	-
F_1-Phe	0.080 +/- 0.002	2.8 +/- 0.2	7	0.1-0.5	7
F_2-Phe	0.0047 +/- 0.0001	4.1 +/- 0.5	12	0.04-1	1/3
F_3-Phe	0.039 +/- 0.001	2.4 +/- 0.2	11	0.06-0.6	3
Y156F	15 +/- 1	2.3 +/- 0.2	15	1-5	-
Y156TAG					
Phe	17 +/- 1	1.7 +/- 0.1	15	1-4	-
OMe-Phe		No response			
F_1-Phe	14 +/- 1	2.0 +/- 0.1	20	0.1-5	1/1.2
F_2-Phe	49 +/- 3	1.8 +/- 0.1	13	0.2-4	3
F_3-Phe	65 +/- 5	1.7 +/- 0.1	11	0.3-2	4
Cha		No response			
Y206F	0.25 +/- 0.01	2.7 +/- 0.1	17	0.6-17	-
Y206TAG					
Phe	0.25 +/- 0.01	2.5 +/- 0.1	20	0.06-12	-
F_1-Phe	1.4 +/- 0.1	2.8 +/- 0.5	15	0.4-6	6
F_2-Phe	>100		20	0.1-1	
OMe-Phe	0.64 +/- 0.01	2.9 +/- 0.1	11	0.3-6	3
Br-Phe	1.5 +/- 0.1	3.1 +/- 0.1	11	1-13	6
CN-Phe	43 +/- 1	2.7 +/- 0.1	19	0.8-7	172

Table 4.5. Unnatural amino acid mutagenesis of aromatic binding site residues. Data were obtained from a receptor containing the wild type signal peptide. All mutants have the T6'S background mutation.

Mutation	EC_{50} (mM)	Hill	n	I_{max} (μA)	Fold Shift
WT	0.35 +/- 0.01	2.5 +/- 0.2	20	0.4-4	-
T6'S	0.0080 +/- 0.0005	2.4 +/- 0.3	27	0.06-8	-
Y156F	6.4 +/- 0.4	1.6 +/- 0.1	17	1-4	800
Y156TAG					
Phe	4.8 +/- 0.3	1.6 +/- 0.1	7	0.2-2	-
F_3-Phe	32 +/- 2	1.4 +/- 0.1	7	0.06-0.4	7
Y206F	0.10 +/- 0.01	2.6 +/- 0.3	14	0.14-7	-
Y206TAG					
Phe	0.16 +/- 0.01	3.0 +/- 0.2	8	0.07-0.30	-
F_1-Phe	0.64 +/- 0.01	2.8 +/- 0.1	9	0.04-0.34	4
F_2-Phe	>100		8	0.1-0.6	>250
OMe-Phe	0.56 +/- 0.01	1.8 +/- 0.1	11	0.1-1.4	4
Br-Phe	0.98 +/- 0.03	2.5 +/- 0.1	15	0.08-6	6
CN-Phe	19 +/- 1	2.8 +/- 0.2	14	0.8-6	119
Me-Phe	0.098 +/- 0.003	2.4 +/- 0.1	12	0.05-7	1/1.8

lower the cation-π binding ability. Such a study shows no electrostatic interaction between the ligand and either F96 or Y156, as indicated by the very small losses-of-function upon incorporation of F_3-Phe, a highly electron-deficient ring system (Table 4.4).

In contrast, electron-withdrawing groups added to Y206 strongly impacted receptor function. As before, we study substituted Phe analogues to avoid complications associated with lowering the pK_a of a Tyr residue when electron-withdrawing groups are added. Most telling is the large effect for 4-CN-Phe vs 4-Br-Phe. The two substituents present a similar steric perturbation, but only CN is strongly deactivating in a cation-π interaction. We were unable to study the series of fluorinated Phe derivatives that we have previously employed because 3,5-F_2-Phe gave receptors that did not reach their

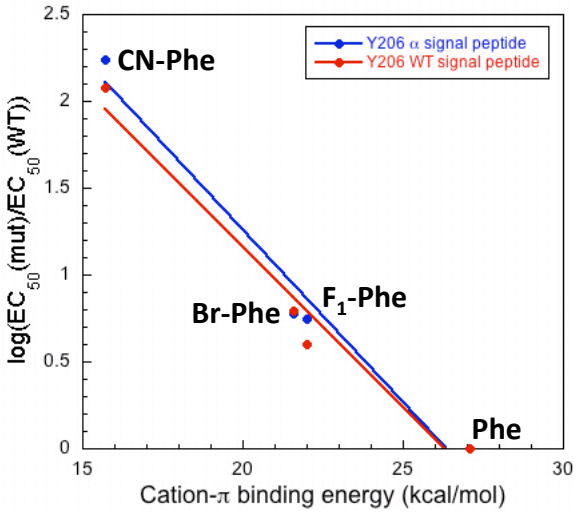

Figure 4.7. Plot of cation-π binding energy vs. mutant receptor loss-of-function at Y206. A linear trend is indicative of an electrostatic interaction with the face of the residue examined. Data for both the wild type and α signal peptide-containing templates are plotted together and indicate no effect of altering the signal peptide on receptor function

maximal response upon application of our highest concentration of glutamate, 100 mM. There is apparently a strong steric penalty for substituents in the meta position at residue 206, where the side chains of T201(195) and T203(197) could be impacted, as incorporation of 3,5-Me_2-Phe also resulted in nonfunctional receptors. As such, our study is restricted to 4-substituted Phe derivatives. With this more limited data set, a linear plot of calculated cation-π binding energy and the ratio of the mutant EC_{50} to the wild type could be obtained (Figure 4.7). Although this is a limited data set, we feel the correlation of Figure 5, along with the very large CN/Br ratio (~20) makes a compelling case for a cation-π interaction to Y206.

In addition to the 3,5-F_2Phe mutation, full turnover of the dose-response curve was not seen for 4-CN-Phe in the α signal peptide-containing template (Figure 4.8). The α signal peptide was required to obtain suppression data at the F96 and Y156 sites, however suppression data could be obtained for both the wild type and α signal peptide-containing Y206 mutations. Data was obtained in both templates for Y206 mutations to ensure that the signal peptide did not affect receptor function (Tables 4.4 and 4.5). To estimate an EC_{50} value, obtained data were fit to the Hill equation. As shown in Figure 5, very similar results are obtained for receptors with either the α or the β signal peptide,

providing evidence that altering the signal peptide has no effect on receptor function and boosting confidence in the EC_{50} values obtained for the receptors with the α signal

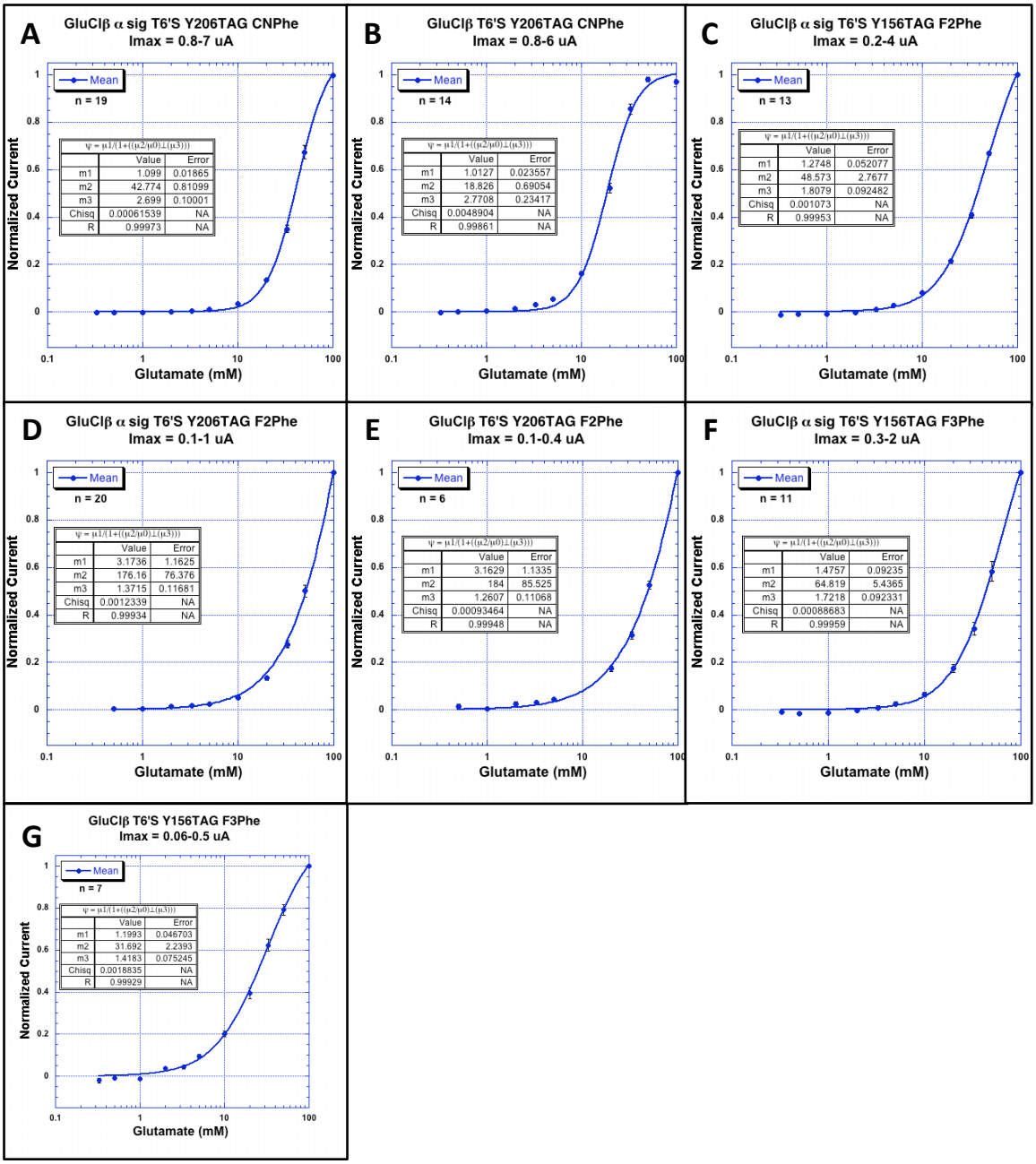

Figure 4.8. EC_{50} plots of mutant receptors that demonstrate a large loss-of-function. **(A)** Y206CNPhe with the α signal sequence **(B)** Y206CNPhe with the WT β signal sequence **(C)** Y156F_2Phe **(D)** Y206F_2Phe with the α signal sequence **(E)** Y206F_2Phe with the WT β signal sequence **(F)**Y156F_3Phe with the α signal sequence **(G)** Y156F_3Phe the WT β signal sequence.

peptide. The Y206 3,5-F_2-Phe mutant in both constructs began to respond to glutamate but did not near the turnover point. These data were fit to the Hill equation (Figure 4.8), but we do not believe that the resulting EC_{50} value is an accurate indication of receptor function. We have therefore reported this mutation as having an EC_{50} of >100 mM. The D loop tryptophan was not examined because it is not located near the binding site in the crystal structure.

Probing other Noncovalent Interactions. In addition to a strong cation-π interaction, other noncovalent interactions between glutamate and the receptor were identified. Two arginine residues on the complementary subunit, R40(37) and R59(56), were predicted by the crystal structure to form ionic interactions with the main chain carboxylate and the side chain carboxylate of glutamate, respectively (Figure 4.5). These interactions are confirmed through receptor mutagenesis. The R59 residue appears to be more sensitive to mutagenesis than R40 because R59 could not tolerate mutation to alanine, whereas R40A demonstrated a large but measurable loss-of-function of approximately 140-fold (Table 4.6). Mutagenesis of either residue to glutamate resulted in a non-functional receptor. The importance of a stabilizing positive charge on the complementary face of the binding site is further demonstrated by mutagenesis of a nearby lysine residue, K176(171), on the F loop of the complementary subunit. This residue is predicted to be 4.5 Å from the side chain of glutamate and does not participate in a functionally important ligand binding interaction, as indicated by the small 2-fold loss-of-function upon mutagenesis to alanine. Interestingly, however, mutagenesis of this lysine residue to glutamate resulted in a large 70-fold loss-of-function, indicating either the repulsive

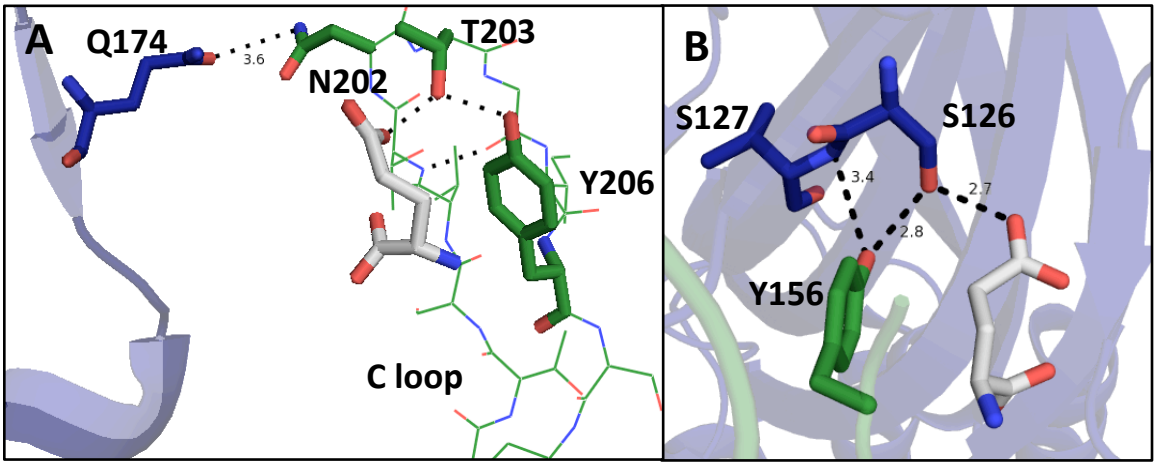

Figure 4.9. Predicted hydrogen bond interactions between the primary and complementary subunits near the ligand-binding site in the 3RIF crystal structure. Residues on the primary face are shown in green, residues on the complementary face in blue, and glutamate in white. Hydrogen bond network between **(A)** the C loop of the primary subunit and the F loop of the complementary subunit the B loop of the primary subunit and the E loop of the complementary subunit **(B)** the B loop of the primary subunit and the E loop of the complementary subunit.

Table 4.6. Conventional mutagenesis of binding site residues. All mutants have the T6'S background mutation.

Mutation	EC50 (mM)	Hill	n	Fold Shift	Ω	ΔΔG (kcal/mol)
WT (T6'S)	0.0080 +/- 0.0005	2.4 +/- 0.3	27	-		
R40A	1.1 +/- 0.1	2.1 +/- 0.1	17	140		
R40E		No response				
R59A		No response				
R59E		No response				
K176A	0.017 +/- 0.001	2.2 +/- 0.1	17	2		
K176E	0.54 +/- 0.02	1.8 +/- 0.1	14	70		
Y206A		No response				
Y206F	0.10 +/- 0.01	2.6 +/- 0.3	14	13		
T203A	0.64 +/- 0.01	2.3 +/- 0.1	19	80		
T203A/Y206F	0.21 +/- 0.01	2.2 +/- 0.1	18	26	1/37	2.1
Q174A	0.11 +/- 0.01	2.4 +/- 0.2	14	14		
N202A	0.010 +/- 0.001	3.3 +/- 0.2	16	1.25		
Q174A/Y206F	0.92 +/- 0.04	2.2 +/- 0.2	13	115	0.67	0.23
Y156A		No response				
Y156F	6.4 +/- 0.4	1.6 +/- 0.1	17	800		
S126A	4.7 +/- 0.1	2.5 +/- 0.1	22	590		
S126A/Y156F		No response				

effect of introducing a negative charge near the carboxylates of the ligand or interference of the ligand-binding interactions with R40 or R59.

Two inter-subunit hydrogen bond networks are predicted by the GluClα crystal structure: one between the C loop of the primary subunit and the F loop of the complementary subunit and another between the B loop of the primary subunit and the E loop of the complementary subunit (Figure 4.9). Motivation to study the former comes from previous studies in the muscle-type nAChR, where an inter-subunit hydrogen bond between an aspartate side chain (γD174/δD180) on the complementary subunit and a backbone nitrogen (αS191) on the β-hairpin turn of the C loop was shown to be important for channel gating[42]. This backbone nitrogen was later shown to be optimally positioned by a hydrogen bond network initiating from a neighboring vicinal disulfide bond (αC192/αC193) on the C loop[43]. While the GluCl receptors, as well as all non-α nAChRs, lack this vicinal disulfide, other structural motifs may have evolved to perform the same function.

The GluClα crystal structure predicts an intra-subunit hydrogen bond between the side chains of T203(197) and Y206(200) on loop C in approximately the same relative position as the vicinal disulfide. Additionally, a glutamine, Q174(169), is located two residues away from the aspartates on the F loop in the γ and δ subunits of the nAChR and is poised to interact with the side chain of an asparagine on the β-hairpin turn of the C loop, N202(196). While these interactions are different than those observed in the muscle type nAChR, they have the potential to be functionally analogous.

To analyze these potential interactions, mutant cycle analysis was performed. The data indicate a strong functional coupling between the side chains of T203 and Y206

with a coupling strength of 2.1 kcal/mol (Table 4.6), between the T203A and Y206F mutants. A 14-fold loss-of-function was observed for the Q174A mutant, providing evidence that this side chain is important for receptor function. Interestingly, the N202A mutant gives wild type receptors, despite a clear hydrogen bond between Q174 and N202 in the crystal structure. No functional coupling was observed between Y206 and Q174. These findings do not support a long-range functional coupling between structural and/or ligand-binding elements on the C loop and an inter-subunit hydrogen bond with the F loop, as was observed in the nAChR. The only other polar neighbor of Q174 is an asparagine also on the complementary subunit, N36(33), suggesting that no functionally important inter-subunit interaction exists between the C loop of the primary subunit and the F loop of the complementary subunit. It is possible that the salt-bridges formed between the two arginine residues on the complementary subunit and the carboxylates of the ligand are sufficient to shape the ligand binding site on the complementary side and an additional interaction between the C and F loops would be redundant. These strong interactions are absent in the nAChRs because acetylcholine is neutral on the side that binds the complementary subunit, and additional interactions may be necessary to hold the binding site together.

While the functional coupling between the side chains of T203 and Y206 is likely unrelated to the effects caused by the vicinal disulfide, it provides support for the ligand-binding interactions previously discussed and predicted by the crystal structure. T203 is predicted to act as a hydrogen bond donor to the side chain carboxylate of glutamate and as a hydrogen bond acceptor to the hydroxyl of Y206. The hydrogen bond between Y206 and T203 likely strengthens the cation-π binding energy of the tyrosine due to an increase

in electrostatic potential on the ring system, caused by the electron donating properties of the acidic phenol. These effects were previously predicted with gas phase calculations of phenol and formamide, a hydrogen bond acceptor, where a hydrogen bond significantly enhanced a cation-π interaction in the gas phase[44]. This may account for why tyrosine, a weaker cation-π binder than tryptophan in isolation, is capable of forming such a strong cation-π interaction with glutamate in this receptor and why tyrosines are overrepresented in cation-π interactions in Cys-loop receptors relative to phenylalanine. It can also be argued that the hydrogen bond exists to position Y206 in an orientation optimal for a strong cation-π interaction. It is important to note that the cation-π interaction determined here was measured with phenylalanine derivatives that lack the hydrogen bond to T203. Data indicate a cation-π binding strength similar to other primary amines as indicated by the slope of the cation-π plot[38,40,41,45]. Regardless of mechanism, we experimentally observe the importance of this hydrogen bond with the Y206F mutation, which results in a 13-fold loss of function. The directionality of hydrogen bonding predicted by the crystal structure is confirmed by incorporation of 4-MeO-Phe at Y206. This mutation does not reverse the loss-of-function seen in the Y206F mutant, and therefore provides evidence that Y206 is acting as a hydrogen bond donor. The T203A mutation resulted in an 80-fold loss-of-function, likely caused by breaking both its interaction to glutamate and Y206.

In addition to inter-subunit interactions between the C and F loops, the crystal structure suggests a hydrogen bond interaction between the side chains of Y156 on the B loop of the primary subunit and S126 on the E loop of the complementary subunit. Mutagenesis of these residues individually to remove the polar side chain resulted in a

large loss-of-function of 800-fold and 590-fold, respectively (Table 4.6). These large and similar losses-of-function indicate that an interaction between the two side chains is likely to occur and is important for receptor function, however functional coupling could not be determined because the EC_{50} of the double mutant could not be measured. The high EC_{50} values of the single mutants are near the limit of our detection, and therefore any additional loss-of-function would be difficult to measure because of the high glutamate concentrations required.

In other anion-selective Cys-loop receptors where a tyrosine is found at the aromatic position on loop B, different effects are observed upon mutagenesis of the tyrosine to phenylalanine. In the glycine receptor, this residue is naturally a phenylalanine, and therefore a hydrogen bond with the complementary subunit is not possible. In the $GABA_C$ receptor, a less than 5-fold loss of function is observed upon mutagenesis of tyrosine to phenylalanine[40]. However, in the $GABA_A$ receptor, a large 400-fold loss-of-function was observed, similar to that seen here in the GluClβ receptor[45]. Interestingly, substitution of tyrosine with 4-MeO-Phe was able to recover the receptor to wild type EC_{50} in $GABA_A$, indicating that the tyrosine acts as a hydrogen bond acceptor, whereas in GluClβ, substitution with 4-MeO-Phe led to a non-functional receptor indicating that it acts as a donor. These data suggest that the interactions between the primary and complementary subunits vary, even between highly related receptors, and that a hydrogen bond at this site is not a universal feature of Cys-loop receptors.

In summary, a series of interactions were examined in the GluClβ receptor that were predicted by the crystal structure of the homologous GluClα receptor. Unnatural amino acid mutagenesis indicates a strong cation-π interaction with a tyrosine residue on

loop C, Y206. This ligand-binding interaction is a conserved feature of the mammalian Cys-loop receptors studied to-date, and is found here in a distant invertebrate homolog. While this interaction shows that many of the features between distant classes of Cys-loop receptors are conserved, many interactions were found that are receptor-specific. An inter-subunit hydrogen bond between loops C and F shown to be important in the muscle type nAChR is absent in GluClβ. Conversely, an important inter-subunit interaction between loops B and E in GluClβ is absent in many more closely related anion-selective homologs. These data indicate that while the crystal structure of a receptor can serve as a good model for other homologous receptors, care must be taken when extrapolating structural information.

References

1. Thompson, A.J., Lester, H.A., and Lummis, S.C., The structural basis of function in Cys-loop receptors. *Q Rev Biophys*, **2010**. *43*(4): p. 449-499.
2. Coe, J.W., Brooks, P.R., Vetelino, M.G., Wirtz, M.C., Arnold, E.P., Huang, J., Sands, S.B., Davis, T.I., Lebel, L.A., Fox, C.B., Shrikhande, A., Heym, J.H., Schaeffer, E., Rollema, H., Lu, Y., Mansbach, R.S., Chambers, L.K., Rovetti, C.C., Schulz, D.W., Tingley, F.D., 3rd, and O'Neill, B.T., Varenicline: an alpha4beta2 nicotinic receptor partial agonist for smoking cessation. *J Med Chem*, **2005**. *48*(10): p. 3474-3477.
3. Cupp, E.W., Bernardo, M.J., Kiszewski, A.E., Collins, R.C., Taylor, H.R., Aziz, M.A., and Greene, B.M., The effects of ivermectin on transmission of Onchocerca volvulus. *Science*, **1986**. *231*(4739): p. 740-742.
4. Miyazawa, A., Fujiyoshi, Y., Stowell, M., and Unwin, N., Nicotinic acetylcholine receptor at 4.6 A resolution: transverse tunnels in the channel wall. *J Mol Biol*, **1999**. *288*(4): p. 765-786.
5. Unwin, N., Refined structure of the nicotinic acetylcholine receptor at 4A resolution. *J Mol Biol*, **2005**. *346*(4): p. 967-989.
6. Brejc, K., van Dijk, W.J., Klaassen, R.V., Schuurmans, M., van Der Oost, J., Smit, A.B., and Sixma, T.K., Crystal structure of an ACh-binding protein reveals the ligand-binding domain of nicotinic receptors. *Nature*, **2001**. *411*(6835): p. 269-276.
7. Hilf, R.J. and Dutzler, R., X-ray structure of a prokaryotic pentameric ligand-gated ion channel. *Nature*, **2008**. *452*(7185): p. 375-379.

8. Hilf, R.J. and Dutzler, R., Structure of a potentially open state of a proton-activated pentameric ligand-gated ion channel. *Nature*, **2009**. *457*(7225): p. 115-118.
9. Bocquet, N., Nury, H., Baaden, M., Le Poupon, C., Changeux, J.P., Delarue, M., and Corringer, P.J., X-ray structure of a pentameric ligand-gated ion channel in an apparently open conformation. *Nature*, **2009**. *457*(7225): p. 111-114.
10. Hibbs, R.E. and Gouaux, E., Principles of activation and permeation in an anion-selective Cys-loop receptor. *Nature*, **2011**. *474*(7349): p. 54-80.
11. Campbell, W.C., Ivermectin: an update. *Parasitol Today*, **1985**. *1*(1): p. 10-16.
12. Campbell, W.C., Fisher, M.H., Stapley, E.O., Albers-Schonberg, G., and Jacob, T.A., Ivermectin: a potent new antiparasitic agent. *Science*, **1983**. *221*(4613): p. 823-828.
13. Aziz, M.A., Diallo, S., Diop, I.M., Lariviere, M., and Porta, M., Efficacy and tolerance of ivermectin in human onchocerciasis. *Lancet*, **1982**. *2*(8291): p. 171-173.
14. Lester, H.A., Dibas, M.I., Dahan, D.S., Leite, J.F., and Dougherty, D.A., Cys-loop receptors: new twists and turns. *Trends Neurosci*, **2004**. *27*(6): p. 329-336.
15. Miller, P.S. and Smart, T.G., Binding, activation and modulation of Cys-loop receptors. *Trends Pharmacol Sci*, **2010**. *31*(4): p. 161-174.
16. Van Arnam, E.B., Dougherty, D. A., Functional Probes of Drug–Receptor Interactions Implicated by Structural Studies: Cys-Loop Receptors Provide a Fertile Testing Ground. *Journal of Medicinal Chemistry*, **2014**.
17. Etter, A., Cully, D.F., Schaeffer, J.M., Liu, K.K., and Arena, J.P., An amino acid substitution in the pore region of a glutamate-gated chloride channel enables the coupling of ligand binding to channel gating. *J Biol Chem*, **1996**. *271*(27): p. 16035-16039.
18. Slimko, E.M. and Lester, H.A., Codon optimization of Caenorhabditis elegans GluCl ion channel genes for mammalian cells dramatically improves expression levels. *J Neurosci Methods*, **2003**. *124*(1): p. 75-81.
19. Kao, C., Zheng, M., and Rudisser, S., A simple and efficient method to reduce nontemplated nucleotide addition at the 3 ' terminus of RNAs transcribed by T7 RNA polymerase. *Rna-a Publication of the Rna Society*, **1999**. *5*(9): p. 1268-1272.
20. Nowak, M.W., Gallivan, J.P., Silverman, S.K., Labarca, C.G., Dougherty, D.A., and Lester, H.A., In vivo incorporation of unnatural amino acids into ion channels in Xenopus oocyte expression system. *Ion Channels, Pt B*, **1998**. *293*: p. 504-529.
21. Filatov, G.N. and White, M.M., The role of conserved leucines in the M2 domain of the acetylcholine receptor in channel gating. *Mol Pharmacol*, **1995**. *48*(3): p. 379-384.
22. Labarca, C., Nowak, M.W., Zhang, H., Tang, L., Deshpande, P., and Lester, H.A., Channel gating governed symmetrically by conserved leucine residues in the M2 domain of nicotinic receptors. *Nature*, **1995**. *376*(6540): p. 514-516.
23. Frazier, S.J., Cohen, B.N., and Lester, H.A., An engineered glutamate-gated chloride (GluCl) channel for sensitive, consistent neuronal silencing by ivermectin. *J Biol Chem*, **2013**. *288*(29): p. 21029-21042.

24. Placzek, A.N., Grassi, F., Meyer, E.M., and Papke, R.L., An alpha7 nicotinic acetylcholine receptor gain-of-function mutant that retains pharmacological fidelity. *Mol Pharmacol*, **2005**. *68*(6): p. 1863-1876.
25. Yakel, J.L., Lagrutta, A., Adelman, J.P., and North, R.A., Single amino acid substitution affects desensitization of the 5-hydroxytryptamine type 3 receptor expressed in Xenopus oocytes. *Proc Natl Acad Sci U S A*, **1993**. *90*(11): p. 5030-5033.
26. Xiu, X., Puskar, N.L., Shanata, J.A., Lester, H.A., and Dougherty, D.A., Nicotine binding to brain receptors requires a strong cation-pi interaction. *Nature*, **2009**. *458*(7237): p. 534-537.
27. Marotta, C.B., Dilworth, C.N., Lester, H.A., and Dougherty, D.A., Probing the non-canonical interface for agonist interaction with an alpha5 containing nicotinic acetylcholine receptor. *Neuropharmacology*, **2014**. *77*: p. 342-349.
28. Zhong, W.G., Gallivan, J.P., Zhang, Y.O., Li, L.T., Lester, H.A., and Dougherty, D.A., From ab initio quantum mechanics to molecular neurobiology: A cation-pi binding site in the nicotinic receptor. *Proceedings of the National Academy of Sciences of the United States of America*, **1998**. *95*(21): p. 12088-12093.
29. Pertzoff, V.A., The solubility of glutamic acid in water and certain organic solvents. *Journal of Biological Chemistry*, **1933**. *100*(1): p. 97-104.
30. Kearney, P.C., Zhang, H., Zhong, W., Dougherty, D.A., and Lester, H.A., Determinants of nicotinic receptor gating in natural and unnatural side chain structures at the M2 9' position. *Neuron*, **1996**. *17*(6): p. 1221-1229.
31. Zerangue, N., Schwappach, B., Jan, Y.N., and Jan, L.Y., A new ER trafficking signal regulates the subunit stoichiometry of plasma membrane K(ATP) channels. *Neuron*, **1999**. *22*(3): p. 537-548.
32. Boyd, G.W., Doward, A.I., Kirkness, E.F., Millar, N.S., and Connolly, C.N., Cell surface expression of 5-hydroxytryptamine type 3 receptors is controlled by an endoplasmic reticulum retention signal. *J Biol Chem*, **2003**. *278*(30): p. 27681-27687.
33. Mossessova, E., Bickford, L.C., and Goldberg, J., SNARE selectivity of the COPII coat. *Cell*, **2003**. *114*(4): p. 483-495.
34. Xu, J., Zhu, Y., and Heinemann, S.F., Identification of sequence motifs that target neuronal nicotinic receptors to dendrites and axons. *J Neurosci*, **2006**. *26*(38): p. 9780-9793.
35. Kracun, S., Harkness, P.C., Gibb, A.J., and Millar, N.S., Influence of the M3-M4 intracellular domain upon nicotinic acetylcholine receptor assembly, targeting and function. *Br J Pharmacol*, **2008**. *153*(7): p. 1474-1484.
36. Castillo, M., Mulet, J., Aldea, M., Gerber, S., Sala, S., Sala, F., and Criado, M., Role of the N-terminal alpha-helix in biogenesis of alpha7 nicotinic receptors. *J Neurochem*, **2009**. *108*(6): p. 1399-1409.
37. Pons, S., Sallette, J., Bourgeois, J.P., Taly, A., Changeux, J.P., and Devillers-Thiery, A., Critical role of the C-terminal segment in the maturation and export to the cell surface of the homopentameric alpha 7-5HT3A receptor. *Eur J Neurosci*, **2004**. *20*(8): p. 2022-2030.
38. Beene, D.L., Brandt, G.S., Zhong, W., Zacharias, N.M., Lester, H.A., and Dougherty, D.A., Cation-pi interactions in ligand recognition by serotonergic (5-

HT3A) and nicotinic acetylcholine receptors: the anomalous binding properties of nicotine. *Biochemistry*, **2002**. *41*(32): p. 10262-10269.

39. Puskar, N.L., Xiu, X.A., Lester, H.A., and Dougherty, D.A., Two Neuronal Nicotinic Acetylcholine Receptors, alpha 4 beta 4 and alpha 7, Show Differential Agonist Binding Modes. *Journal of Biological Chemistry*, **2011**. *286*(16): p. 14618-14627.
40. Lummis, S.C., D, L.B., Harrison, N.J., Lester, H.A., and Dougherty, D.A., A cation-pi binding interaction with a tyrosine in the binding site of the GABAC receptor. *Chem Biol*, **2005**. *12*(9): p. 993-997.
41. Pless, S.A., Millen, K.S., Hanek, A.P., Lynch, J.W., Lester, H.A., Lummis, S.C., and Dougherty, D.A., A cation-pi interaction in the binding site of the glycine receptor is mediated by a phenylalanine residue. *J Neurosci*, **2008**. *28*(43): p. 10937-10942.
42. Gleitsman, K.R., Kedrowski, S.M.A., Lester, H.A., and Dougherty, D.A., An Intersubunit Hydrogen Bond in the Nicotinic Acetylcholine Receptor That Contributes to Channel Gating. *Journal of Biological Chemistry*, **2008**. *283*(51): p. 35638-35643.
43. Blum, A.P., Gleitsman, K.R., Lester, H.A., and Dougherty, D.A., Evidence for an extended hydrogen bond network in the binding site of the nicotinic receptor: role of the vicinal disulfide of the alpha1 subunit. *J Biol Chem*, **2011**. *286*(37): p. 32251-32258.
44. Mecozzi, S., West, A.P., and Dougherty, D.A., Cation-pi interactions in aromatics of biological and medicinal interest: Electrostatic potential surfaces as a useful qualitative guide. *Proceedings of the National Academy of Sciences of the United States of America*, **1996**. *93*(20): p. 10566-10571.
45. Padgett, C.L., Hanek, A.P., Lester, H.A., Dougherty, D.A., and Lummis, S.C., Unnatural amino acid mutagenesis of the GABA(A) receptor binding site residues reveals a novel cation-pi interaction between GABA and beta 2Tyr97. *J Neurosci*, **2007**. *27*(4): p. 886-892.

Chapter 5

M4 helix properties in the GluClα receptor tune the coupling of ligand binding and channel gating

Abstract

Despite the ability of the GluClα receptor to bind glutamate, the receptor is not activated by glutamate in the absence of allosteric modulators such as ivermectin. In contrast, the homologous GluClβ homomeric and GluClαβ heteromeric receptors are efficiently activated by glutamate. The ability of GluClα to bind glutamate indicates that the receptor's dysfunction is due to a lack of coupling between the ligand-binding domain and the transmembrane pore-forming domain. Through the synthesis of a series of GluClα/β chimeras, it was found that by modifying the C-terminal residues of GluClα, including the C-terminal half of the M4 helix, glutamate sensitivity could be restored. The C-termini of GluCl subunits are short disordered sequences that are positioned to interact with the extracellular domain of the receptor, specifically the Cys-loop, which is characteristic of this class of proteins. Additional chimera and mutagenesis studies have failed to provide evidence for a defective C-terminus-Cys-loop interaction in GluClα. Instead, membrane-protein interactions or M4 helix structure/dynamics may be responsible for this decoupling.

Introduction

Fast synaptic transmission occurs through the propagation of an electrical signal by a class of ligand-gated ion channels known as the Cys-loop receptors. In these

receptors, a ligand-binding event in the extracellular domain initiates a cascade of receptor movements that ultimately results in the opening of the pore lining M2 helix and the flow of ions across the membrane. These two domains are located over 40 Å apart in the folded receptor, and the mechanism by which this signal is propagated is not yet fully understood[1,2].

The activation process is thought to occur in a wave-like manner with discreet domain movements that ultimately lead to an increase in ion permeability across the membrane[3]. These movements initiate at the ligand-binding site and propagate step-wise toward the transmembrane region[4,5]. Proper communication in the form of structural compatibility between the extracellular and transmembrane domains is crucial for the coupling of ligand binding and channel gating[6,7]. Many of the regions shown to be important for successful channel gating are found at the interface of the two domains including the pre-M1 linker[8,9], the "pin in socket" interaction between extracellular loop 2 and the M2-M3 loop[10-12], the Cys-loop[13], and the extracellular C-terminal domain[14,15]. Additionally, maintaining an overall charge pattern at the interface between the two domains was shown to be important for gating[16].

In addition to these interfacial regions, other factors and regions distant from the binding site have been shown to be important for the creation of functional receptors and the coupling of ligand binding to channel gating. These factors include the lipid composition surrounding the receptor[17] and the properties of the transmembrane regions[18], of which proper tuning is required for receptor assembly and ligand-induced activation. The fourth transmembrane helical domain, TM4, has been implicated as a lipid-sensing domain that serves to translate the information of the surrounding

membrane to the rest of the receptor[17,19]. It has also been suggested to serve as a hinge in the gating mechanism[20]. Linear free-energy analysis of the muscle-type nAChR supports concurrent motion of TM4 helix residues along with residues on the mid-section of TM2 (13', 11', 7', and 3') that are estimated to move in the middle of the gating process[4,21], therefore supporting the importance of this helix in the gating mechanism.

Disruption of regions important for channel gating can lead to receptors with lower ligand efficacy or in the most extreme case, to receptors that are nonfunctional. Decoupling of ligand-binding and channel gating events can occur through point mutations to residues important for gating[22-24], varied properties of receptor domains[25,26], or through modulation of the lipid bilayer surrounding the receptor[17,27]. In *Xenopus laevis* oocytes, the homomeric GluClα receptor is shown to be insensitive to its native ligand, glutamate, in the absence of an allosteric modulator that stabilizes the open conformation, ivermectin[24]. The receptor is known to have a functional binding site because the receptor was crystalized with glutamate bound in the presence of ivermectin, and additional channel activation can be elicited by glutamate after application of ivermectin[2]. Functional response to glutamate in the absence of ivermectin can be regained with a point mutation of a TM2 helix pore-lining residue, T2'A[24], or by expressing the channel in an alternate heterologous expression system such as HEK293 cells[28]. These findings support a mechanism of glutamate-insensitivity that involves dysfunction of the gating mechanism rather than ligand-binding event. It also suggests that membrane effects might play a role in this decoupling.

In this study, chimeras between GluClα and the homologous GluClβ receptor, both from *Caenorhabditis elegans*, were created to determine regions of the receptor

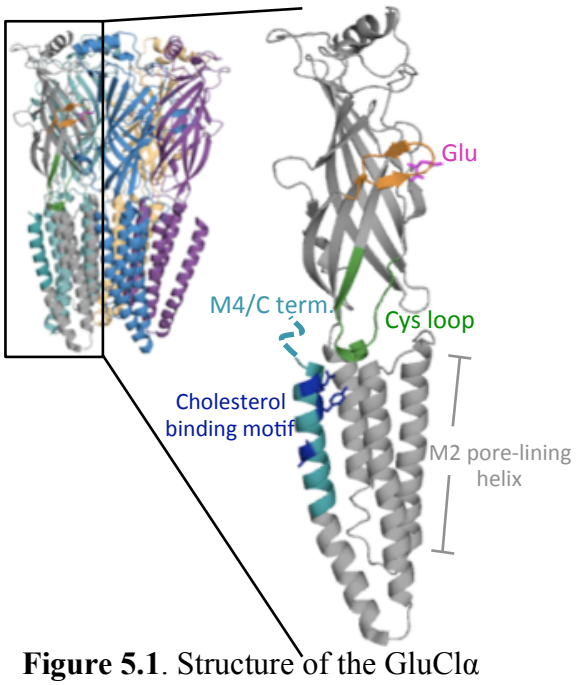

Figure 5.1. Structure of the GluClα receptor (PDB ID: 3RIF) with regions of interest highlighted.

responsible for this decoupling. The GluClβ receptor was selected because it is the closest homolog to GluClα and is fully activated by glutamate in *X. laevis* oocytes. GluClα/β chimeras implicate the C-terminal half of the M4 helix of GluClα as having defective properties that prevent channel activation (Figure 5.1). Mutagenesis of amino acids in this region indicates that no individual residue is responsible for this effect, but rather the properties of the entire helix are involved. Removal of a putative cholesterol binding motif near the C-terminus of TM4, found in the GluClα and not the GluClβ receptor, resulted in ~10% regain of glutamate-induced response relative to ivermectin. No deficiency of coupling between the Cys-loop and the C-terminus was identified. These findings indicate that the properties of TM4, while distant from both the ligand binding and channel gate domains, exert significant effects on receptor function. Direct interactions with the surrounding membrane likely have a strong influence on the structure and dynamics of this helix, which is translated to the ligand binding domain and channel gate through unknown mechanisms.

Methods

Molecular biology. The mammalian codon optimized GluClα and β receptors from *C. elegans*[29] were used in the pcDNA3.1 vector for HEK293T experiments. The receptors were subcloned into the pGEMhe vector and the stop codon of the GluClβ receptor was mutated from TAG to TGA for *Xenopus laevis* oocyte experiments. Mutagenesis of the GluClβ receptor, including amino acid deletions, was performed using the QuikChange protocol (Stratagene). The cDNA was linearized using SbfI (New England Biolabs) and mRNA was produced from the linearized plasmids by using the T7 mMessage Machine kit (Ambion) for *X. laevis* oocyte experiments.

Chimeras. Chimeras were synthesized by mutating in an EcoRI restriction enzyme site (GAATTC) in both the GluClα and GluClβ receptors at the desired cut site. First, the inherent EcoRI site in the GluClα M3-M4 loop (AT**GAATTC**C) was removed using silent mutations (AT**GAACAG**C) to eliminate undesired cutting. The mutated receptors were then cut with EcoRI and HindIII (5' of the encoded gene) and the fragments were separated by gel electrophoresis on a 1% agarose gel. The resulting bands were isolated and purified using a gel extraction kit (Qiagen) and the desired GluClα and GluClβ fragments were ligated together using DNA ligase. The engineered EcoRI restriction site was then mutated back to the wild type α/β or β/α sequence and mRNA was produced as described above.

Oocyte preparation and injection. Stage V-VI *Xenopus laevis* oocytes were harvested and injected with RNA as previously described[30]. For all constructs, 12.5 ng of receptor mRNA was injected 48 hours before recording.

Transfection of HEK293T cells. Cells were grown in DMEM:F12 (1:1) media with GlutaMAX-I (Gibco). 60-90% confluent HEK293T cells in 35 mm dishes were transfected with 2 μg of DNA using the *Trans*IT-mRNA reagent. Transfection was performed by manufacturers instructions using 3.75 μL of Boost Reagent and 7.5 μL of *Trans*IT in serum and antiobiotic free media. The DNA and reagent complexes were added directly to the media over the cells and cells were incubated for 24 hours at 37^{o}C and 5% CO_2. After 24 hours the cells were harvested and plated in 96-well plates (one 35 mM dish was used to fill 3 wells in a 96-well plate) and allowed to incubate for an additional 24 hours before FlexStation3 recording.

Methyl-β-cyclodextrin removal of cholesterol. For methyl-β-cyclodextrin (MβCD) experiments in *X. laevis* oocytes, 4 cells were placed in 2 mL of varying concentrations of MβCD (50 μM, 500 μM, or 5 mM) in ND96+ for the specified amount of time (0.5, 1, 1.5, or 2 hours). Cells were then washed 3X with ND96+ before recording.

For HEK293T experiments, media containing 0, 100 μM, 1 mM, and 10 mM MβCD were added to cells plated in a 96 well plate. Cells were incubated in the presence of MβCD for 2 hours before the media was exchanged after a PBS wash step.

Data Collection and analysis. All oocyte experiments were performed on an OpusXpress 6000A (Axon Instruments) using two-electrode voltage clamp mode. The recording buffer was calcium-free ND96 (96 mM NaCl, 2 mM KCl, 1 mM $MgCl_2$, and 5 mM HEPES, pH 7.5). The initial holding potential was -60 mV. Data were sampled at 125 Hz and filtered at 50 Hz. A calcium-free ND96 prewash was applied for 30 s (1 mL/min.) followed by application of agonist for 15 s (4 mL/min.). Agonist was then washed out with calcium-free ND96 buffer for 116 s (3 mL/min.). Agonist-induced currents were measured from the baseline. Glutamate dose solutions were made in calcium-free ND96 buffer from a 50 mM (pH 7.5) stock solution made in the same buffer. A 10 μM solution of ivermectin was made in calcium-free ND96 buffer from a 50 mM stock solution made in DMSO.

All HEK293T experiments were performed using a FlexStation3 (Molecular Devices). After a 48 hour incubation period, the media above the cells was removed and the cells were washed with Flex Buffer (115 mM NaCl, 1 mM KCl, 1 mM $CaCl_2$, 1 mM $MgCl_2$, 10 mM D-glucose, and 10 mM HEPES at pH 7.5)[31]. The cells in the 96-well plate were incubated with 100 μL/well of a 1:2 dilution of FLIPR Membrane Potential Assay Kit (blue) for 30 minutes at 37°C and 5% CO_2 and read using the FlexStation3. Wells were excited at 530 nm and fluorescence was recorded at 565 nm using a 550 nm filter at low photomultiplier tube sensitivity after application of 100 μL of agonist to the wells. Fluorescence data were collected every 1.52 seconds for 180 seconds and data were analyzed using the SOFTmax Pro software (Molecular Devices). The peak values for each well in a column of the 96-well plate were normalized to the maximum value.

Data were fit to the Hill equation, $I_{norm} = 1/(1 + (EC_{50}/A))\ n_H$, where I_{norm} is the normalized current peak at [agonist] = A, EC_{50} is the concentration of agonist that elicits a half-maximum response, and n_H is the Hill coefficient. EC_{50} values were obtained by averaging the I_{norm} values for each agonist concentration and fitting those values to the Hill equation.

Results and Discussion

Implication of the M4 helix in GluClα receptor insensitivity to glutamate. Chimeras between GluClα and GluClβ were synthesized to identify regions responsible for GluClα insensitivity to glutamate. A previous study indicated that the GluClα extracellular domain possesses sufficient ligand binding elements, as evidenced by the functionality of a GluClα/β chimera with an extracellular (EC) GluClα domain and a transmembrane (TM) GluClβ domain[24]. This finding also suggests that a decoupling of ligand binding and channel gating events, originating in the TM domain of the receptor, is the reason for glutamate insensitivity in GluClα. We have duplicated their data here, and have created additional receptor chimeras to determine if there are TM regions other than the channel gate that contribute to the impaired coupling between ligand binding and channel gating in GluClα. Chimeras are indicated by the order of splicing (α/β indicates N-terminal GluClα elements and C-terminal GluClβ elements and the reverse for β/α) and the approximate location of splicing. The exact site of receptor splicing is indicated in Figure 5.2. Because ivermectin is a full allosteric agonist at the wild-type GluClα receptor, we can measure the efficacy of glutamate at the mutant receptors as the percent response to glutamate relative to ivermectin.

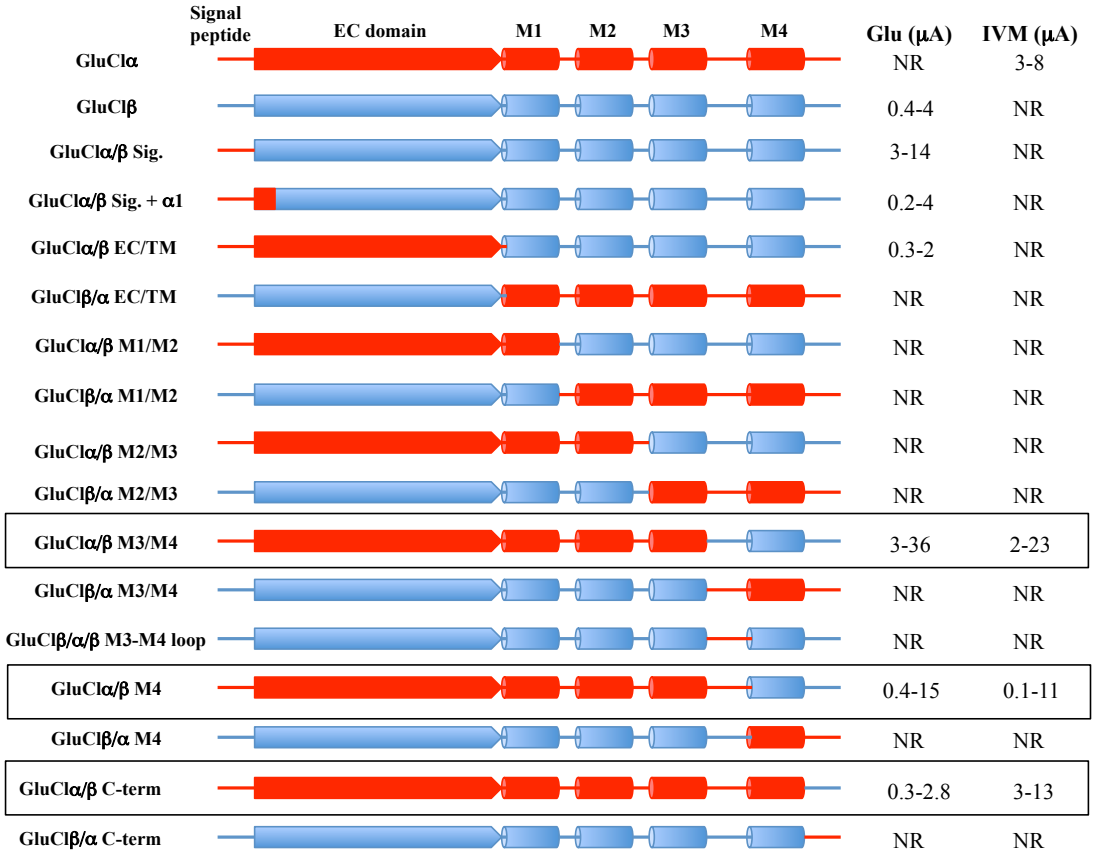

Figure 5.2. Chimeras synthesized in this study. Red indicates GluClα and blue GluClβ.

Table 5.1. Functional data of synthesized chimeras

	EC_{50} Glu (mM)	Hill	n	I_{max} Glu (μA)	I_{max} IVM (μA)
GluClα		No Response			3-7
GluClα:β (1:1)	0.48 +/- 0.01	3.3 +/- 0.1	7	4-24	7-9
GluClβ	0.35 +/- 0.01	2.5 +/- 0.2	20	0.4-4	NR
α/β EC/TM	0.00078 +/- 0.00007	2.1 +/- 0.4	15	0.3-2	NR
β/α EC/TM		No response			NR
α/β M1-M2		No response			NR
β/α M1-M2		No response			NR
α/β M2-M3		No response			NR
β/α M2-M3		No response			NR
α/β M3-M4 loop	0.11 +/- 0.01	2.1 +/- 0.1	22	3-36	2-23
β/α M3-M4 loop		No Response			NR
α/β M4	0.54 +/- 0.03	2.5 +/- 0.3	19	0.4-15	0.1-11
β/α M4		No Response			NR
GluClα/β C-term	2.8 +/- 0.5	1.4 +/- 0.1	7	0.4-3	3-13
GluClβ/α C-term		No response			-

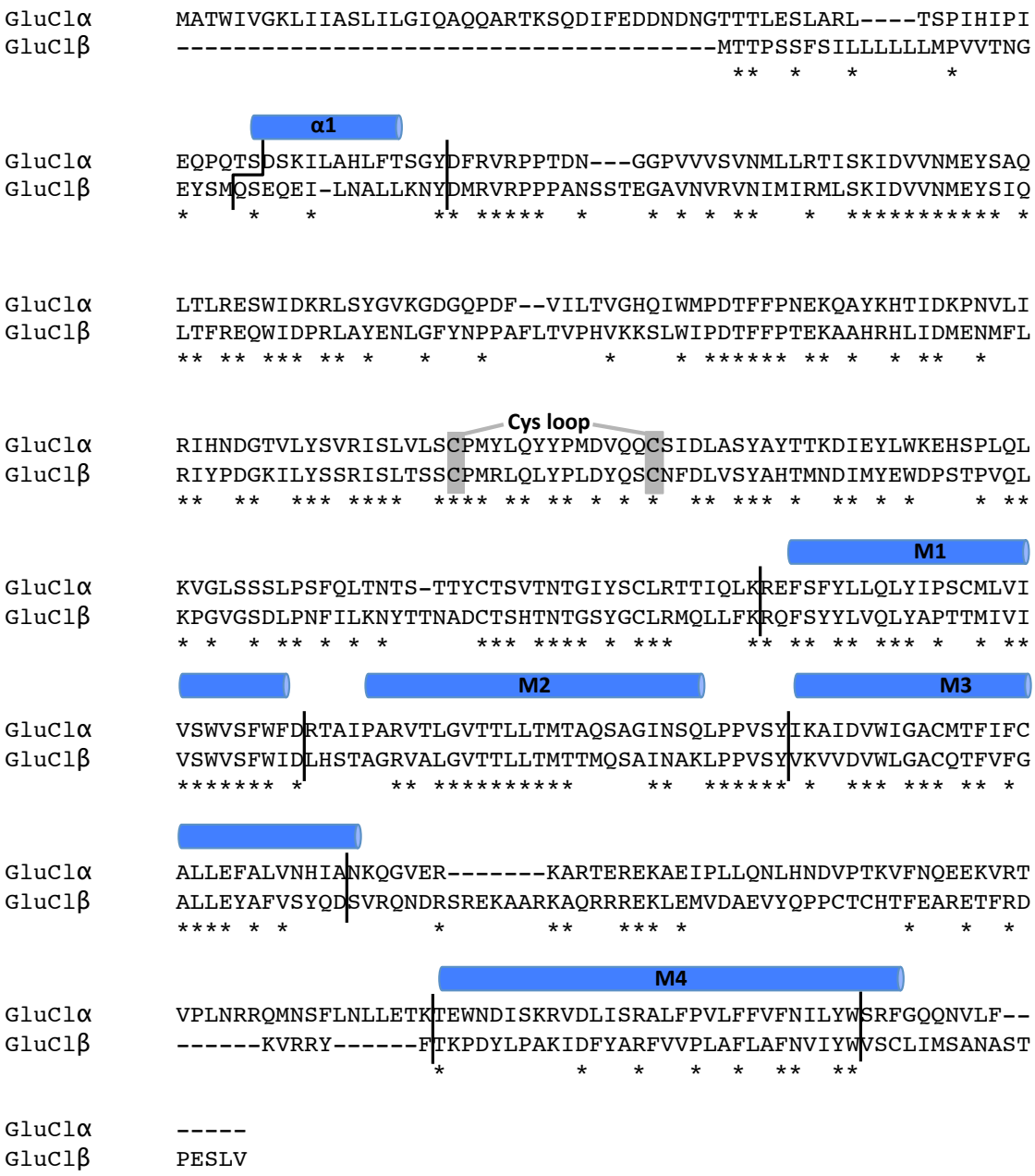

Figure 5.3. Sites of receptor splicing for chimera synthesis.

In addition to the α/β EC/TM chimera, chimeras with the receptors spliced between helices for both α/β and β/α were created (Figures 5.2 and 5.3). While a majority of these chimeras were non-functional, chimeras that are primarily GluClα, except for the M3-M4 loop and/or M4 helix, demonstrated robust glutamate responses in

addition to response to ivermectin (Table 5.1). Conversely, receptors that were primarily GluClβ at the N-terminal end did not respond to glutamate with any C-terminal fragments of GluClα. The GluClα/β-C-term chimera demonstrated functional response to glutamate, however the response to glutamate was ~10-20% that of ivermectin. This indicates impaired coupling when the entire GluClα M4 helix is present and suggests that properties of both the M4 helix and the C-terminus are responsible for this effect. Relative response of the GluClα/β chimeras including or excluding the β M3-M4 loop were similar for both glutamate and ivermectin. These findings indicate that the M3-M4 loop is not involved in glutamate insensitivity, and that the putative RxR endoplasmic reticulum (ER) retention motifs do not prevent export to the membrane in the chimeras. It is interesting to note that the GluClβ receptor with the GluClα M3-M4 loop was non-functional. This is likely attributed to impaired communication between the GluClα M3-M4 loop and the GluClβ receptor rather than a problem with the GluClα M3-M4 helix itself, as evidenced by the functional response to glutamate of both the GluClα/β-M3-M4 loop and M4 chimeras. The EC_{50} values of the GluClα/β-M3-M4 loop and TM4 chimeras are comparable to that of the wild type GluCl receptors. The EC_{50} of the original α/β EC/TM chimera is a ~500-fold gain-of-function compared to the other chimeras. This chimera also demonstrates some constitutive activity as evidenced by large leak currents in the absence of agonist and lower current response to applied glutamate.

Properties of the C-terminus and M4 helix are responsible for decoupling ligand binding and channel gating in GluClα. Upon identification of the M4 helix as a

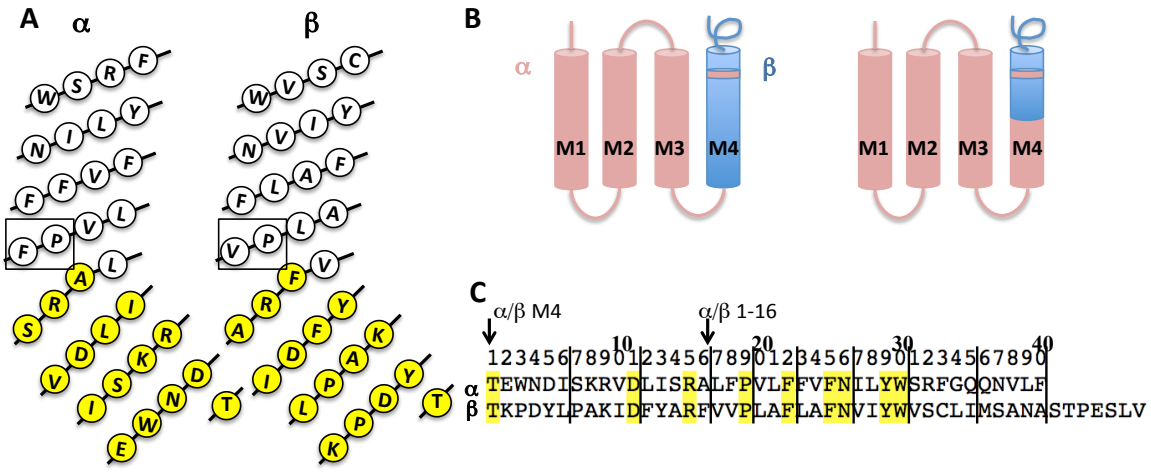

Figure 5.4. Sequence and location of residues in the GluClα and β M4 helices. **(A)** Approximate location of residues and shape of TM4, residues 1-16 are highlighted in yellow. **(B)** Cartoon of mutagenesis to GluClα/β-M4 (left) and GluClα/β-M4,1-16 (right). **(C)** Sequence alignment of TM4 and C-terminus residues. Residues conserved between the two receptors are highlighted in yellow.

Table 5.2. Mutagenesis of M4 residues in the GluClα/β-M4 chimera

	EC_{50} Glu (mM)	Hill	n	I_{max} Glu (μA)	I_{max} IVM (μA)
α/β M4	0.54 +/- 0.03	2.5 +/- 0.3	19	0.4-15	0.1-11
1-6	0.46 +/- 0.01	2.1 +/- 0.1	13	5-18	ND
1-11	0.72 +/- 0.02	1.9 +/- 0.1	7	0.3-19	ND
1-16	0.78 +/- 0.01	1.7 +/- 0.1	32	1-25	4-5
1-19	High leak currents, small response (~5% IVM)				0.5-15
1-22		No response			1-2
1-30	2.8 +/- 0.5	1.4 +/- 0.1	7	0.4-3	3-13
19-40		No response			NR
22-40		No response			NR
25-40		No response			~100 nA
29-40	0.84 +/- 0.01	2.0 +/- 0.1	10	0.5-15	1-4
36-40	1.3 +/- 0.1	2.5 +/- 0.2	8	1-5	ND
-C-term	0.20 +/- 0.01	1.2 +/- 0.1	18	2-18	ND
1-6, -C-term 7			3	0.1-0.5	0.3-1
1-11, 36-40		No response			NR
1-16, 29-40		No response			0.02-0.15
1-6, 29-40	1.3 +/- 0.1	1.9 +/- 0.1	15	0.4-8 (~15%)	5-34
1-11, 29-40		No response			0.3-2
1-16, -C-term 7	0.55 +/- 0.02	1.8 +/- 0.1	14	1-16	ND
1-16,ANA→VLF	0.89 +/- 0.03	2.1 +/- 0.1	5	0.2-0.7	ND

domain capable of uncoupling ligand binding from gating, mutagenesis was performed to narrow the residues involved (Table 5.2). Numbering for mutations made in the M4 helix begin at the N-terminus of the M4 helix as residue 1 (threonine) and continue through to the C-terminus of the GluClα receptor and end at residue 40 (phenylalanine) (Figure 5.4). The M4 helix is predicted to end at residue 30 in this numbering scheme, and so residues 31-40 are assumed to be the extracellular C-terminus residues. It was found that the first 16 residues of the M4 helix in the GluClα/β-M4 chimera could be mutated to the corresponding GluClα residues with no loss of sensitivity to glutamate. Extending the chimera to have GluClα residues at the 1-19 and 1-22 positions of the M4 helix led to receptors that had little or no response to glutamate, but demonstrated robust response to ivermectin. Some function (10-20%) was regained when the entire M4 helix (residues 1-30) was mutated to GluClα residues, as was previously mentioned. These data indicate that the nature of amino acids in the 17-C-terminus region of the M4 helix is important for determining glutamate sensitivity.

In addition to mutating residues from the N-terminus of the M4 helix, residues were also mutated from the C-terminus of the receptor in the GluClα/β-M4 chimera to further narrow the dysfunctional region. Because the C-terminus of GluClβ is seven residues longer than the C-terminus of GluClα, these extra residues were truncated as a first step to receptor mutagenesis. Truncation of these residues in the GluClα/β-M4 chimera gave individual oocytes with EC_{50} values that varied over an order of magnitude (Figure 5.5). Further mutagenesis to make the C-terminus more GluClα-like abolished this effect. We initially supposed this effect could be caused by a partial disruption of an *N*-linked glycosylation motif (NxS) in the C-terminus of GluClβ. Truncation of the

Table 5.3. Removal of and mutagenesis to a putative N-linked glycosylation site on the C-terminus of the GluClβ and GluClα/β-M4 and M4,1-16 chimeras. All constructs have the GluClβ C-terminus.

Chimera	EC_{50} (mM)	Hill	n	I_{max} (μA)	Fold shift
GluClβ	0.35 +/- 0.01	2.5 +/- 0.2	20	0.4-3.9	-
NAS (-TPESLV)	0.38 +/- 0.01	2.1 +/- 0.1	12	1.5-20	1
LAS (-TPESLV)	0.30 +/- 0.01	2.0 +/- 0.2	6	0.07-0.33	1/1.3
NAS->DAS	0.34 +/- 0.01	2.2 +/- 0.1	15	0.3-16	1
NAS->LAS	0.20 +/- 0.01	2.4 +/- 0.2	7	5-12	1/1.8
NAS out (-NASTPESLV)	No response				
GluClα/β M4	0.54 +/- 0.03	2.5 +/- 0.3	19	0.4-15	-
NAS (-TPESLV)	*Multiple populations*		*13*	*6-23*	*1*
LAS (-TPESLV)	*Multiple populations*		*7*	*1-30*	
NAS->DAS	1.0 +/- 0.1	1.8 +/- 0.1	15	0.4-16	1.9
NAS->LAS	*Multiple populations*		*6*	*6-24*	
NAS out (-NASTPESLV)	*Multiple populations*		*16*	*5-16*	*1.9*
GluClα/β 1-16	0.78 +/- 0.01	1.7 +/- 0.1	32	1.5-25	-
NAS (-TPESLV)	0.55 +/- 0.02	1.8 +/- 0.1	14	1-16	1/1.4
LAS (-TPESLV)	No data				
NAS->DAS	0.86 +/- 0.04	2.0 +/- 0.2	7	0.9-9	1.1
NAS->LAS	*0.54 +/- 0.04*	*1.6 +/- 0.1*	*7*	*4-17*	*1/1.4*
NAS out (-NASTPESLV)	0.63 +/- 0.01	2.0 +/- 0.1	15	0.4-13	1/1.2

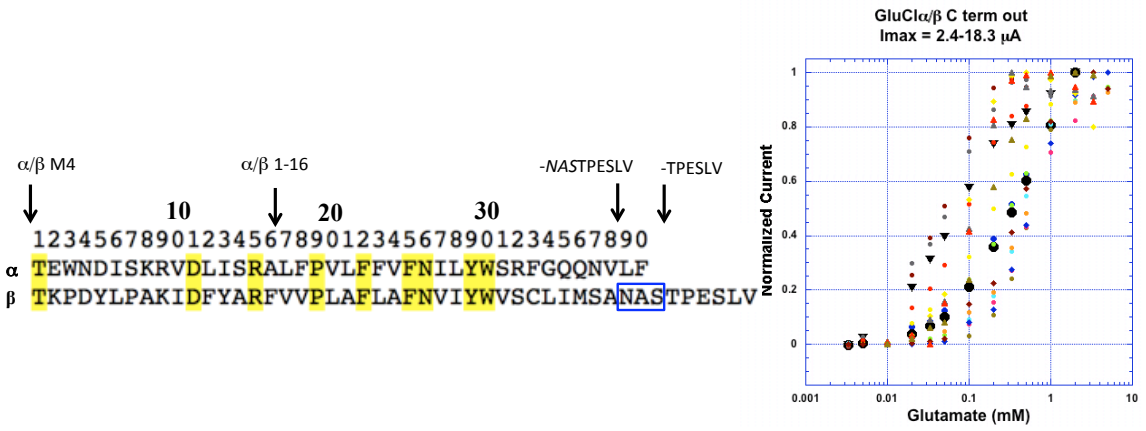

Figure 5.5. Location of NAS *N*-linked glycosylation motif at the C-terminus of GluClβ and scatter plot of GluClα/β-M4,(-TPESLV) highlighting the variability of responses in different oocytes.

seven C-terminal residues removes the serine in this motif, but not the asparagine or the subsequent alanine (Nx(A) of the motif), and could therefore lead to altered glycosylation efficiencies. Mutagenesis of asparagine to leucine in the C-terminal truncation GluClα/β-M4 chimera, which would abolish any glycosylation at this site, did not change the variability of oocyte EC_{50} and did not have an effect on receptor function (Table 5.3). Additionally, mutagenesis of the NxS glycosylation motif to DxS, which removes the nitrogen of the side chain to be glycosylated, in the chimera lacking the C-terminal truncation had no effect on receptor function, further supporting that glycosylation either does not occur at this site, or that it is not functionally relevant. These effects were not observed in the wild-type GluClβ receptor and were only observed in the N→L, but not the N→D, mutation in the GluClα/β-M4,1-16 chimera, indicating a potentially important electrostatic interaction between the asparagine and another region of the receptor in this chimera. These data provide evidence that properties of both the M4 helix and the C-terminus of the receptor are dependent on each other, and that altering either can affect the ability of the receptor to function properly. We also conclude that the variability in EC_{50} is likely due to different coupling states of the receptor. This phenomenon could be caused by weakening/changing the interaction(s) between the modified C-termini and the receptor that is shown here to be required for activation. These interactions, if less stable, could be more sensitive to variability in membrane environment of the specific oocyte.

When the remainder of the C-terminus (residues 29-40) was mutated to be GluClα-like, the receptor demonstrated similar functional properties as the parent GluClα/β-M4 chimera. This finding, when combined with previously discussed data, indicates that while the composition of the C-terminus is important for receptor function,

neither the M4 helix or the C-terminus of the GluClα receptor alone are responsible for glutamate insensitivity in the wild-type receptor. We observe this in the functional mutant GluClα/β-M4 chimeras, where the entire receptor is GluClα-like with the exception of either the C-terminus (1-16 for fully functional, 1-30 for partially) or the M4 helix (29-40). Therefore some combination of properties of the two domains must exacerbate impaired coupling of ligand binding and channel gating. Attempts to mutate GluClβ residues to their α counterparts in the GluClα/β-M4,1-16 or 29-40 chimeras were unsuccessful. These data indicate that distant residues on the M4 helix and C-terminus are functionally connected through unknown mechanisms. Two possible hypotheses to explain this phenomenon are that either the properties of the M4 helix in the *X. laevis* membrane directly affect the ability of the C-terminus to form necessary interactions, or that weaker interactions of the C-terminus prevent the M4 helix from forming important interactions with the M1 and M3 helices required for receptor function.

Mutagenesis of the M4 helix. The GluClα receptor contains a Phe-Pro motif near the middle of the M4 helix that is absent in the GluClβ receptor. This motif has been previously shown to affect the *cis-trans* preference of the proline backbone[32], which could lead to alternate conformations of the M4 helix in the GluClα and β receptors. In the GluClα crystal structure, this proline initiates a kink in the M4 helix at the i-4 position, which could provide flexibility of the C-terminal portion of the M4 helix. To determine whether the Phe-Pro motif has a functional role in the GluCl receptors, the motif was mutated into GluClβ and out of GluClα. No change in receptor EC_{50} or

glutamate sensitivity was observed for either mutant, indicating that this motif does not play a functional role in receptor activation (Table 5.4).

Next, residues within the 17-30 amino acid region in the M4 helix were mutated one helix turn at a time, from GluClβ-like to GluClα-like, to determine if specific residue mismatches were responsible for the impaired gating properties of the receptor. Mutations were made in both the GluClα/β-M4 and M4,1-16 chimeras to determine whether the effects of mutagenesis were influenced by the properties of the rest of the M4 helix. Different batches of cells gave data that were inconsistent, likely due to the large leak currents observed (> 1 μA). Large leak currents indicate either poor cell health or constitutive activation (channel opening in the absence of agonist). These leak currents increased steadily with each glutamate application and gave data that did not fit the Hill equation. One healthier batch of cells indicated a biphasic fit for some of the mutants, with the appearance of a high-sensitivity component, with an EC_{50} of ~0.02 mM glutamate, that accounted for ~20% of the response. The current response of these mutants to glutamate was ~5-25% that observed with ivermectin application. These data were not reproduced, therefore no interpretation of these mutations is considered.

Table 5.4. Mutagenesis of the Phe-Pro motif in the M4 helix of GluClα. Residue numbering is relative to the start of the M4 helix.

GluCl	EC_{50} (mM)	Hill	n	Fold shift	I_{max} (μA)
β WT	0.35 +/- 0.01	2.5 +/- 0.2	20	-	0.4-4
β V18F	0.89 +/- 0.02	1.9 +/- 0.1	7	1.3	1.4-15
α F18V	No response				

Properties of the receptor, including the M4 helix, determine requirements for the length of the C-terminus. C-terminal truncations were made to the wild-type GluClβ receptor and the GluClα/β-M4 and M4,1-16 chimeras to determine requirements for C-terminus length. The length of the C-terminus has previously been shown to affect receptor trafficking and formation of functional ligand binding sites[14,15]. In these studies, truncation of the 5-HT_{3A} C-terminus, in either the wild-type receptor or α7 EC binding domain chimera, resulted in impaired ligand sensitivity and surface expression with results that were independent of the identity of the extracellular binding domain. Here, we show that the GluCl receptors are also sensitive to C-terminal truncation, however the amount of truncation that was tolerated was dependent on the identity of the rest of the receptor.

The wild-type GluClβ receptor was shown to be the most sensitive to C-terminal truncation with a complete loss of function upon removal of the last 9 amino acids, which results in a C-terminus that is two residues shorter than the wild-type GluClα receptor (Figure 5.6 and Table 5.5). Conversely, truncation of the terminal 9 amino acids on the GluClα/β-M4 chimeras had no effect on receptor function. Removal of an additional two amino acids (-11) resulted in a decrease in functional response to glutamate in the GluClα/β-M4,1-16 chimera, but not in the GluClα/β-M4 chimera, and truncation to -13 further reduced the GluClα/β-M4,1-16 response and decreased the response of the GluClα/β-M4 chimera as well. It is important to note that all of the receptors considered here in the C-terminal truncations studies have an identical GluClβ-like C-terminal domain, but vary in the GluClα-like or GluClβ-like character of the rest of the receptor. Therefore, the variations in functionality of the truncated constructs are likely due to

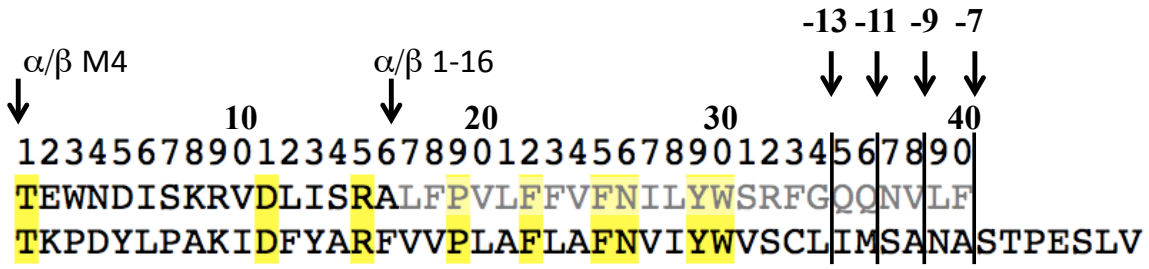

Figure 5.6. Sites of C-terminus truncation. The GluClα sequence is hidden from residue 17-40 because all constructs considered in this study have GluClβ-like character in this region at a minimum.

Table 5.5. C-terminal truncation of GluClβ and GluClα/β-M4 and M4,1-16 chimeras

	EC_{50} (mM)	Hill	n	I_{max} (μA)	Fold shift
WT					
GluClβ	0.35 +/- 0.01	2.5 +/- 0.2	20	0.4-3.9	-
GluClα/β-M4	0.54 +/- 0.03	2.5 +/- 0.3	19	0.4-15	-
GluClα/β-M4,1-16	0.78 +/- 0.01	1.7 +/- 0.1	32	1.5-25	-
C-term 7 out					
GluClβ	0.38 +/- 0.01	2.1 +/- 0.1	12	1-20	1
GluClα/β-M4	0.56 +/- 0.04	1.2 +/- 0.1	13	6-23	1
GluClα/β-M4,1-16	0.55 +/- 0.02	1.8 +/- 0.1	14	1-16	1/1.4
C term 9 out					
GluClβ		No response			
GluClα/β-M4	1.0 +/- 0.1	1.1 +/- 0.1	16	5-16	1.9
GluClα/β-M4,1-16	0.63 +/- 0.01	2.0 +/- 0.1	15	0.4-13	1/1.2
C-term 11 out					
GluClβ		No response			
GluClα/β-M4	0.83 +/- 0.04	2.0 +/- 0.2	15	5-25	1.5
GluClα/β-M4,1-16	1.6 +/- 0.1	2.2 +/- 0.1	13	0.4-3	2.1
C-term 13 out					
GluClβ		No response			
GluClα/β-M4	0.75 +/- 0.06	1.8 +/- 0.2	7	0.1-1.2	1.4
GluClα/β-M4,1-16	3.3 +/- 0.6	1.0 +/- 0.1	8	0.07-0.4	4.2

different functional interactions between the C-terminus and the corresponding receptor. This can be interpreted as the two receptors (GluClα and β) having different interactions between the C-terminus and its interaction partner or that the two receptors have different

activation mechanisms that have varied requirements for C-terminus coupling to another domain of the receptor.

In the GluClβ receptor, a strong requirement was found for having an extended C-terminal domain, whereas a lesser requirement was demonstrated for the GluClα-like receptors. One interpretation for this is that the GluClβ receptor needs a longer C-terminus so that it can interact with residues distal from the M4 helix either through specific or global electrostatic interactions. This is supported by a large loss of functional response to glutamate in the N→L mutation of the -9 residue (from the end of the C-terminus) in the GluClβ -7 C-terminal truncation (Table 5.3). These combined data indicate that this residue, potentially in addition to others toward the M4 helix, participates in an important electrostatic interaction with another residue in the GluClβ receptor. This effect would not be observed in the chimeras if the partner residue was not conserved in the GluClα receptor, if there were other functionally analogous interactions, or if the C-terminus was less important in the activation mechanism of GluClα. The difference in truncation sensitivity in the two GluClα/β-M4 chimeras indicates that the C-terminus is important for activation, and that properties of the M4 helix affect coupling interactions between the C-terminal domain and its interaction partner in the receptor. These effects could be caused by differences in the dynamics or structure of the M4 helix in the membrane, which could affect the placement and flexibility of the C-terminal domain. These interactions in the GluClα receptor may be more global and less specific than they are in the GluClβ receptor because of the tolerance of the GluClβ C-terminus. A defective GluClα C-terminus or interaction between the C-terminus and its interaction partner in the receptor can be ruled out because of the full response to glutamate in the

GluClα/β-M4,29-40 chimera, which contains only a GluClβ-like M4 helix. Instead, membrane properties of the M4 helix are likely responsible for the observed glutamate insensitivity. Studies were not performed to determine whether the lack of response to glutamate in the C-terminal truncations was due to impaired surface expression or receptor activation. We assume that C-terminal truncation in the GluCl receptors is not causing ER retention, as was observed in the 5-HT_{3A} receptors, because no ER retention motif is found in the EC or TM regions that would need to be masked by this domain.

Functional interactions between the C-terminus and the extracellular domain of GluClα were not identified. The C-terminal domain of Cys-loop receptors has long been predicted to make a functional interaction with the extracellular ligand binding domain[14,16,17,32]. The interaction partner of the C-terminus has been speculated to be the Cys-loop, which is supported by direct contacts observed in the GluClα crystal structure (Figure 5.7). To determine whether there are specific interactions between the Cys-loop and the C-terminus in the GluCl receptors, chimeras with matched and mismatched Cys-loop and C-terminal domains were synthesized (Table 5.6 and Figure 5.8). Of these chimeras, only the GluClα with the β C-terminus and GluClβ with the α Cys-loop were functional. These data further support our findings that glutamate insensitivity in GluClα is not caused by a lack of coupling between the C-terminus and Cys-loop. If it were, glutamate sensitivity would be recovered in the GluClα receptor by introducing both the β Cys-loop and C-terminus, which should form a functional pair. The data also suggest that the inherent properties of the GluClα Cys-loop are not flawed because incorporation of this sequence into GluClβ results in a fully functional receptor. Despite these findings

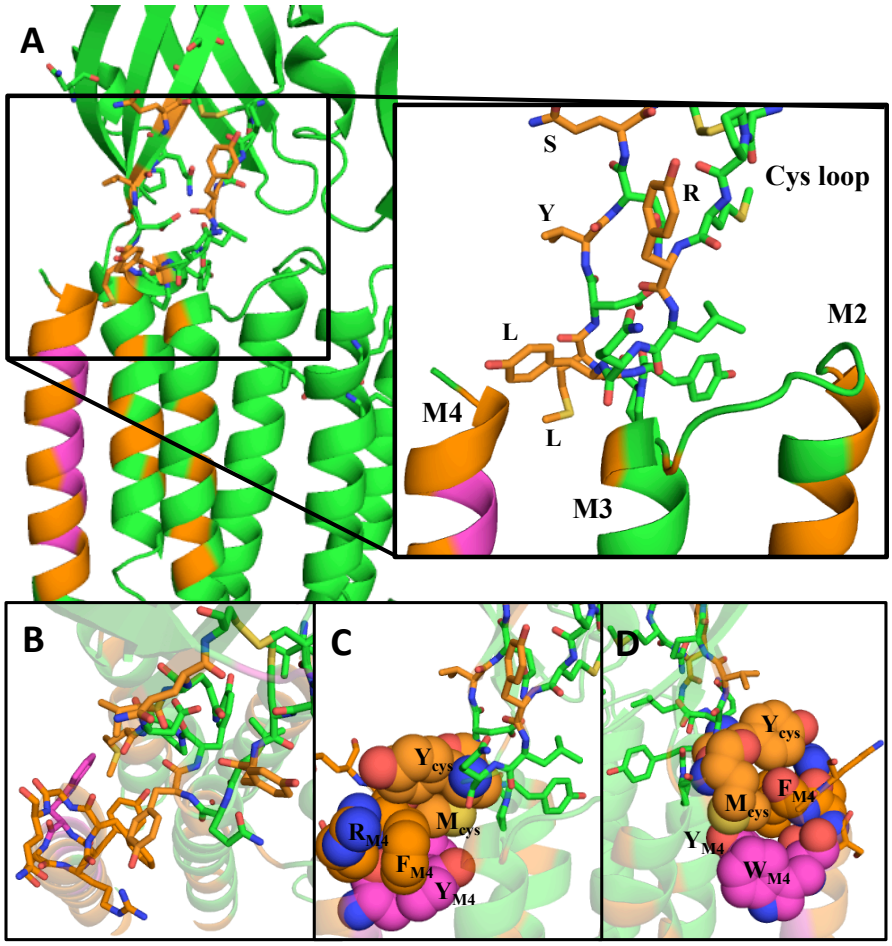

Figure 5.7. Crystal structure of the Cys-loop-C-terminus interactions predicted by the GluClα crystal structure. Green and purple residues are conserved between the GluClα and β receptors, purple residues are located in the 17-34 region of the M4 helix. Orange residues are not conserved between the two receptors. Crystallographic data is not available for residues 35-40. **(A)** Side view of the Cys-loop. Residue labels indicate the corresponding amino acid in GluClβ. **(B)** Top down view of the Cys-loop and C-terminus. **(C)** Side view from the M3 helix of the Cys-loop and C-terminus. Residues predicted to contact each other are shown as space-filling. **(D)** The same interactions as seen from the M1 helix.

not providing evidence for a functional interaction between the two domains, the chimeras indicate that these regions are important for receptor activation, as shown by a lack of response to both glutamate and ivermectin in a majority of the chimeras examined.

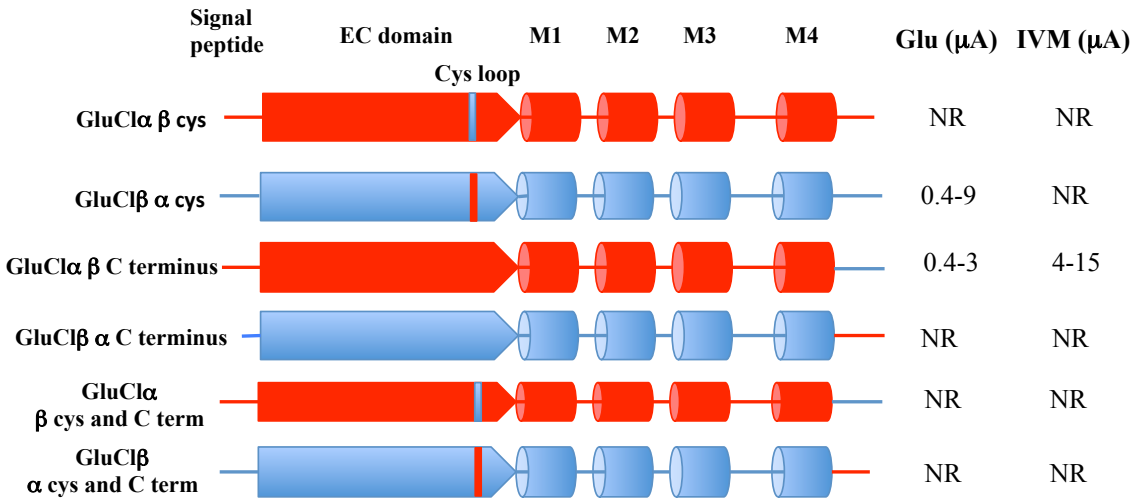

Figure 5.8. Cartoon representation of chimeras examined in this study.

Table 5.6. Cys-loop and C-terminus chimera data

Chimera	EC_{50} (mM)	Hill	n	I_{max} Glu (μA)	IVM (μA)
GluClα β Cys-loop		No response			NR
GluClβ α Cys-loop	0.57 +/- 0.01	2.2 +/- 0.1	15	0.4-9	-
GluClα β C	2.8 +/- 0.5	1.4 +/- 0.1	7	0.4-3	3-13
GluClβ α C		No response			-
GluClα β Cys and C		No response			NR
GluClβ α Cys and C		No response			-

Because we could not confirm a functional interaction between the Cys-loop and the C-terminus, we sought to identify other potential sites of interaction between the C-terminus and the EC domain of the receptor. Near the Cys-loop on the β9 strand of the EC domain is an asparagine residue in an *N*-linked glycosylation motif in both the GluClα and β receptors (Figure 5.9). Glycosylation of this residue could obstruct interaction between the C-terminus and the Cys-loop, or could provide additional polar functional groups for the C-terminus to interact with. To determine the importance of glycosylation at this site, the motif was altered or removed. An NxS motif is found in GluClα and an NxT motif in GluClβ, both of which have been shown to encode *N*-linked

glycosylation in eukaryotes with varying rates and efficiencies[33,34]. Therefore, to determine whether the two glycosylation motifs lead to differences in glycosylation patterns or efficiencies in *X. laevis* oocytes, the motifs were swapped in the two receptors. The glycosylation motifs were also removed in both receptors by mutating the asparagine to alanine. In both cases, no change in receptor function was observed (Table 5.7). These data suggest that the GluCl receptors are not glycosylated in *X. laevis* oocytes or that there is no functional role for glycosylation at this site in the GluClβ receptor. It is possible that there is a functional role for glycosylation at this site in GluClα, and the lack of glycosylation in *X. laevis* oocytes is involved in glutamate insensitivity.

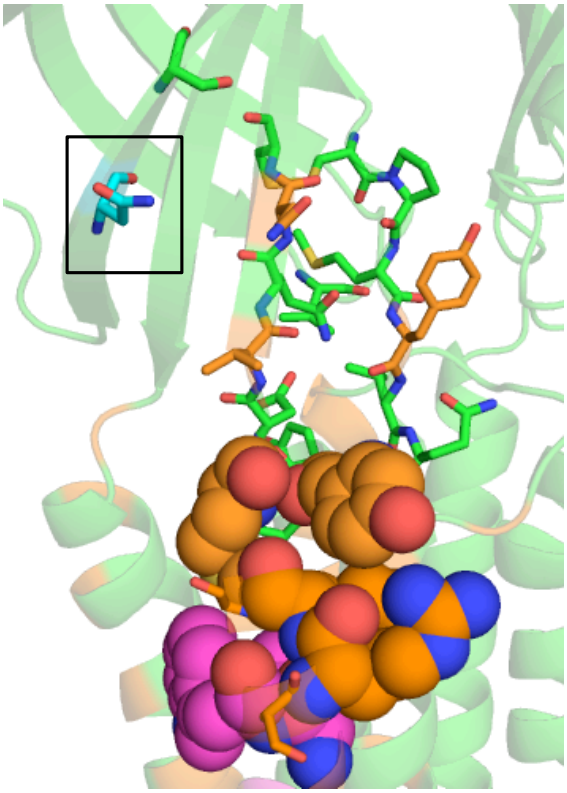

Figure 5.9. Interaction of C-terminus residues in the GluClα crystal structure (3RIF) with the Cys-loop. The asparagine in the *N*-linked glycosylation motif is indicated in cyan.

Because the GluClα receptor could only be crystalized when the six C-terminal residues (35-40) were deleted, these residues can be assumed to be unstructured in the ligand-bound state (assuming the crystal structure represents a physiologically relevant state). Therefore, any interaction the C-terminus makes with another region of the receptor is likely transient or low affinity, and therefore cannot be captured in a static snapshot of the receptor. While the length and composition (in the GluClβ receptor) were

Table 5.7. Modulation and removal of a putative N-linked glycosylation site on the β9 sheet of the extracellular domain.

	EC_{50} (mM)	Hill	n	I_{max} (μA)	Fold shift
GluClα NxS→NxT	No response to glutamate, response to IVM				
GluClα NxS→AxS	No response to glutamate, response to IVM				
GluClβ NxT→NxS	0.57 +/- 0.01	2.2 +/- 0.1	7	0.2-4	1.6
GluClβ NxT→AxT	0.28 +/- 0.01	2.0 +/- 0.1	8	0.3-1	1/1.25

shown to be important for receptor activation, no binding partner was identified for the C-terminus. REFER analysis also does not indicate that the Cys-loop (or any other region of the EC domain) and the M4 helix/C-terminus act as a functional unit because both domains move at different, and not subsequent, stages of the activation process[4]. We therefore cannot make any conclusions about the role of the C-terminus in receptor activation.

Probing membrane properties: examination of cholesterol-receptor interactions and effect of incubation temperature. The crystal structure of the GluClα receptor shows a kink and bulge at approximately the midpoint of the M4 helix. This kink is likely caused by a break in hydrogen bonding of the helical backbone by a proline residue conserved amongst the anion-selective Cys-loop receptors and the prokaryotic ligand-gated ion channels. This break in the helix occurs at the i-4 residue from the proline, which in the GluClα receptor is an arginine at the 15th residue on the helix. Along with the kink, a bulge occurs at the subsequent alanine residue (residue 16 on the helix) because of a partial unwinding of the helix. The C-terminal region of this helix, following this kink and bulge, is the region shown in this study to cause glutamate insensitivity in GluClα as indicated by the GluClα/β-M4,1-16 chimera. We hypothesize that either intrinsic

properties of this part of the helix or interactions with the surrounding membrane are responsible for glutamate insensitivity.

In the GluClα receptor, a putative cholesterol-binding motif (L/V-X_{1-5}-Y-X_{1-5}-R/K, where X is between 1 and 5 amino acids of any type[35,36]) was identified near the C-terminal end of the M4 helix (Figure 5.10a). This motif (and its inverted counterpart) is found in a number of other Cys-loop receptors[37-39], as well as other membrane proteins[38,40], and is thought to aid in the incorporation of membrane proteins into cholesterol-rich lipid domains[41]. Indeed, sterol interaction with the M4 helix has been shown to modulate function in the *Torpedo* nAChR[42,43] and $GABA_A$ receptor[44], as well as in the TM domains of a number of G protein-coupled receptors. Mutagenesis[43], computational studies[27], and lipid modulation[17,45] indicate a lipid-dependent uncoupling of ligand-binding and TM domains in Cys-loop receptors displaying cholesterol-binding motifs in the M4 helix in the absence of crucial lipid-protein interactions. Ligand-gated ion channels that lack this cholesterol recognition motif have been found to be less sensitive to cholesterol modulation[46].

Mutagenesis to remove the cholesterol recognition motif led to a partial regain of function in the GluClα receptor (Figure 5.10b). The $Vx_4Yx_2R \rightarrow Ax_4Ax_2A$ mutation gave glutamate-induced currents with a maximum response that was ~10% the currents observed in response to ivermectin. The YxR→AxA mutant also gave similar responses, but mutagenesis of individual residues in the motif had little-to-no effect on receptor activation. The relative responses to glutamate and ivermectin varied between cell batches, indicating that inherent variability between oocytes can affect receptor activity.

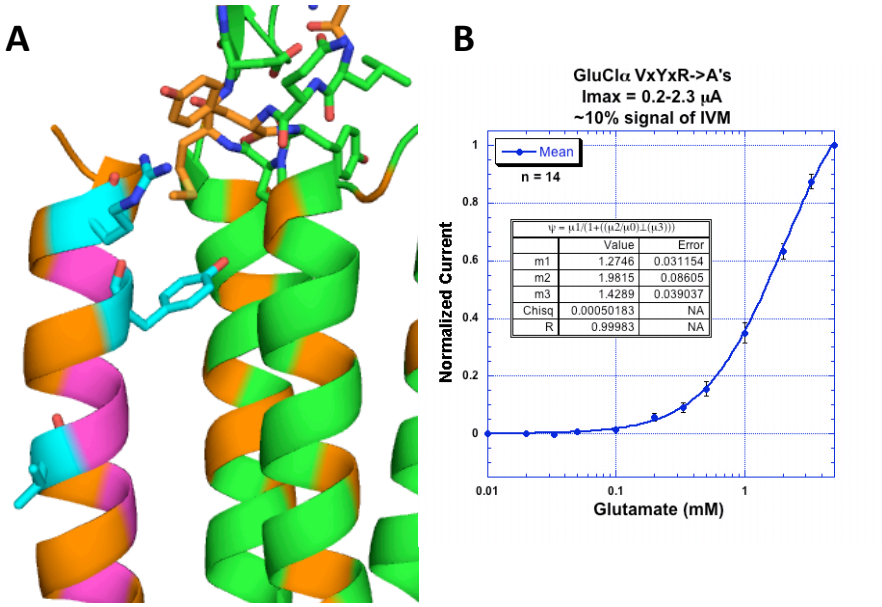

Figure 5.10. Cholesterol binding motif in the GluClα receptor. (A) Crystal structure of residues in the motif (B) dose-response curve of removal of the putative cholesterol binding motif.

To visualize the putative cholesterol binding site, cholesterol was docked into the crystal structure of GluClα (Figure 5.11). This was performed by dragging the coordinates for cholesterol into the binding site predicted by the recognition motif. No energy minimization was performed to optimize cholesterol binding to the receptor. By rough fit, the cholesterol molecule fits well in the predicted binding site. The hydroxyl of cholesterol could easily be bound by the arginine side chain and the planar hydrophobic core of cholesterol could be stabilized by stacked aromatic residues formed by TM3/TM4 helical interactions. The GluClα M4 helix also differs from the GluClβ receptor in that it has larger hydrophobic residues on the periphery of the putative cholesterol binding site. These residues, along with the polar and aromatic contacts, could form a hydrophobic binding pocket that bound cholesterol with high-affinity. Mutagenesis of these large hydrophobic residues in addition to the VxYxR→AxAxA mutations, did not increase

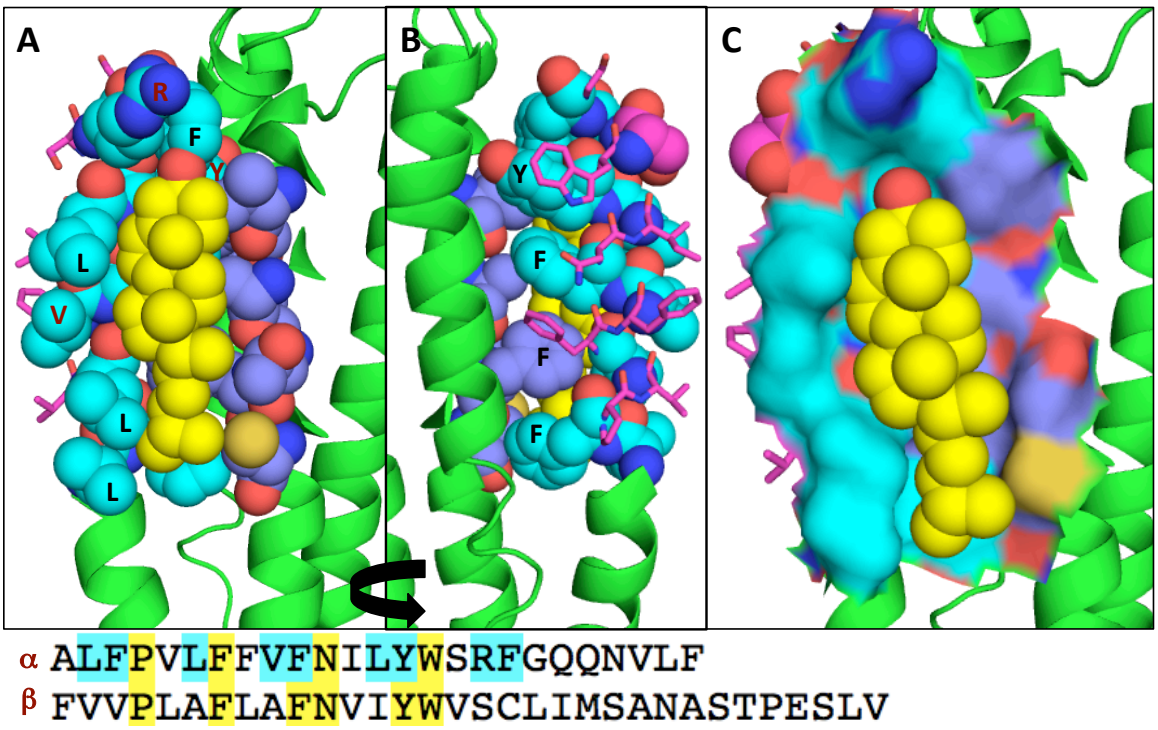

Figure 5.11. Putative cholesterol binding site. Residues in cyan are on the M4 helix, residues in blue are on the M3 helix, and cholesterol is shown in yellow. Cholesterol was docked into the GluClα structure with no energy minimization. **(A)** and **(B)** front and back view of the putative cholesterol binding site, respectively. **(C)** Surface contour of the two helices.

response to glutamate and in most cases, resulted in a non-functional receptor. These findings indicate that the arginine and tyrosine residues are the crucial components of cholesterol binding, and that small hydrophobic side chains in the M4 helix disfavor receptor activation.

Attempts to remove cholesterol, using methyl-β-cyclodextrin (MβCD), were not effective. Incubation of oocytes in low concentrations of MβCD (50 or 500 μM) prior to data collection did not result in glutamate-induced currents of the wild type receptor. Incubation with a higher concentration (5 mM) resulted in cells with large leak currents indicative of compromised cell health. MβCD incubation of oocytes expressing the VxYxR→AxAxA mutations also resulted in low current responses to applied glutamate,

however poor cell health gave data that did not fit the Hill equation (data not shown). Similar data were found with GluCl receptors expressed in HEK293T cells. We therefore conclude that in the GluClα receptor, cholesterol acts as a negative allosteric modulator, which is contrary to the effects observed in the muscle-type nAChR and $GABA_A$ receptors. While we are able to see this effect through receptor mutagenesis, cholesterol depletion with MβCD has not proved to be an effective way to remove tightly bound cholesterol. This would not be surprising if a high-affinity cholesterol binding site was present, because of the large concentration of cholesterol found in the membrane and the fact that MβCD is only capable of binding and sequestering free cholesterol molecules.

Negative allosteric modulation by cholesterol could occur through many different mechanisms. In the crystal structure, which was obtained without cholesterol in the crystallization matrix, the arginine residue in the cholesterol binding motif is predicted to form a hydrogen bond interaction with a tyrosine on the Cys-loop. This tyrosine is a leucine in the GluClβ receptor, further providing evidence that these receptors do not have conserved interactions between the C-terminus and the EC domain. Mutagenesis of this tyrosine to alanine in GluClα resulted in a non-functional receptor that did not respond to either glutamate of ivermectin, indicating its importance in the activation mechanism. While we were not able to provide evidence for a functional coupling between the Cys-loop and the C-terminus, data were collected in cells with high concentrations of cholesterol. It is possible that the hydroxyl of cholesterol binds the arginine, thereby preventing a potentially important interaction between the C-terminus and the Cys-loop. It is also possible that bound cholesterol changes the properties of the membrane environment sensed by the receptor. Cholesterol is known to increase the

thickness of the membrane[47], which could prevent helical tilting of the M4 helix, thought to be part of the activation mechanism[48] because of the energetic penalty of burying polar residues in the hydrophobic membrane. Also, bound cholesterol could stabilize M3-M4 helix interactions and preclude TM helical movement. Regardless of mechanism, cholesterol likely plays a role in receptor activation. While we are not able to definitively prove a direct TM4-cholesterol interaction, data in this study suggest cholesterol as a negative allosteric modulator. The existence and location of the cholesterol recognition motif on the M4 helix coincides well with chimera data and removal of this motif results in a partial regain of function. Additional experiments are required to determine the nature of this interaction.

While the "cholesterol as a negative allosteric modulator" hypothesis works for experiments in *X. laevis* oocytes, the hypothesis does not hold for other heterologous expression systems. The GluClα receptor was shown to be functional when expressed in HEK293 cells[28], which also have a high concentration of cholesterol in the lipid bilayer. It is possible, however, that properties of the membrane or the receptor in the membrane vary at the different incubation temperatures of the expression systems (18^{o}C for *X. laevis* oocytes and 37^{o}C for HEK293 cells). Because we couldn't incubate or record on oocytes at 37^{o}C, HEK293T cells expressing wild-type GluClα were assayed at 25^{o}C and 37^{o}C to determine whether a decrease in temperature had an effect on response to applied glutamate. While some days of recording indicated a slight loss of receptor response at the lower temperature, the data were not consistent between trials. It is also possible that the observed slight loss of signal was due to cell health issues.

References

1. Unwin, N., Refined structure of the nicotinic acetylcholine receptor at 4A resolution. *J Mol Biol*, **2005**. *346*(4): p. 967-989.
2. Hibbs, R.E. and Gouaux, E., Principles of activation and permeation in an anion-selective Cys-loop receptor. *Nature*, **2011**. *474*(7349): p. 54-80.
3. Cederholm, J.M., Schofield, P.R., and Lewis, T.M., Gating mechanisms in Cys-loop receptors. *Eur Biophys J*, **2009**. *39*(1): p. 37-49.
4. Purohit, P., Mitra, A., and Auerbach, A., A stepwise mechanism for acetylcholine receptor channel gating. *Nature*, **2007**. *446*(7138): p. 930-933.
5. Grosman, C., Zhou, M., and Auerbach, A., Mapping the conformational wave of acetylcholine receptor channel gating. *Nature*, **2000**. *403*(6771): p. 773-776.
6. Bouzat, C., Gumilar, F., Spitzmaul, G., Wang, H.L., Rayes, D., Hansen, S.B., Taylor, P., and Sine, S.M., Coupling of agonist binding to channel gating in an ACh-binding protein linked to an ion channel. *Nature*, **2004**. *430*(7002): p. 896-900.
7. Kash, T.L., Jenkins, A., Kelley, J.C., Trudell, J.R., and Harrison, N.L., Coupling of agonist binding to channel gating in the GABA(A) receptor. *Nature*, **2003**. *421*(6920): p. 272-5.
8. Mercado, J. and Czajkowski, C., Charged residues in the alpha1 and beta2 pre-M1 regions involved in GABAA receptor activation. *J Neurosci*, **2006**. *26*(7): p. 2031-2040.
9. Hu, X.Q., Zhang, L., Stewart, R.R., and Weight, F.F., Arginine 222 in the pre-transmembrane domain 1 of 5-HT3A receptors links agonist binding to channel gating. *J Biol Chem*, **2003**. *278*(47): p. 46583-46589.
10. Miyazawa, A., Fujiyoshi, Y., and Unwin, N., Structure and gating mechanism of the acetylcholine receptor pore. *Nature*, **2003**. *423*(6943): p. 949-955.
11. Kash, T.L., Kim, T., Trudell, J.R., and Harrison, N.L., Evaluation of a proposed mechanism of ligand-gated ion channel activation in the GABAA and glycine receptors. *Neurosci Lett*, **2004**. *371*(2-3): p. 230-234.
12. Lynch, J.W., Rajendra, S., Pierce, K.D., Handford, C.A., Barry, P.H., and Schofield, P.R., Identification of intracellular and extracellular domains mediating signal transduction in the inhibitory glycine receptor chloride channel. *EMBO J*, **1997**. *16*(1): p. 110-120.
13. Schofield, C.M., Jenkins, A., and Harrison, N.L., A highly conserved aspartic acid residue in the signature disulfide loop of the alpha 1 subunit is a determinant of gating in the glycine receptor. *J Biol Chem*, **2003**. *278*(36): p. 34079-34083.
14. Pons, S., Sallette, J., Bourgeois, J.P., Taly, A., Changeux, J.P., and Devillers-Thiery, A., Critical role of the C-terminal segment in the maturation and export to the cell surface of the homopentameric alpha 7-5HT3A receptor. *Eur J Neurosci*, **2004**. *20*(8): p. 2022-2030.
15. Butler, A.S., Lindesay, S.A., Dover, T.J., Kennedy, M.D., Patchell, V.B., Levine, B.A., Hope, A.G., and Barnes, N.M., Importance of the C-terminus of the human 5-HT3A receptor subunit. *Neuropharmacology*, **2009**. *56*(1): p. 292-302.

16. Xiu, X., Hanek, A.P., Wang, J., Lester, H.A., and Dougherty, D.A., A unified view of the role of electrostatic interactions in modulating the gating of Cys loop receptors. *J Biol Chem*, **2005**. *280*(50): p. 41655-41666.
17. daCosta, C.J. and Baenziger, J.E., A lipid-dependent uncoupled conformation of the acetylcholine receptor. *J Biol Chem*, **2009**. *284*(26): p. 17819-17825.
18. Haeger, S., Kuzmin, D., Detro-Dassen, S., Lang, N., Kilb, M., Tsetlin, V., Betz, H., Laube, B., and Schmalzing, G., An intramembrane aromatic network determines pentameric assembly of Cys-loop receptors. *Nature Structural & Molecular Biology*, **2010**. *17*(1): p. 90-98.
19. Barrantes, F.J., Bermudez, V., Borroni, M.V., Antollini, S.S., Pediconi, M.F., Baier, J.C., Bonini, I., Gallegos, C., Roccamo, A.M., Valles, A.S., Ayala, V., and Kamerbeek, C., Boundary Lipids In The Nicotinic Acetylcholine Receptor Microenvironment. *Journal of Molecular Neuroscience*, **2010**. *40*(1-2): p. 87-90.
20. Caballero-Rivera, D., Cruz-Nieves, O.A., Oyola-Cintron, J., Torres-Nunez, D.A., Otero-Cruz, J.D., and Lasalde-Dominicci, J.A., Tryptophan scanning mutagenesis reveals distortions in the helical structure of the deltaM4 transmembrane domain of the Torpedo californica nicotinic acetylcholine receptor. *Channels (Austin)*, **2012**. *6*(2): p. 111-123.
21. Mitra, A., Bailey, T.D., and Auerbach, A.L., Structural dynamics of the M4 transmembrane segment during acetylcholine receptor gating. *Structure*, **2004**. *12*(10): p. 1909-1918.
22. Lummis, S.C., Beene, D.L., Lee, L.W., Lester, H.A., Broadhurst, R.W., and Dougherty, D.A., Cis-trans isomerization at a proline opens the pore of a neurotransmitter-gated ion channel. *Nature*, **2005**. *438*(7065): p. 248-252.
23. Saul, B., Kuner, T., Sobetzko, D., Brune, W., Hanefeld, F., Meinck, H.M., and Becker, C.M., Novel GLRA1 missense mutation (P250T) in dominant hyperekplexia defines an intracellular determinant of glycine receptor channel gating. *Journal of Neuroscience*, **1999**. *19*(3): p. 869-877.
24. Etter, A., Cully, D.F., Schaeffer, J.M., Liu, K.K., and Arena, J.P., An amino acid substitution in the pore region of a glutamate-gated chloride channel enables the coupling of ligand binding to channel gating. *J Biol Chem*, **1996**. *271*(27): p. 16035-16039.
25. Han, L., Talwar, S., and Lynch, J.W., The Relative Orientation of the TM3 and TM4 Domains Varies between alpha 1 and alpha 3 Glycine Receptors. *ACS Chem Neurosci*, **2013**. *4*(2): p. 248-254.
26. Chen, X.B., Webb, T.I., and Lynch, J.W., The M4 transmembrane segment contributes to agonist efficacy differences between 1 and 3 glycine receptors. *Molecular Membrane Biology*, **2009**. *26*(5-7): p. 321-332.
27. Brannigan, G., Henin, J., Law, R., Eckenhoff, R., and Klein, M.L., Embedded cholesterol in the nicotinic acetylcholine receptor. *Proceedings of the National Academy of Sciences of the United States of America*, **2008**. *105*(38): p. 14418-14423.
28. Frazier, S.J., Cohen, B.N., and Lester, H.A., An engineered glutamate-gated chloride (GluCl) channel for sensitive, consistent neuronal silencing by ivermectin. *J Biol Chem*, **2013**. *288*(29): p. 21029-21042.

29. Slimko, E.M. and Lester, H.A., Codon optimization of Caenorhabditis elegans GluCl ion channel genes for mammalian cells dramatically improves expression levels. *J Neurosci Methods*, **2003**. *124*(1): p. 75-81.
30. Nowak, M.W., Gallivan, J.P., Silverman, S.K., Labarca, C.G., Dougherty, D.A., and Lester, H.A., In vivo incorporation of unnatural amino acids into ion channels in Xenopus oocyte expression system. *Ion Channels, Pt B*, **1998**. *293*: p. 504-529.
31. Lummis, S.C.R., Thompson, A.J., Bencherif, M., and Lester, H.A., Varenicline Is a Potent Agonist of the Human 5-Hydroxytryptamine(3) Receptor. *Journal of Pharmacology and Experimental Therapeutics*, **2011**. *339*(1): p. 125-131.
32. Limapichat, W., Lester, H.A., and Dougherty, D.A., Chemical Scale Studies of the Phe-Pro Conserved Motif in the Cys Loop of Cys Loop Receptors. *Journal of Biological Chemistry*, **2010**. *285*(12): p. 8976-8984.
33. Marshall, R.D., Glycoproteins. *Annu Rev Biochem*, **1972**. *41*: p. 673-702.
34. Bause, E. and Legler, G., The role of the hydroxy amino acid in the triplet sequence Asn-Xaa-Thr(Ser) for the N-glycosylation step during glycoprotein biosynthesis. *Biochem J*, **1981**. *195*(3): p. 639-644.
35. Li, H. and Papadopoulos, V., Peripheral-type benzodiazepine receptor function in cholesterol transport. Identification of a putative cholesterol recognition/interaction amino acid sequence and consensus pattern. *Endocrinology*, **1998**. *139*(12): p. 4991-4997.
36. Li, H., Yao, Z., Degenhardt, B., Teper, G., and Papadopoulos, V., Cholesterol binding at the cholesterol recognition/ interaction amino acid consensus (CRAC) of the peripheral-type benzodiazepine receptor and inhibition of steroidogenesis by an HIV TAT-CRAC peptide. *Proc Natl Acad Sci U S A*, **2001**. *98*(3): p. 1267-1272.
37. Baier, C.J., Fantini, J., and Barrantes, F.J., Disclosure of cholesterol recognition motifs in transmembrane domains of the human nicotinic acetylcholine receptor. *Sci Rep*, **2011**. *1*: p. 69.
38. Burger, K., Gimpl, G., and Fahrenholz, F., Regulation of receptor function by cholesterol. *Cell Mol Life Sci*, **2000**. *57*(11): p. 1577-1592.
39. Fantini, J. and Barrantes, F.J., How cholesterol interacts with membrane proteins: an exploration of cholesterol-binding sites including CRAC, CARC, and tilted domains. *Front Physiol*, **2013**. *4*: p. 31.
40. Hanson, M.A., Cherezov, V., Griffith, M.T., Roth, C.B., Jaakola, V.P., Chien, E.Y., Velasquez, J., Kuhn, P., and Stevens, R.C., A specific cholesterol binding site is established by the 2.8 A structure of the human beta2-adrenergic receptor. *Structure*, **2008**. *16*(6): p. 897-905.
41. Epand, R.M., Thomas, A., Brasseur, R., and Epand, R.F., Cholesterol interaction with proteins that partition into membrane domains: an overview. *Subcell Biochem*, **2010**. *51*: p. 253-278.
42. Blanton, M.P., Xie, Y., Dangott, L.J., and Cohen, J.B., The steroid promegestone is a noncompetitive antagonist of the Torpedo nicotinic acetylcholine receptor that interacts with the lipid-protein interface. *Mol Pharmacol*, **1999**. *55*(2): p. 269-278.
43. Santiago, J., Guzman, G.R., Rojas, L.V., Marti, R., Asmar-Rovira, G.A., Santana, L.F., McNamee, M., and Lasalde-Dominicci, J.A., Probing the effects of membrane cholesterol in the Torpedo californica acetylcholine receptor and the

novel lipid-exposed mutation alpha C418W in Xenopus oocytes. *J Biol Chem*, **2001**. *276*(49): p. 46523-46532.
44. Sooksawate, T. and Simmonds, M.A., Effects of membrane cholesterol on the sensitivity of the GABA(A) receptor to GABA in acutely dissociated rat hippocampal neurones. *Neuropharmacology*, **2001**. *40*(2): p. 178-84.
45. Barrantes, F.J., Cholesterol effects on nicotinic acetylcholine receptor. *J Neurochem*, **2007**. *103 Suppl 1*: p. 72-80.
46. Labriola, J.M., Pandhare, A., Jansen, M., Blanton, M.P., Corringer, P.J., and Baenziger, J.E., Structural sensitivity of a prokaryotic pentameric ligand-gated ion channel to its membrane environment. *J Biol Chem*, **2013**. *288*(16): p. 11294-11303.
47. Nezil, F.A. and Bloom, M., Combined influence of cholesterol and synthetic amphiphillic peptides upon bilayer thickness in model membranes. *Biophys J*, **1992**. *61*(5): p. 1176-1183.
48. Xu, Y., Barrantes, F.J., Luo, X., Chen, K., Shen, J., and Jiang, H., Conformational dynamics of the nicotinic acetylcholine receptor channel: a 35-ns molecular dynamics simulation study. *J Am Chem Soc*, **2005**. *127*(4): p. 1291-1299.

Appendix A

Light-induced modulation of a voltage-gated potassium channel by a $Ru(bpy)_2$-polyunsaturated fatty acid derivative

Intent

The goal of this project was to shift the I-V curve of the Shaker potassium channel in *X. laevis* oocytes toward the left (gain-of-function) upon incubation with and irradiation of $Ru(bpy)_2$-polyunsaturated fatty acid derivatives. This appendix provides initial data about the effects of the first of these compounds, $Ru(bpy)_2$-linoleic acid.

Results and Discussion

Effect of polyunsaturated fatty acids on channel function. It has previously been shown that polyunsaturated fatty acids (PUFAs) interact with a variety of membrane proteins either through direct allosteric interactions or by alteration of the physical properties of the surrounding membrane[1-7]. Specifically, in voltage-gated potassium channels, PUFAs have been shown to shift the current-voltage (I-V) relationship of the channel in an electrostatic and pH dependent manner[8,9]. In these studies, docosahexaenoic acid (DHA), an ω-3 PUFA with six units of unsaturation, was shown to shift the conductance vs. voltage curve in a dose-dependent manner toward the left on the voltage axis indicating that PUFAs can lead to hyperpolarization of the membrane. This effect was more dramatic at higher pH values, pH 9 vs. pH 7.5. Conversely, a rightward shift was observed when the negatively charged carboxylate group was replaced with a positively charged amino group, and no shift was observed for the neutral methyl ester,

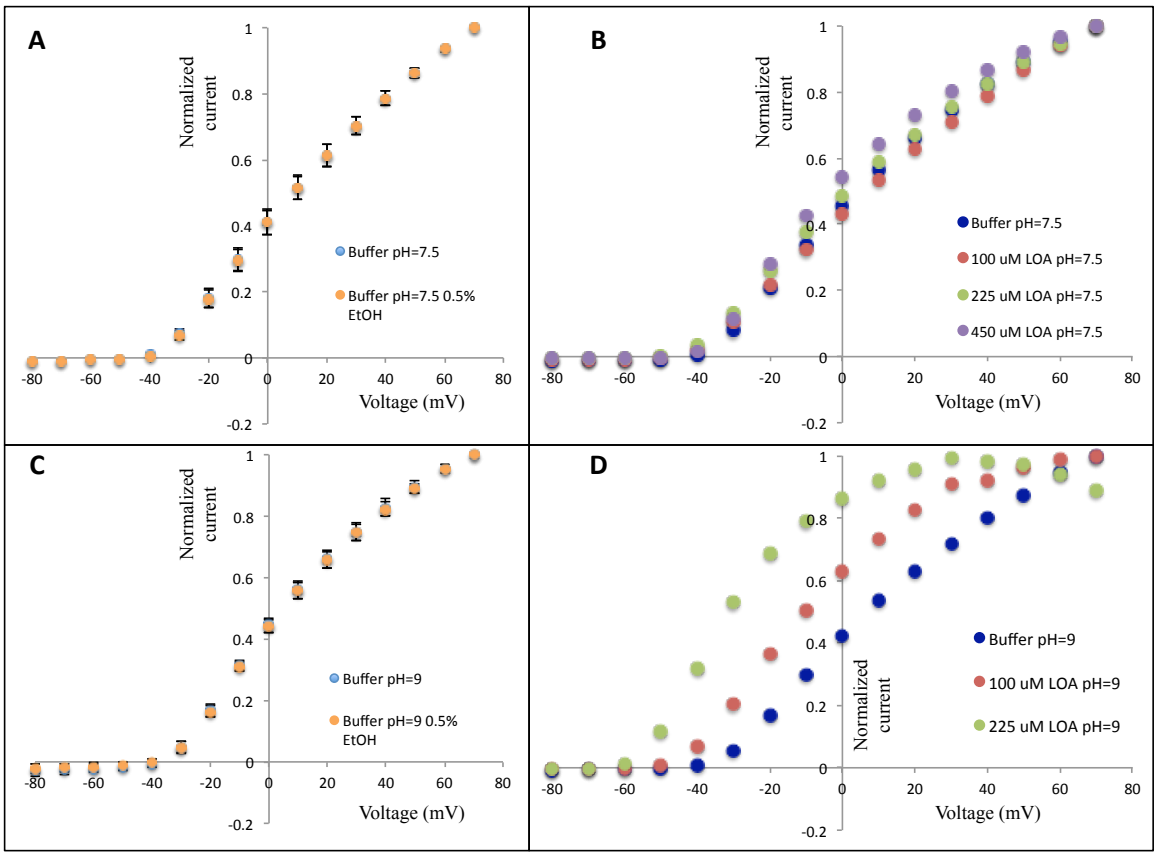

Figure A1. Dose-dependent electrostatic effect of linoleic acid on Shaker potassium channels. **(A** and **C)** I-V curve of Shaker IR upon application of buffer and buffer + ethanol used to make the highest concentration LOA solution: pH 7.5 or pH 9, respectively. **(B** and **D)** I-V curve of Shaker IR upon application of buffer and increasing concentrations of LOA: pH 7.5 and pH 9, respectively.

implying an electrostatic effect. These studies were repeated here with linoleic acid (LOA), an ω-6 PUFA with two unsaturations. A similar leftward shift was observed upon addition of LOA to *X. laevis* oocytes overexpressing the Shaker IR potassium channel, which was both dose-dependent and more pronounced at higher pH values (Figure A1). These data therefore support the previous studies and indicate that LOA behaves similarly to DHA. Small concentrations of ethanol from the LOA stock solution (up to 0.5%) had no effect on channel function at pH 7.5 or pH 9.

A light-absorbing Ru(bpy)$_2$ group alters the effect of LOA on channel function. A 100 μM dose of Ru(bpy)$_2$LOA and a <100 μM dose of Ir(bpy)$_2$LOA were applied separately to cells overexpressing Shaker IR and were irradiated with 455 nm light for 15 seconds after a 1 minute incubation (Figure A3). While a 100 μM dose of LOA gave no shift in the I-V curve of the channel at pH 7.5, a 100 μM dose of Ru(bpy)$_2$LOA resulted in a large rightward (loss-of-function) shift and cell death before irradiation could be performed. No shift was observed for Ir(bpy)$_2$LOA

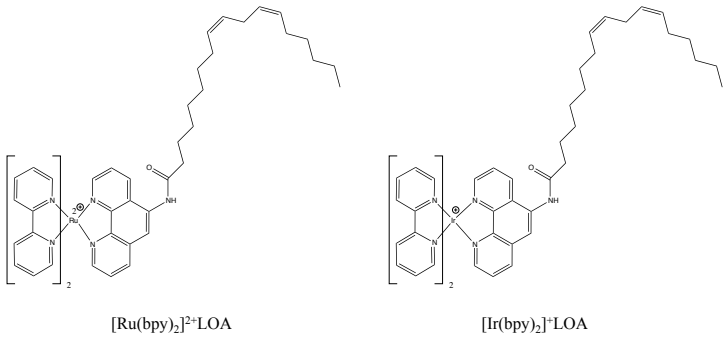

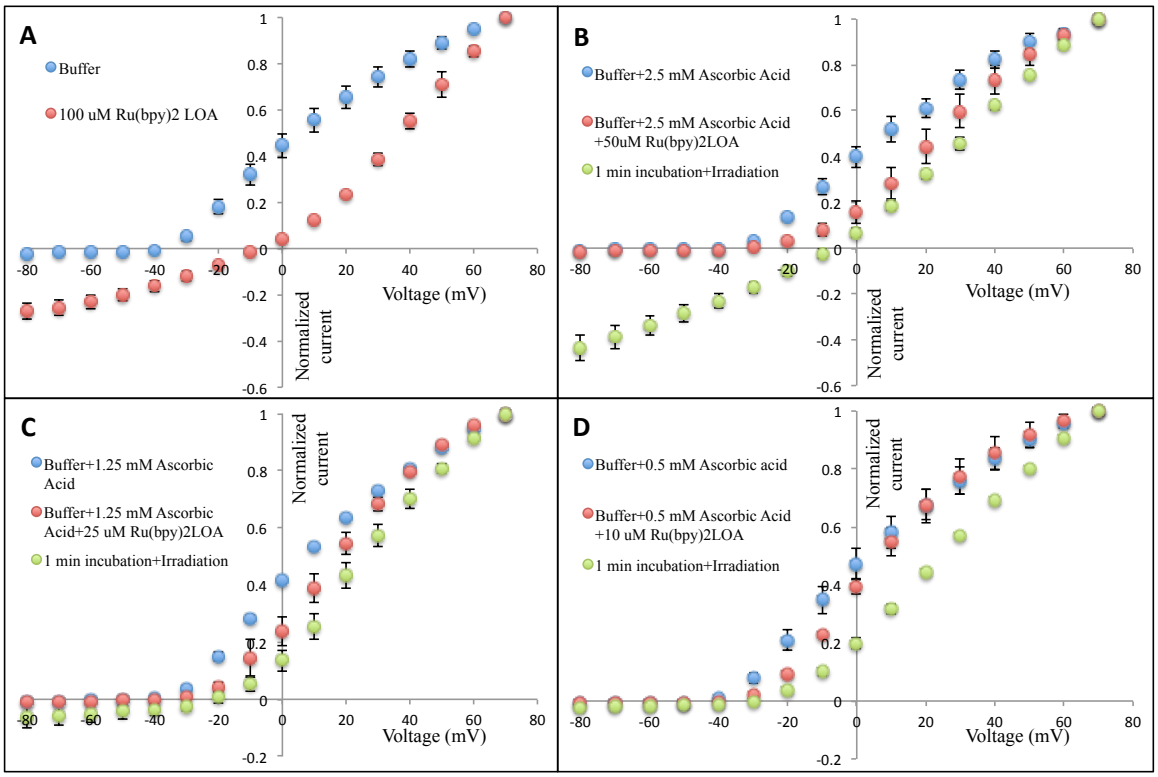

Figure A3. Shifts in I-V curve of Shaker IR in response to decreasing doses of Ru(bpy)$_2$LOA before and after irradiation with 455 nm light. **(A)** 100 μM Ru(bpy)$_2$LOA **(B)** 50 μM Ru(bpy)$_2$LOA, **(C)** 25 μM Ru(bpy)$_2$LOA, **(D)** 25 μM Ru(bpy)$_2$LOA

(data not shown). This may be due to the lesser charge of the complex, +1 vs. +2, or because of the potentially low concentration of the drug solution.

Ascorbic acid was used as an electron donor to favor reduction of the Ru^{2+} complex upon light absorption to Ru^{1+} over oxidation to $Ru^{3+.}$ It was thought that upon irradiation of light, favoring the redox chemistry of the complex toward reduction would result in a leftward shift of the I-V curve relative to the Ru^{2+} complex because of the electrostatic effects previously observed with PUFAs. Because application of 100 µM of the complex led to rapid cell death, lower concentrations were applied to *X. laevis* oocytes and were tested for their effects on channel function. Minimal cell death was observed upon application of 50 µM, 25 µM, and 10 µM $Ru(bpy)_2LOA$. However, irradiation with 455 nm light lead to reduced cell health in both the 50 µM and 25 µM dose, indicated by leak currents at low membrane potentials (< -20 mV). We therefore

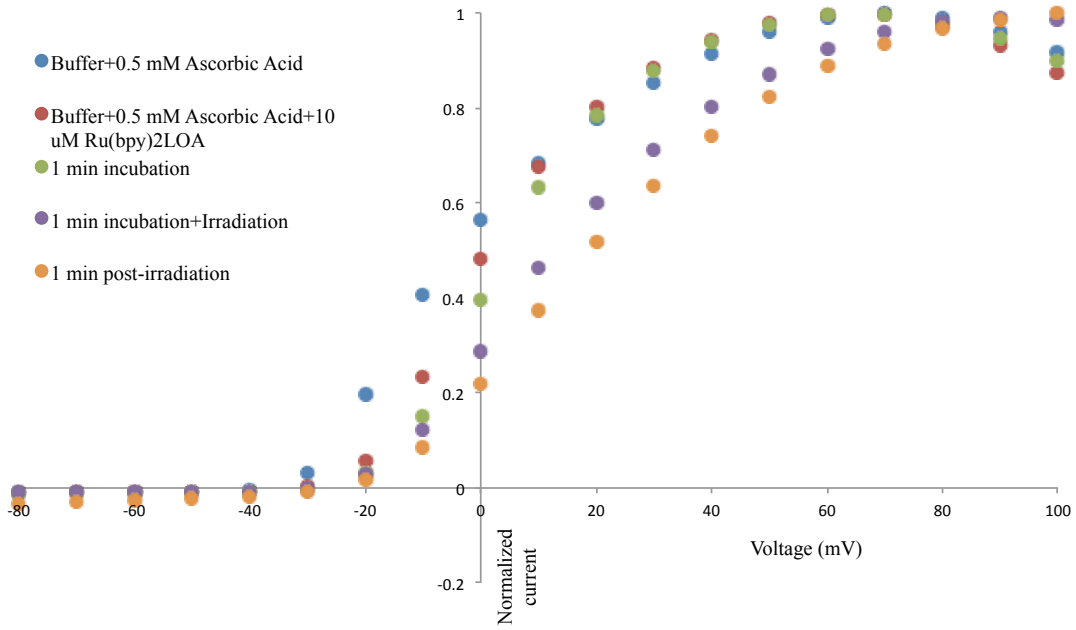

Figure A4. Shifts of the I-V curve of Shaker IR. Data are shown before application of $Ru(bpy)_2LOA$, after application of the complex, after a 1 minute incubation period, after irradiation with 455 nm light, and after a 1 minute post-irradiation dark incubation.

determined that 10 μM was an ideal concentration for maintaining cell health and observing the effects of the complex on receptor function.

Application of $Ru(bpy)_2LOA$ led to a rightward shift of the I-V curve, with more dramatic shifts observed at higher concentrations of the complex. This shift, opposite of what was observed with LOA, is likely due to the +2 charge of the complex compared to the -1 charge of LOA. Upon irradiation, contrary to our expectations, the I-V curve shifted further to the right, indicating either that oxidation of the complex was observed or that another mechanism was responsible for the observed shift. After a one-minute post-irradiation period in the dark, the large rightward shift observed upon irradiation did not decrease, and a slight shift further to the right was observed instead (Figure A4).

Concurrent studies performed by our collaborators with a $Ru(bpy)_2C17$ complex in HEK293 and INS cells showed that irradiation of cells incubated with the complex led to an increase in action potential firing[10]. This effect increased in the presence of reducing compounds (ascorbic acid and ferrocyanide) and decreased in the presence of oxidizing compounds (ferricyanide). It was concluded that the $Ru(bpy)_2C17$ complex induced depolarization of the membrane in the presence of reducing compounds (more negative at the extracellular surface) and hyperpolarization of the membrane in the presence of oxidizing compounds (more positive). Therefore, instead of demonstrating effects similar to PUFAs, irradiation led to a change in the bulk charge of the extracellular space near the membrane, therefore affecting the opening and closing of voltage-gated ion channels. These results provide evidence that what we observed with the $Ru(bpy)_2LOA$ complex at the Shaker IR channel was not due to oxidation of the complex upon irradiation, but instead due to changes in membrane polarization.

Methods

Molecular Biology and electrophysiology. The Shaker potassium channel (inactivation domain removed) was in the pBSTA plasmid. Plasmid DNA was linearized with NotI restriction endonuclease and *in vitro* transcribed mRNA was created using runoff transcription and Ambion's T7 mMessage Machine Enzyme kit. 100 mM stock solutions of linoleic acid and $Ru(bpy)_2LOA$ were made in ethanol and stored at -80^oC. The mass of the iridium complex was unknown and assumed to be less than the ruthenium complex. A stock solution was made with an equal volume of ethanol and was further diluted identically to the ruthenium complex to make the drug solution that was used. We therefore report the concentration as <100 μM, however it is likely to be <<100 μM. For Shaker IR overexpression, 5 ng of mRNA was injected into stage V-VI *X. laevis* oocytes 24 hours prior to recording.

Data were collected with an OpusXpress6000A (Axon Instruments) using two-electrode voltage clamp mode. Recording buffers were ND96 pH 7.5 (96 mM NaCl, 2 mM KCl, 1 mM $MgCl_2$, 5 mM HEPES, 1.8 mM $CaCl_2$, pH 7.5) or ND96 pH 9 (96 mM NaCl, 2 mM KCl, 1 mM $MgCl_2$, 5 mM CHES, 1.8 mM $CaCl_2$, pH 9.0). Initial holding potential was -80 mV, and currents were measured as the voltage was jumped between -80 mV and +70 mV in 10 mV increments. Cells were irradiated with a 455 nm LED for 15 seconds prior to and throughout the duration of data collection for the irradiation curve.

Synthesis. $Ru(bpy)_2LOA$ and $Ir(bpy)_2LOA$ molecules were synthesized by Melanie Pribisko-Yen in the Grubbs group.

References

1. Feller, S.E. and Gawrisch, K., Properties of docosahexaenoic-acid-containing lipids and their influence on the function of rhodopsin. *Current Opinion in Structural Biology*, **2005**. *15*(4): p. 416-422.
2. Feller, S.E., Gawrisch, K., and MacKerell, A.D., Polyunsaturated fatty acids in lipid bilayers: Intrinsic and environmental contributions to their unique physical properties. *Journal of the American Chemical Society*, **2002**. *124*(2): p. 318-326.
3. Grossfield, A., Feller, S.E., and Pitman, M.C., Contribution of omega-3 fatty acids to the thermodynamics of membrane protein solvation. *Journal of Physical Chemistry B*, **2006**. *110*(18): p. 8907-8909.
4. Bendahhou, S., Cummins, T.R., and Agnew, W.S., Mechanism of modulation of the voltage-gated skeletal and cardiac muscle sodium channels by fatty acids. *American Journal of Physiology-Cell Physiology*, **1997**. *272*(2): p. 592-600.
5. Kang, J.X. and Leaf, A., Evidence that free polyunsaturated fatty acids modify Na+ channels by directly binding to the channel proteins. *Proceedings of the National Academy of Sciences of the United States of America*, **1996**. *93*(8): p. 3542-3546.
6. Xu, X.P., Erichsen, D., Borjesson, S.I., Dahlin, M., Amark, P., and Elinder, F., Polyunsaturated fatty acids and cerebrospinal fluid from children on the ketogenic diet open a voltage-gated K channel: A putative mechanism of antiseizure action. *Epilepsy Research*, **2008**. *80*(1): p. 57-66.
7. Xiao, Y.F., Sigg, D.C., and Leaf, A., The antiarrhythmic effect of n-3 polyunsaturated fatty acids: Modulation of cardiac ion channels as a potential mechanism. *Journal of Membrane Biology*, **2005**. *206*(2): p. 141-154.
8. Borjesson, S.I., Hammarstrom, S., and Elinder, F., Lipoelectric modification of ion channel voltage gating by polyunsaturated fatty acids. *Biophysical Journal*, **2008**. *95*(5): p. 2242-2253.
9. Borjesson, S.I., Parkkari, T., Hammarstrom, S., and Elinder, F., Electrostatic Tuning of Cellular Excitability. *Biophysical Journal*, **2010**. *98*(3): p. 396-403.
10. Rohan, J.G., Citron, Y.R., Durrell, A.C., Cheruzel, L.E., Gray, H.B., Grubbs, R.H., Humayun, M., Engisch, K.L., Pikov, V., and Chow, R.H., Light-triggered modulation of cellular electrical activity by ruthenium diimine nanoswitches. *ACS Chem Neurosci*, **2013**. *4*(4): p. 585-593.

Appendix B

Screening of physostigmine analogs against ligand-gated ion channels*

*Work done in collaboration with Christopher Marotta

Abstract

The goal of this project was to screen novel compound synthesized by the Reisman group for activation or inhibition of a variety of ligand-gated ion channels. These molecules were synthesized using their group's novel methodology and demonstrate structural similarity to physostigmine, a positive allosteric modulator of nicotinic acetylcholine receptors (nAChRs) and a clinically used inhibitor of acetylcholinesterase. In this study, five compounds were screened for their activity at seven ligand-gated ion channels: the α7, α4β2, and muscle-type nAChRs and the 5-HT_{3A}, $GABA_{A(\alpha\beta\gamma)}$, glycine, and GluR2 receptors. Most compounds were channel blockers of the nAChRs at moderate concentrations, however, one compound, **86**, demonstrated positive allosteric modulation of the GABAαβγ receptor in addition to channel block of the nAChRs.

Results and discussion

Compound screening against ligand-gated ion channels. Five novel physostigmine analogs were screened against a panel of ligand-gated ion channels (Figure B1). These compounds were tested for their ability to activate the receptor alone (agonist) or for their ability to activate or inhibit the receptor in the presence of the native agonist (allosteric

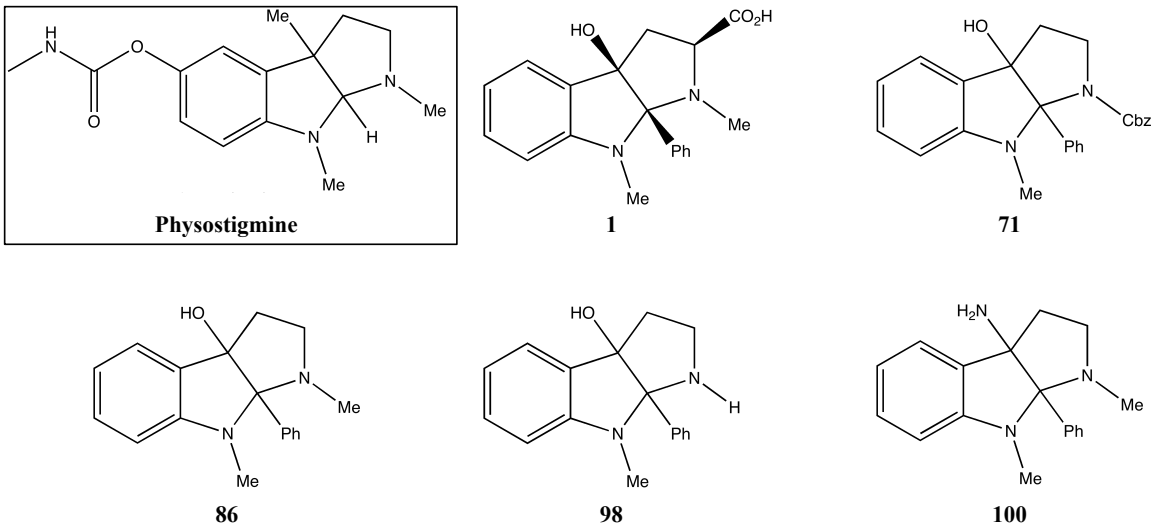

Figure B1. Chemical structures of physostigmine and the five novel compounds tested in this screen.

modulator, antagonist, or channel blocker). All compounds were tested at a concentration of 20 μM and were tested in combination with an EC_{50} concentration of the native agonist. Therefore, the percent increase or decrease in signal reported is relative to the response elicited by an EC_{50} value of the agonist. While these compounds might have shown stronger effects at higher concentrations, we were limited by the amount of many of the compounds that we had and the solubility of the compounds in buffer. We were also only interested in determining "hits" at moderate concentrations that could potentially be used physiologically.

Of the five compounds tested at seven receptors, only compound **86** at $GABA_A$ showed any response to application of the compound in the absence of agonist. The 20 μM dose of **86** at $GABA_A$ elicited a current response that was approximately 5-10% that of the current observed with the EC_{50} agonist dose, however the compound was not sufficiently soluble in buffer to determine a dose-response curve or relative efficacy.

Table B1. Percent change in current observed upon co-application of an EC_{50} dose of agonist and 20 μM of the indicated compound relative to the agonist alone. Negative values represent a decrease of observed current and positive values represent an increase.

	1	**71**	**86**	**98**	**100**
Muscle (9')	-21 +/- 0.6	-29 +/- 3	-53 +/- 3	-7 +/- 3	-81 +/- 6
α4β2 (9')	-28 +/- 2	-47 +/- 4	-29 +/- 6	-11 +/- 2	-44 +/- 2
α7 (6')	-62 +/- 4	-68 +/- 7	-92 +/- 4	-57 +/- 10	-96 +/- 3
5-HT_{3A}	-3 +/- 2	-23 +/- 4	-3 +/- 5	3 +/- 12	-11 +/- 8
$GABA_{A\alpha\beta\gamma}$	-27 +/- 4	-27 +/- 11	52 +/- 10	-27 +/- 21	10 +/- 5
GluR2	-6 +/- 0.7	-0.2 +/- 2	-9 +/- 6	-11 +/- 5	-12 +/- 5
Glycine	-6	-9 +/- 9	3 +/- 7	18 +/- 10	-16 +/- 6

When the compounds were co-applied with an EC_{50} dose of the respective agonist, a variety of responses were observed in the different receptors (Table B1). The most common phenotype was a decrease in observed current relative to the EC_{50} dose alone, indicating an inhibitory role for these compounds. It is likely that this inhibition of current is due to open channel block, which is observed with high concentrations of physostigmine (>20 μM)[1]. This effect was most pronounced in the nAChRs, specifically the α7 receptor, with between 57% and 96% block for all compounds tested. Current inhibition was also observed in the $GABA_A$ and 5-HT_{3A} receptors in response to some of the compounds (-27% for **1**, **71**, and **98** at $GABA_A$ and -23% for **71** at the 5-HT_{3A} receptor). No significant inhibition or activation was observed (<-20% or >20%, respectively) upon application of any of the compounds to the GluR2 or glycine receptors. Interestingly, in addition to slight agonist activity at the $GABA_A$ receptor, **86** elicited a significant *increase* in current when combined with an EC_{50} dose of GABA, indicating the compound can act both as an agonist and as a positive allosteric modulator. Similar studies at the $GABA_{A(\alpha\beta)}$ receptor were inconclusive. Agonist activity or positive allosteric modulation was not observed at any of the other receptors. All compounds

resulted in different levels of inhibition/activation of the receptors examined, indicating some level of specificity of each compound for certain receptors over others.

Characterization of the binding interaction of the physostigmine analogs. An IC_{50} curve for compound **1**, the most water soluble and plentiful compound we had for study, was determined against acetylcholine (ACh) at the α7 (T6'S) and the $\alpha4_3\beta2_2$ receptors (Figure B2). Large variability was observed between cells at low compound concentrations (<10 μM) indicating that the compound may have a slow on-rate and that full inhibition was not achieved in the drug application time used. The IC_{50} of **1** at α7 was determined to be approximately 5 μM with a Hill coefficient of -0.8 indicating that there is likely a single binding site in the receptor, thus favoring these compounds as channel blockers. Because of the presence of five identical subunits in α7, this receptor has five identical agonist binding sites, and so a competitive inhibitor could have multiple molecules bound and a Hill coefficient greater than 1. Values were similar for the α4β2 receptor with an IC_{50} of 8 μM and a Hill coefficient of -1.2. At the maximum dose of 100 μM nearly full inhibition of current is observed in both receptors.

To provide evidence that the physostigmine analogs are acting through an open channel blocking mechanism, voltage jump experiments were performed (Figure B3). The goal of these experiments was to indicate a voltage-dependence of the channel blockers by observing a difference between the negative to positive and the positive to negative voltage jumps. This has previously been performed on the open channel blocker hexamethonium at α4β2 nAChRs[2]. While we did not observe the same voltage-dependence as in the hexamethonium studies, this is likely due to our molecule being a

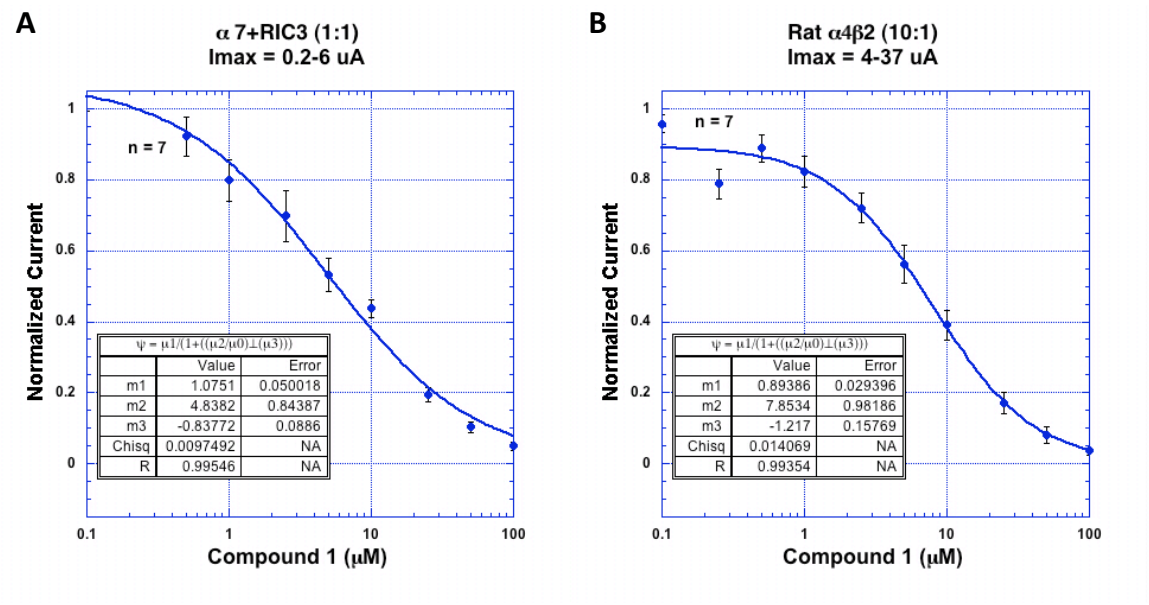

Figure B2. IC_{50} curve of **1** at the **(A)** α7 and **(B)** $\alpha4_3\beta2_2$ nAChRs. m2 is the IC_{50} value and m3 is the Hill coefficient.

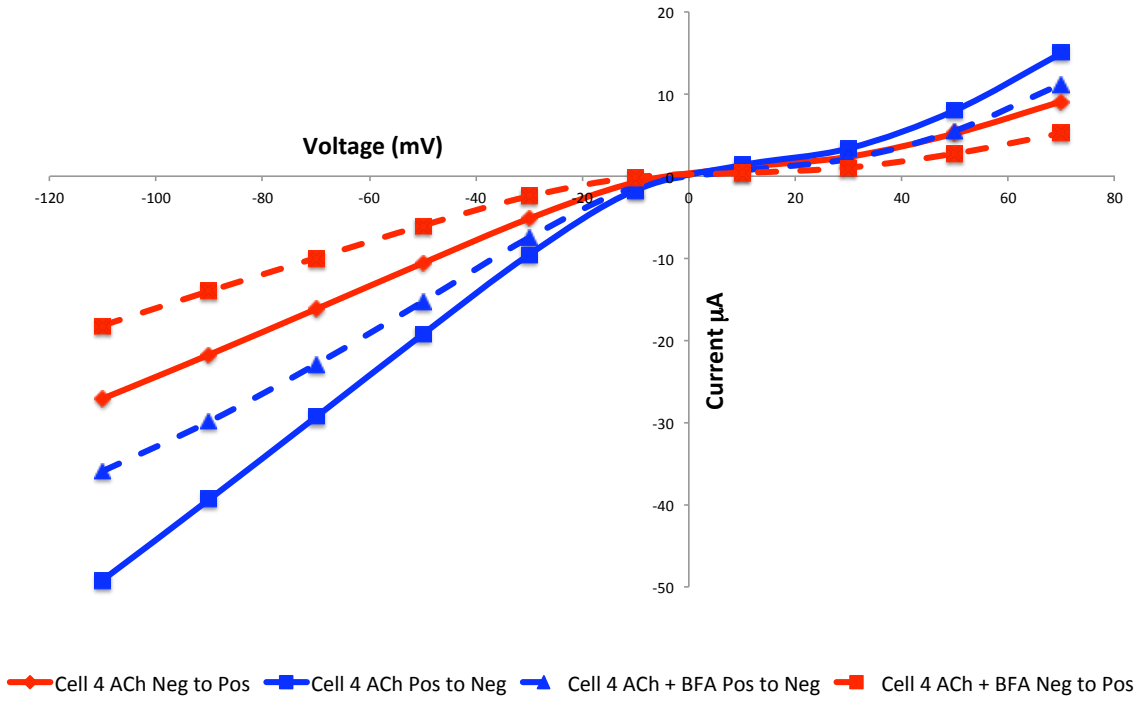

Figure B3. Voltage jump of $\alpha4_3\beta2_2$ in the presence of ACh and ACh+**1** jumped from -110 to +70 mV and subsequently +70 to -110 mV.

net neutral molecule and theirs a positively charged molecule, rather than ours not being an open channel blocker. Performing these experiments on the other positively charged physostigmine agonists would likely have shown a larger effect. The Hill coefficients they observed were similar to what we observed for our molecule (-0.7 to -0.9), as were the IC_{50} values (3-19 μM).

Conclusions

The physostigmine analogs examined here demonstrate properties similar to physostigmine itself. At low concentrations of physostigmine, it acts as a weak agonist and positive allosteric modulator of nAChRs (similar to **86** at $GABA_A$) and at higher concentrations exhibits open channel blocking activity[1]. We observe an inhibition of current of the various nAChRs tested here by a co-application of 20 μM of the physostigmine analogs and an EC_{50} dose of the native agonist. This is also observed to a lesser extent in the $GABA_A$ and 5-HT_{3A} receptors. The IC_{50} and Hill coefficient values for these novel compounds are similar to what is observed for other nAChR open channel blockers, providing evidence for a channel blocking mechanism of these compounds. Perhaps at lower ligand concentrations the compounds would have exhibited channel activation and positive allosteric modulation, however these tests were not performed. It would be interesting to examine more closely the properties of **86** at the $GABA_A$ receptor, for example, an EC_{50} value, whether channel blocking is observed at higher concentrations, and determination of the binding site of the compound. However, solubility in buffer will likely be a problem for these studies.

Methods

Percent inhibition/activation of receptors by the compounds was determined by the methods shown in Figure B4. First, three consecutive EC_{50} doses of the native agonist were applied with a 3-5 minute washout in between applications. This was followed by a 20 μM concentration of the ligand being tested and a subsequent 20 μM ligand + agonist EC_{50} dose with no washout in between to test for agonist and antagonist, allosteric modulation, and channel block activity, respectively. The second and third current responses were averaged together and the compound and compound+agonist responses were normalized to this value to give a percent change. The ability for the ligand to be washed out of the receptor was then measured by two successive agonist applications. Agonist EC_{50} values used in these experiments were: 100 μM ACh (α7 T6'S), 1.2 μM ACh (muscle-type L9'A), 0.5 μM ACh ($\alpha4_3\beta2_2$ L9'A), 110 μM glycine (glycine receptor), 3 μM 5-HT ($5\text{-}HT_{3A}$), 14 μM glutamate (GluR2), and 11 μM GABA ($GABA_{A\alpha\beta\gamma}$). ND96 Ca^{2+} free buffer was used for the muscle-type and α4β2 nAChRs, the glycine, $5\text{-}HT_{3A}$, and GluR2 receptors. ND96 was used for the $GABA_A$ and α7 nicotinic acetylcholine receptors.

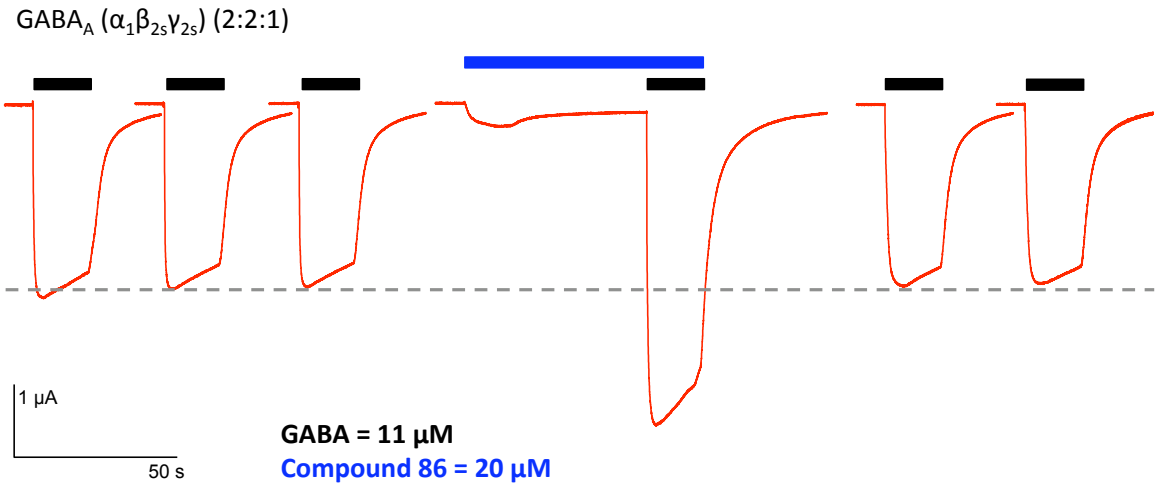

Figure B4. Protocol used for testing novel compounds against ligand-gated ion channels for agonist, antagonist, allosteric modulator, and channel blocker properties.

References

1. Militante, J., Ma, B.W., Akk, G., and Steinbach, J.H., Activation and block of the adult muscle-type nicotinic receptor by physostigmine: single-channel studies. *Mol Pharmacol*, 2008. *74*(3): p. 764-776.
2. Buisson, B. and Bertrand, D., Open-channel blockers at the human alpha 4 beta 2 neuronal nicotinic acetylcholine receptor. *Molecular Pharmacology*, 1998. *53*(3): p. 555-563.